**RIJKSUNIVERSITEIT GENT**

FACULTEIT VAN DE LANDBOUWWETENSCHAPPEN

Seminarie voor Toegepaste Wiskunde
en Biometrie

# SIMULATIE VAN DE WATERBEWEGING IN DE BUNGOR SERIES (TYPIC PALEUDULT) IN RELATIE TOT DE BODEMEROSIE

# SIMULATION OF WATER MOVEMENT IN THE BUNGOR SERIES (TYPIC PALEUDULT) IN RELATION TO SOIL EROSION

door

WAN SULAIMAN BIN WAN HARUN

A thesis presented to the Faculty of Agricultural Sciences, Ghent
in partial fulfilment of requirements for the degree of
Doctor in Agricultural Sciences

Proefschrift voorgedragen tot het bekomen van de graad van
Doctor in de Landbouwkundige Wetenschappen
op gezag van

**Rektor Prof. Dr. J. HOSTE**



Deken :
**Prof. Dr. Ir. A. COTTENIE**

Promotor :
**Prof. Ir. G. C. VANSTEENKISTE**

Bijstelling:

Agricultural exploitation of waste tin mining land is feasible with the intervention of Government Authorities.

(Landbouwkundige uitbating van gronden verlaten door de tin-mijnbouw is goed mogelijk indien de overheid gepast tussenkomt.)

# ACKNOWLEDGEMENTS

The contributions of various individuals and institutions towards the realisation of this thesis are gratefully acknowledged.

Foremost, I wish to express my sincere gratitude to the promotor of this thesis, Prof. ir. G.C. Vansteenkiste for his guidance and encouragement throughout the course of the study and for his valuable criticism during the preparation of the manuscript. To Prof. Dr. ir. M. De Boodt, I would like to express my indebtedness for allowing me the use of the Soil Physics laboratory facilities, for his generous help and for serving on the jury.

Similar words of thanks and appreciation are also extended to the members of the reading committee, Prof. Dr. ir. A. Rotti, Prof. ir. G.A. Heyndrickx and Dr. ir. R. Hartmann for their constructive comments and criticism. I am also deeply obliged to the other members of the jury, Prof. Dr. ir. A. Cottenie, Prof. Dr. ir. F. Pauwels, Prof. ir. L. Baert and Prof. ir. Van Ruymbeke for their interest in the work.

This study could not have been possible without the sponsorship of the University of Agriculture Malaysia; to the Vice-chancellor, Tan Sri Prof. Mohd. Rashdan bin Hj. Baba and the Dean of Agriculture, Prof. Mohd. Zain bin Karim, my utmost gratitude for their consent and encouragement.

Likewise, the financial support of the Algemeen Bestuur van de Ontwikkelingssamenwerking (A.B.O.S.) during my study in Belgium is gratefully acknowledged and in particular, my appreciation to Mevr. Kilani - van den Broeck and Madame G. Dekoninck for their kind help.

Special words of thanks go to Dr. ir. A. Calus and ir. J. Callewier for their unceasing help with the computer facilities and to Dr. ir. H. Verplancke and Mr. O. Willems for their assistance in the laboratory.

I am also grateful to Dr. ir. F. de Schutter and ir. J. Spriet for fruitful discussions on the finite element method and the pattern recognition method, respectively.

Words of thanks are also due to ir. L.M. Maene for sending me the soil samples, Mevr. De Paepe - Gevaert for her special care in typing this manuscript and Mr. R. Van Rijk for the preparation of slides.

Needless to say, there are many friends and personnel of the Department of Applied Mathematics and Biometry and the Laboratory of Soil Physics and Horticultural Soil Science I have failed to mention but who, in one way or another, have contributed towards the realisation of this manuscript; to these people, my heartfelt thanks.

Finally, this thesis is dedicated to my wife, Jaenah and my children Wan Imran, Wan Azhar and Wan Norazian whose love and moral support helped me to the completion of this study.

# CONTENTS

# INTRODUCTION

Modeling and simulation of soil water flow has long been a subject of interest in water resources planning, soil management and conservation, soil-plant relationships as well as from purely soil physical aspects. Interest was generated because of the desire to quantify the processes taking place coupled with the intent on an optimal management of our soil and water resources.

A current problem of interest is that of soil erosion. Erosion studies to date have concentrated mainly on the soil surface, on the one hand, i.e., the top few centimetres which is the primary site for management and control, and the rain characteristics, on the other. The role of the soil profile and the incidental water movement in it have received less attention. Even though soil detachment is mainly caused by splash erosion (Hudson, 1971), soil losses can only occur when surface water is present to carry away the detached soil. This happens only when rain exceeds infiltrability. The volume of runoff water as well as the time of commencement of ponding (or runoff) is, thus, of prime interest in any consideration of soil erosion. One ought to complement small runoff-plot measurements with water flow studies in the soil profile because the soil profile is the most important means of conducting rain water from the surface to groundwater.

The rate of water movement depends on the hydraulic properties of the soil, namely, the hydraulic conductivity and water retention characteristics. Both vary spatially and are largely dependent upon pore size distribution. Within a profile, the profile development as manifested in the genetic and morphological horizons is probably the most important single factor that influences the pore size distribution and, hence, the hydraulic properties of the soil. An increasing hydraulic conductivity with depth means that the rate of water movement through the soil will be surface limiting meaning that the infiltration rate will be controlled by the surface horizon. On the other hand, the presence of less permeable horizon(s) below increases the importance of the lower horizon(s) in the long term movement of water.

To acquire a quantitative appreciation of the flow behaviour under these conditions one inevitably has to resort to the numerical model

based on Richards' equation (Richards, 1931).

Most numerical procedures dealing with Richards' equation are based on the finite difference approach which can treat fairly difficult problems. However, this approach is often difficult to apply in complex flow domains. Therefore, recently, attention has been shifted to the finite element method (Neuman et al., 1975 ; Cushman and Kirkham, 1978) which is capable of treating in a natural manner such complexities as irregularly shaped boundaries, soil heterogeneity and arbitrary anisotropy. Evidence, however, seem to indicate the existence of some underlying problem in the application of the finite element method to saturated and partly saturated soils.

The objectives of the study are therefore, formulated as follows :

1. to simulate water movement in a soil series found on slopes in Peninsular Malaysia, namely, the Bungor Series (an ultisol) during rain, with the aim of quantifying the influence of hydraulic properties of the soil profile on the accompanying infiltration-runoff relationship.
2. to make a comparative study of the finite difference and finite element spatial approximation methods in the study of unsaturated soil water movement.

In pursuing these two objectives it also becomes necessary to examine the relative merits of the two forms of the unsaturated flow equation, namely, the moisture-based equation and the pressure-based equation.

It is obviously desirable to acquire *in situ* measurements of the hydraulic properties and the relevant field variables of the water flow model. In view of certain limitations, however, this is not yet possible. Therefore, disturbed samples are used instead and measurements are made on them in the laboratory. Doubtless to say, this does impose some limitation on the applicability of the results when interpreting them in the light of actual field conditions. Nonetheless, it is believed that this investigation will contribute towards a further understanding of the complex process occurring in the soil surface zone and a familiarization of the hydrologic behaviour of Malaysian soils. It is worthwhile to note that to date there has been no published work on water movement in Malaysian soils. Whether Darcy's law is valid for the description of unsaturated water movement in these highly weathered soils is still to be seen.

CHAPTER 1

# A SIMULATION APPROACH TO THE STUDY OF SOIL WATER MOVEMENT

## 1.1. SIMULATION AND MODELING

Simulation may be defined as a technique of solving problems by following the changes over time of a dynamic model of a system without attempting to solve the equation(s) of the model analytically (Gordon, 1969). Its usage in soil and groundwater studies is becoming popular because of the difficulties associated with experimental studies on the real soil and groundwater systems. By simulation much insight can be gained into the behaviour of the system without resorting to elaborate experimental setup, which eventually, as often does, prove to be still inadequate.

Simulation studies in general consists of three basic steps :

- definition of the problem,
- development of a model to represent the process under study,
- use of the model, i.e., design and execution of simulation runs to answer specific questions that have been posed.

The first and the last step are self-explanatory and demand no further elaboration. The second step, namely, model development is the crux of the simulation process.

*Model Development*

Model development or modeling is as much an art as it is a science. Many variants to model development exist depending upon the type of system to be modelled and simulated (see for example, Isermann, 1975 ; Vansteenkiste, 1972, 1975). Nevertheless, three fundamental stages can be identified. The first is the formulation of a mathematical model to represent the process or system being studied. This can be achieved by a theoretical analysis based on physical laws to generate basic equations which are then solved to give a model with definite structure and parameters. Most models in soil water systems are obtained in this manner since water flow is essentially a field problem governed by potential

theories/laws. Alternatively, when the process cannot be described by physical laws, one can start with an assumed structure based on some a-priori knowledge of the process.

In either case, the next stage of the modeling process is that of parameter identification. Measured input and output of the system are used to determine the parameters of the model by such methods as curve fitting and least squares parameter optimization, the particular technique employed, again depends in large measure on the type of model to be identified.

The final stage in the model development is validation of the model. Results of simulation runs are compared to real world data to see if the model behaves as expected. Here, a large degree of subjectivity is involved. Few criteria for "goodness of fit" exist and it is eventually left to the researcher, relying upon his background experience to decide whether the model is a valid representation of the process being studied.

A more recent approach to model building is a form of pattern recognition. One starts with a number of candidate models whose structures are considered to be different patterns and identification is seen as a task in recognizing the patterns using experience and available information (Karplus, 1972 ; Vansteenkiste, 1978a). In this approach, emphasis is on the characteristics of the model rather than the actual parameter values.

An essential part of modeling which has not been identified as a fundamental step is the development of mathematical and computer techniques for handling the model. This aspect is especially important in distributed parameter systems, whereby the governing equations (models) are mostly nonlinear partial differential equations. The success of the simulation depends to a large extent on the development reliable techniques for solving such equations.

## 1.2. DEFINITION OF THE PROBLEM

In Peninsular Malaysia soil erosion is a major cause for the deterioration of the environment. In an effort to alleviate the problem a number of studies have been carried out and are still underway on the measurement and assessment of soil erodibility and rain erosivity (Maene et al., 1977).

Pertinent to the problem are such information as the intensity of rain that can initiate runoff for a given soil, the approximate time of commencement of runoff during a rainfall event and the accompanying infil-

tration-runoff relationship. While most of the information can be obtained by direct runoff-plot measurements, it is also desirable to assess the role of the soil profile in the global erosion problem. Thus, the primary objective of the present study is to obtain quantitative estimates of the above mentioned factors from a study of the water movement within the soil profile. Such estimates can be a further aid in the management and control of soil erosion.

As a large number of water flow models are already in existence, the approach to the present study is to select one that is particularly suited to the underlying problem and to proceed from there within the general framework of system simulation. The next section presents a brief review of some of the existing water flow models.

## 1.3. SOIL WATER FLOW MODELS

Soil water flow models are required in many problem areas such as land and water resource planning, conservation, management and research. The level of sophistication of the model is dictated by the scale of the problem and the purpose for which it is developed. Two broad classes can be defined, namely, the macroscopic models and the semi-macroscopic ones.

### 1.3.a. Macroscopic Models

In the evaluation or assessment of erosion several runoff-infiltration models are available. At the scale of a catchment, the maximum rate of runoff can be calculated from the Rational formula (Ramser, 1927), which is

$$V = CIA/360 \tag{1.1}$$

where V is the rate of runoff in $m^3/sec$, I is the rain intensity in mm/hour, A is the catchment area in hectares and C is a dimensionless constant which takes into account the topography, vegetation, infiltrability, soil storage capacity, drainage characteristics and so on.

Ive et al. (1976) proposed a model for medium and small catchments which takes account of the antecedant water content, $\theta$. The model is

$$V_t = (R_t - c)\, f_1(R_t) + R_t f_2(\theta) \tag{1.2}$$

where $V_t$ is the net surface runoff, $R_t$ the rainfall amount, $f_1(R_t)$ and $f_2(\theta)$ are functions determined to minimize the discrepancy between the measured and calculated runoff and c a constant.

1.3.b. Semi-macroscopic Models

(i) Algebraic Models

There are a number of problems in which we only wish to know the water balance of the soil profile. For this purpose algebraic type of equations can be used. In the case of infiltration from ponded water, for instance, the Green and Ampt (1911) equation is widely used. It is

$$t = \frac{1}{K_s}\left[Q - \Delta f(h_o - h_w)\ln\left(\frac{h_o - h_w + Q/\Delta f}{h_o - h_w}\right)\right] \qquad (1.3)$$

where t is the time of accumulated infiltration of an amount Q, $h_o$ is the depth of ponded water, $h_w$ is the soil-water pressure head just above the wet front ($h_w$ is negative), $K_s$ is the hydraulic conductivity in the wetted zone and $\Delta f$ is the "fillable" pore space, that is, the difference between water content before and after passage of water front and assumed constant for a given soil. The term $Q/\Delta f$, therefore, indicates the depth, l of the wet front below the soil surface. Since Q and $Q/\Delta f$ or l both appear in the same equation one cannot predict each independently of the other. However, by assuming that the soil is effectively saturated, in other words, $\Delta f$ is known, then Eq. (1.3) can be used to predict l after which Q can be deduced.

For rainfall or sprinkler irrigation the model of Schwab et al. (1966) gives the relationship between the volume of runoff $V_t$, the daily rainfall amount $R_t$ and the soil storage amount s according to

$$V_t = (R_t - 0.2s)^2/(R_t + 0.8s) \qquad (1.4)$$

This model has been tested over several soils and crop conditions. It can be used in conjunction with Eq. (1.3) to predict various quantities of interest. For example, s in Eq. (1.4) can be related to $\Delta f$ in Eq. (1.3) by $s = \Delta f L$ where L is the soil depth considered. Total infiltration Q, is simply the difference between rainfall amount and runoff. To calculate depth of wetting of a day's rain this value of Q is now substituted in Eq. (1.3) along with a value of $h_o = 0$.

(ii) Darcy Flux Models

In certain problems such as those involving growing plants not only is it desirable to know the water balance of the system but also to know where the water is located relative to the roots. For a 2-dimensional water flow system Baker et al. (1976) and Lambert et al. (1976) assume

that rainfall for one day enters the top layer of the profile and fills it before entering the next layer below. This procedure is repeated until all of the rainfall is accounted for or the soil is filled to field capacity. In the latter case the excess rainfall is considered to be runoff. At all times water moves vertically or horizontally according to Darcy's law in the form

$$v = -D(\theta) \frac{d\theta}{dx} \qquad (1.5)$$

where v is the velocity of flow, $D(\theta)$ is the moisture dependent soil water diffusivity and $d\theta/dx$ the moisture content gradient. Gravity is neglected and the model for soil water flow is symmetrical about the mid-plane.

(iii) Richards' Equation

There are many problems for which neither the algebraic type model nor the Darcian Flux model are accurate enough to predict the water content distribution in the soil. Examples are detailed studies on the effects on water flow of various phenomena such as inhomogeneities, changing surface conditions and variations in hydraulic properties of the soil. These problems require the solution of Richards' equation (Richards, 1931), which can be written as

$$\frac{\partial \theta}{\partial t} = - \nabla.q + S \qquad (1.6)$$

where $\nabla.( )$ is the divergence operator, q is the Darcy flux and S is a source (or sink) term for water. Unless there are plants growing in the soil system S is usually ignored.

Equation (1.6) yields as solution the moisture content as a function of time and position from which the total drainage or infiltration, infiltration rate or evaporation rate and position of wetting front can be deduced. In recent years a large number of simulation models have evolved from Richards' Equation (Freeze, 1969 ; Nimah and Hanks, 1973 ; Feddes et al., 1974 ; Hillel et al., 1975 ; D'Hollander and Impens, 1975).

## 1.4. CHOICE OF WORKING MODEL

In order to meet the objectives of the study Richards' model (equation) or the soil water flow equation has been chosen as the working model. The reasons are as follows. In addition to the water balance, of prime interest is the pattern of water movement in the soil during a rainfall. Various factors such as changing boundary conditions and hetero-

geneities within the soil are easily incorporated in the Richards' model. This model yields the largest number of output information which can be utilized in the physical description of the soil water system. Finally, since experimentation is performed on disturbed samples in the laboratory thereby subjected to less measurement noise, a fairly detailed model such as Richards' equation can be used.

## 1.5. DERIVATION OF RICHARDS' EQUATION

The Buckingham-Darcy flux equation for a rigid, unsaturated porous medium may be written as

$$q = -K(h)\ \nabla\ H \tag{1.7}$$

where q, as defined in (1.6) is the vector flow velocity, K is the hydraulic conductivity and is a function of the pressure head potential h of the soil water, $\nabla$ is the standard del operator and H is the driving potential expressed as the hydraulic head. This equation combines with the equation of continuity (with the sink or source term ignored)

$$\frac{\partial\theta}{\partial t} = -\ \nabla.q \tag{1.8}$$

to provide the flow equation

$$\frac{\partial\theta}{\partial t} = \nabla.(K(h)\ \nabla\ H) \tag{1.9}$$

Choosing the datum plane for the hydraulic head at the xy plane z = 0 and taking z, the position coordinate as positive downwards then H can be expressed as

$$H = h - z \tag{1.10}$$

The pressure head h is negative in unsaturated soil and positive in saturated soil. If the water content and pressure head can be considered as uniquely related, either as $\theta = \theta(h)$ or $h = h(\theta)$, then the left-hand side of Eq. (1.9) can be written as $\partial\theta/\partial t = (d\theta/dh)(\partial h/\partial t)$. Substituting (1.10) and (1.9) and observing that $\nabla.(K\nabla z) = \partial K/\partial z$ for cartesian coordinates result in

$$C\frac{\partial h}{\partial t} = \frac{\partial}{\partial x}\left(K\frac{\partial h}{\partial x}\right) + \frac{\partial}{\partial y}\left(K\frac{\partial h}{\partial y}\right) + \frac{\partial}{\partial z}\left(K\frac{\partial h}{\partial z}\right) - \frac{\partial K}{\partial z} \tag{1.11}$$

which is essentially the governing PDE first derived by Richards (1931).

The term $C = d\theta/dh$ is defined as the specific (or differential) water capacity. The argument for the functions C and K are deliberately left unspecified since $h = h(\theta)$, hence C and K can both be considered to be functions of either h or $\theta$.

Introducing the soil water diffusivity $D(\theta)$ (Childs and Collis-George, 1950) defined as

$$D(\theta) = K(\theta)/C(\theta) \tag{1.12}$$

the pressure-based Eq. (1.11) may now be cast into the "diffusivity" form or the moisture-based equation

$$\frac{\partial \theta}{\partial t} = \frac{\partial}{\partial x}\left(D \frac{\partial \theta}{\partial x}\right) + \frac{\partial}{\partial y}\left(D \frac{\partial \theta}{\partial y}\right) + \frac{\partial}{\partial z}\left(D \frac{\partial \theta}{\partial z}\right) - \frac{\partial K}{\partial z} \tag{1.13}$$

*Discussion*

Implicit in the derivation of Eq. (1.11) are the assumptions that because of the relatively small resistance to flow of air it is possible to ignore the air flow phase, that the air is at atmospheric pressure everywhere in the flow field, that the water and the medium are incompressible, that isothermal conditions prevail and that Darcy's Law applies to flow in partially saturated media.

It should also be noted that from the physical point of view the concept of diffusivity is rather artificial. It was introduced as a device to simplify the governing PDE of flow in unsaturated soils. Indeed, for uniform soils there are advantages of the diffusivity formulation that deserve emphasis. First, $\theta$ can be measured with greater ease, precision and resolution over the complete range from dryness to saturation than the pressure head. Secondly, for a given soil the moisture-based equation is not as strongly non-linear as the pressure-based equation and, therefore, is easier to handle numerically. Finally, if horizontal soil water flow is the prime concern, then in principle the diffusivity function is all that is needed to characterize the flow process. In contrast, both the capacity and conductivity functions are needed in the pressure-based model. Hence, the diffusivity form has been employed by many authors for solving unsaturated flow in homogeneous soils (Philip, 1957 ; Rubin and Steinhardt, 1963 ; Remson et al., 1967).

Application of the diffusivity form to both saturated and unsaturated systems is, however, more complicated as has been demonstrated by Philip (1957b) and Rubin and Steinhardt (1964). The reason is that $\theta$ is

constant in saturated soil and, therefore, cannot provide an indication of the physical state of the water nor the existing potential gradient. Its application to stratified soils will also lead to erroneous results because the diffusivity form of Darcy's Law (Eq. 1.5) with a gravity term included, can artificially yield net flow at the boundaries between layers even when the system is in hydrodynamic equilibrium. The pressure-based equation, on the other hand, simply becomes Laplace's equation when the soil is saturated and regardless of the kind of heterogeneity existing in the system the hydraulic head remains the only driving potential explicitly expressed in the governing equation.

## 1.5. APPROACH TO THE STUDY

The study begins with a known model, thus the main activities are centred on the identification of the parameters of the model, considerations of numerical techniques for handling the model, model validation and simulation in the Bungor Series.

In the parameter identification stage, the structure characterization of the state variable dependent parameters will be attempted using the pattern recognition approach suggested by Vansteenkiste, Bens and Spriet (1978a).

This study deals almost entirely on flow in one dimension since this is the predominant process occurring naturally in the soil in relation to infiltration. Furthermore, initial insight into the differences between the finite difference and finite element methods can be obtained from the simplest geometrical configuration, i.e., a one-dimensional problem. Anomalies observed in the one-dimensional case can then be singled out for further study with two- or three-dimensional problem.

With these in mind and in keeping with the objectives of the study, the layout of the thesis will be as shown in Fig. 1.1.

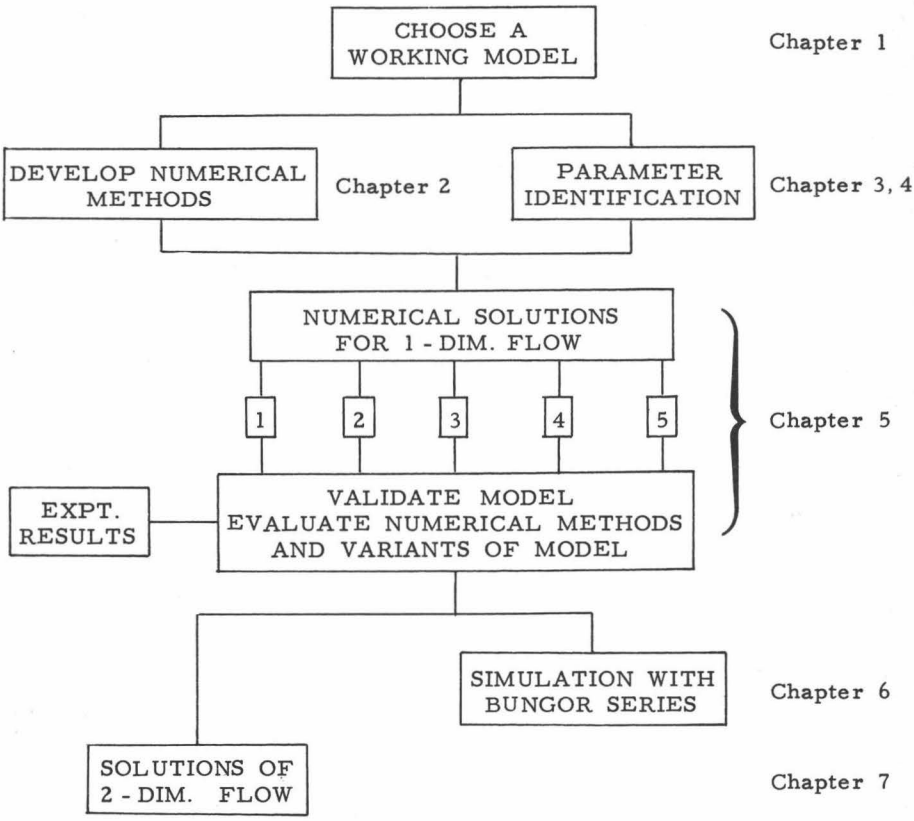


Fig. 1. 1 Layout of the simulation study on soil water movement .

CHAPTER 2

# SOLUTION OF RICHARDS' EQUATION

The majority of existing water flow models entail the solution of Richards' equation in one dimension. This can be written as

$$C \frac{\partial h}{\partial t} = \frac{\partial}{\partial z} \left(K \frac{\partial h}{\partial z}\right) - \frac{\partial K}{\partial z} \tag{2.1}$$

or

$$\frac{\partial \theta}{\partial t} = \frac{\partial}{\partial z} \left(D \frac{\partial \theta}{\partial z}\right) - \frac{\partial K}{\partial z} \tag{2.2}$$

In the foregoing discussion the various techniques of solving Eq. (2.1) and (2.2) are reviewed culminating in the detail treatments of the finite difference and finite element approximation methods.

## 2.1. REVIEW OF METHODS

### 2.1.a. Quasianalytical methods

Richards' equation, due to its strong nonlinearity has no known general analytical solution. However, a specific solution of Eq. (2.2) was first obtained by Philip (1957) for the case of infiltration in an homogeneous semi-infinite soil column subject to the initial and boundary conditions

$$\begin{aligned} \theta(z,0) &= \theta_n \\ \theta(z,t) &= \theta_n \\ \theta(\infty,t) &= \theta_n \end{aligned} \tag{2.3}$$

In a later paper (Philip, 1957b) Eq. (2.1) was solved taking into account a finite water depth over the soil. The initial and boundary conditions in this case are

$$h(z,0) = h_n$$
$$h(0,t) = h_o \qquad (2.4)$$
$$h(\infty,t) = h_n$$

Philip's method led to the solution in the form of a power series in $t^{1/2}$ which may be written as

$$z(f,t) = \phi t^{1/2} + \chi t + \omega t^{3/2} + \ldots + f_m t^{m/2} \qquad (2.5)$$

where $\phi$, $\chi$, $\omega$ and $f_m$ are functions of $\theta$ or h depending on the form of the governing equation. The series converges only for finite t and the solution becomes unreliable as $t \to \infty$. The t-range of convergence depends upon the characteristics of the soil and the initial and boundary conditions.

More recently, Parlange (1971, 1972) developed a quasianalytical solution to the equation

$$\frac{\partial z}{\partial t} + \frac{\partial}{\partial \theta}\left(D \frac{\partial \theta}{\partial z}\right) = \frac{\partial K}{\partial \theta} \qquad (2.6)$$

obtained from Eq. (2.2) via the relation

$$\left(\frac{\partial z}{\partial t}\right)_\theta = -\left(\frac{\partial \theta}{\partial t}\right)_z \left(\frac{\partial z}{\partial \theta}\right)_t$$

The boundary conditions considered were those represented by Eq. (2.3) and (2.4) as well as a constant flux $q_o$ at the soil surface,

$$\theta(z,0) = \theta_n$$
and $$K - D \frac{\partial \theta}{\partial z}(\theta,t) = q_o \qquad (2.7)$$

The solution of Eq. (2.6) subject to conditions (2.7) is

$$z(\theta,t) = \int_{\theta}^{\theta_1(t)} \frac{D(\beta)}{(q_o - K_n)\left|\frac{\beta - \theta_n}{\theta_1(t) - \theta_n}\right| - [K(\beta) - K_n]} \, d\beta$$

where $K_n$ is the hydraulic conductivity at $\theta_n$ and $\theta_1(t)$ is the water content at the soil surface at time t, the latter given by

$$t = \int_{\theta_n}^{\theta_1(t)} \frac{D(\alpha)(\alpha - \theta_n)}{[q_o - K(\alpha)]\,[q_o - K_n]}\, d\alpha$$

Aylor and Parlange (1973) expanded the semi-analytical method to include heterogeneity. The special case considered was for a layered soil with constant imposed flux at the surface and with the initial water content increasing with depth in the upper layer. The solution was obtained graphically based on the assessment of the physical processes involved. The authors emphasized, however, that in cases where the transition between the two layers is less abrupt than in their special case and the difference in porosity greater, further refinement in the physical description at the interface would be necessary.

An interesting linearization and analytical solution to the problem of constant flux at the surface into an infinitely deep homogeneous soil has been provided by Braester (1973), who expressed Eq. (2.2) and condition (2.8) in terms of a diffusivity potential

$$F = \int_{h_n}^{h} K dh = \int_{\theta_n}^{\theta} D d\theta$$

The linearization is accomplished by setting

$$K = K_o\, e^{ch}$$

where $K_o$ and c are constants. Comparison with the numerical solution of Rubin and Steinhardt (1963) showed that while the time variation of $\theta$ at the surface was in good agreement with each other the $\theta$-profiles were more discrepant. The linearized solution does, nevertheless, provide a first approximation which can be improved by perturbation.

The quasianalytical methods such as those of Philip and Parlange, extremely useful as they are in understanding the physics of infiltration are, however, very restrictive in their initial and boundary conditions and therefore, of limited application. For instance, the initial conditions defined by Eq. (2.3), (2.4) and (2.7) are seldom met in practice unless under very dry conditions. Only then could there be uniformity in the soil profile by virtue of negligible hydraulic gradient. Most problems of interest, on the other hand, are concerned with dynamic behaviour of the soil-water-atmospheric environment, subject to changing boundary conditions and with the soil often being heterogeneous. Consequently, methods which

are based entirely on numerical approximation have been developed to overcome the limitations of the quasianalytical methods.

2.1.b. Numerical Methods

The availability of high speed digital computers has, in the last few decades, given new impetus to the solution of complicated mathematical equations. Numerical methods which were once formidable if performed by hand or by means of desk calculators are now easily executed on digital computers and hence are coming into widescale use. Interest in these methods in the field of soil water flow was created because of the need to solve complicated natural hydrologic problems without resorting to simplifications which are mathematically necessary but physically unrealistic.

Numerical methods for the solution of Richards' equation are based on the discretization of the space and time axes. These fall under two main categories, namely, the finite difference (FD) and the finite element (FE) methods, depending on the manner of discretization. To date, most of the attempts have been made using the finite difference method. Some of the important contributions are hereby cited.

One of the earliest works was that of Hanks and Bowers (1962) who applied the finite difference approach to overcome the restriction of uniform initial water content. Equation (2.1) was solved for the case of infiltration from a thin surface film of water ($h(0,t) = 0$) or ponded infiltration into a two-layered soil, each layer having different hydraulic characteristics and different initial water contents. Within each layer, however, the initial water content was uniform.

The problem of infiltration with specified flux was first considered by Rubin and Steinhardt (1963) who solved Eq. (2.2) for a constant rainfall intensity falling on a homogeneous soil of semi-infinite depth at uniform initial (air dry) water content. Only rain intensities less than the saturated conductivity of the soil were considered.

Whisler and Klute (1965) provided FD solution to Eq. (2.1) for infiltration into a soil column initially at equilibrium under gravity with the added refinement that hysteresis was accounted for. Staple (1966) solved Eq. (2.2) for initial infiltration into air dry soil and then used Eq. (2.1) to compute the redistribution of the infiltrated water. Hysteresis was also taken into account for the drying soil.

An even more comprehensive treatment of Eq. (2.1) was that of Freeze (1969). Upper boundary conditions of constant rainfall intensity, ponded water, evaporation and redistribution were considered with a fluctuating

water table at the lower boundary. Watson and Curtis (1975) provided a finite difference analysis of infiltration with airphase effect.

More recently, Haverkamp et al. (1977) concentrated on the numerical aspects by comparing various finite difference schemes for the solution of Eq. (2.1). In comparing the numerical results with experimental results, all the schemes generally performed well for the sandy soil used. The authors, however, indicated that the choice of a particular difference scheme is problem dependent, that is, no one scheme can be best suited for all conditions.

Finite element methods have not enjoyed such widescale use as finite difference methods. The reason is that, even though it is the more powerful method of the two, most soil water flow problems can be satisfactorily represented in one dimension, readily solved by the finite difference method. It is significant to note that conventional solutions of the one-dimensional Richards' equation by the finite element method is yet to be found in the literature. Nevertheless, Cushman and Kirkham (1978) have provided a two-dimensional linearized view of a one-dimensional unsaturated-saturated flow and showed the approach to be more accurate than other analytical or numerical techniques. Another notable contribution has been made by Neuman et al. (1975) for a two-dimensional flow in saturated and partly saturated soils.

## 2.2. THE NUMERICAL APPROACH

For a discussion of the numerical approximation methods and for deriving approximations it is preferable to rewrite Richards' equations in terms of variable u instead of $\theta$ or h. Thus Eq. (2.2), for example, is rewritten as

$$\frac{\partial u}{\partial t}(z,t) = \frac{\partial}{\partial z}\left[D(u)\frac{\partial u}{\partial z} - g\,K(u)\right] \tag{2.8}$$

where g is a constant having a value of +1 for flow in downward direction, 0 for horizontal flow and -1 for flow in upward direction. The initial conditions are

$$u(z,0) = u^{o}(z) \qquad 0 \leq z \leq L \tag{2.9}$$

Two types of boundary conditions can be defined at $z = 0$, namely, one in which u is specified

$$u(0,t) = u_o \tag{2.10a}$$

or, one in which the normal flux is specified (derivative boundary condition) according to

$$\left(D \frac{\partial u}{\partial z} - g K\right)_{z=o} = - q_o \tag{2.10b}$$

Likewise, at z = L, similar conditions may be specified, namely,

$$u(L,t) = u_L \tag{2.11a}$$

or

$$\left(D \frac{\partial u}{\partial z} - g K\right)_{z=L} = - q_L \tag{2.11b}$$

Note that the R.H.S. of Eq. (2.10) and (2.11) may or may not be functions of t. In either case, they are easily handled by the approximation methods.

For convenience in the development of a general algorithm, the discretization of the Richards' equation will be made in two steps beginning with space discretization either by the finite difference or finite element approximation. This reduces the problem to a system of ordinary differential equations. The initial and boundary conditions and the geometry of the problem are treated at the first step. The second step is the discretization of the time axis (Section 2.3). Solving the set of equations resulting from this step yields the approximate solution of the original partial differential equation (Section 2.4).

2.2.a. Finite Difference Method

Finite difference was first introduced as a method to calculate approximately the solution of partial differential equations by Richardson (1910). For a thorough discussion of the finite difference methods for solving partial differential equations one is referred to a number of textbooks (for example, Forsythe and Wasow, 1960 ; Richtmeyer and Morton, 1967). More relevant to the present study is the comprehensive treatment of their applications to soil and groundwater flow, to be found in Remson, Hornberger and Molz (1971).

(i) Theory

The basic idea of these methods is to replace derivatives at a point by ratios of the change in appropriate variables over a small but finite interval, thus giving a pointwise approximation to the governing equations.

Consider a function f(x) sufficiently smooth so that the series de-

veloped below are sensible. Then f may be expanded into a Taylor series about x in the positive direction

$$f(x + \Delta x) = f(x) + \Delta x \frac{df}{dx} + \frac{(\Delta x)^2}{2!} \frac{d^2f}{dx^2} + \frac{(\Delta x)^3}{3!} \frac{d^3f}{dx^3} + \frac{(\Delta x)^4}{4!} \frac{d^4f}{dx^4} + \ldots \tag{2.12}$$

This equation can be solved for (df/dx) to give

$$\frac{df}{dx} = \frac{f(x + \Delta x) - f(x)}{\Delta x} + O(\Delta x)$$

where the term $O(\Delta x)$ represents the remaining terms of the series. A term A is said to be of order $(\Delta x)^n$, written $O((\Delta x)^n)$, if a positive constant C, independent of $\Delta x$, exists such that $|A| < C\,|(\Delta x)^n|$. Thus, as $|(\Delta x)^n| \to 0$, $|A| \to 0$ at least as rapidly.

The *forward difference* approximation to the derivative of f may be obtained by dropping or truncating the $O(\Delta x)$ term and is given by

$$\frac{df}{dx} \approx \frac{f(x + \Delta x) - f(x)}{\Delta x}$$

Expansion of f(x) about x in the negative direction yields

$$f(x + \Delta x) = f(x) - \Delta x \frac{df}{dx} + \frac{(\Delta x)^2}{2!} \frac{d^2f}{dx^2} - \frac{(\Delta x)^3}{3!} \frac{d^3f}{dx^3} + \frac{(\Delta x)^4}{4!} \frac{d^4f}{dx^4} - \ldots \tag{2.13}$$

which is solved to give the *backward difference* approximation to the derivative of f

$$\frac{df}{dx} \approx \frac{f(x) - f(x - \Delta x)}{\Delta x}$$

also with truncation error $O(\Delta x)$.

Further, subtraction of (2.13) from (2.12) results in the *central difference approximation* to the derivative of f

$$\frac{df}{dx} \approx \frac{f(x + \Delta x) - f(x - \Delta x)}{2\Delta x}$$

with a higher order truncation error $O(\Delta x)^2$.

The second derivative follows from the addition of (2.12) and (2.13) to yield

$$\frac{d^2f}{dx^2} = \frac{f(x + \Delta x) - 2f(x) + f(x - \Delta x)}{(\Delta x)^2} + O(\Delta x)^2$$

Finite difference approximation can be easily applied to the partial differential equation (2.8) by making use of a grid superimposed on the z-t plane. Both the space and time discretization can be accomplished concurrently. However, as stated earlier, for the development of a general algorithm and for easy comparison with the finite element method the space and time discretizations will be made separately.

Let the space domain [0,L] be divided into N+1 equidistant points or nodes

$$z_i = i \Delta z \qquad i = 0, 1, \ldots, N$$

$$\Delta z = L/N$$

Then from the earlier derivations, the function u(z,t) and its derivatives with respect to space are approximated at the set of discrete points $z_i$, i = 0, 1, ..., N thus

*Function* : $u(z,t)\Big|_{z_i} \triangleq u(z_i,t) = u_i(t)$

*Derivative* : $\frac{\partial u}{\partial z}(z,t)\Big|_{z_i} \triangleq \frac{1}{\Delta z}\{u_{i+1}(t) - u_i(t)\}$ *Forward difference*

or $\triangleq \frac{1}{\Delta z}\{u_i(t) - u_{i-1}(t)\}$ *Backward difference*

or $\triangleq \frac{1}{2\Delta z}\{u_{i+1}(t) - u_{i-1}(t)\}$ *Central difference*

$$\frac{\partial^2 u}{\partial z^2}(z,t)\Big|_{z_i} \triangleq \frac{1}{(\Delta z)^2}\{u_{i+1}(t) - 2u_i(t) + u_{i-1}(t)\}$$

(ii) Approximation to the θ-Based Equation

*System Equation*

Using the central difference approximation of the space derivative Eq. (2.8) can be written as

$$\frac{\partial u}{\partial t}(z_i,t) = \frac{1}{\Delta z}\{[D(u_{i+1/2})\frac{\partial u_{i+1/2}}{\partial z}(t) - g\,K(u_{i+1/2})] - [D(u_{i-1/2})\frac{\partial u_{i-1/2}}{\partial z}(t) - g\,K(u_{i-1/2})]\} \quad i = 1,2,..N-1$$

which simplifies to

$$\frac{du_i}{dt} = \frac{1}{(\Delta z)^2}\left[D_{i-1/2}\,u_{i-1} - (D_{i-1/2} + D_{i+1/2})u_i + D_{i+1/2}\,u_{i+1}\right]$$

$$- \frac{g}{\Delta z}\left[K_{i-1/2} - K_{i+1/2}\right] \quad i=1,2,\ldots N-1 \qquad (2.14)$$

where $D_{i+1/2} \triangleq D(u_{i+1/2}(t))$ and $K_{i+1/2} \triangleq K(u_{i+1/2}(t))$.

By assuming $D_{i+1/2} = \frac{1}{2}(D_{i+1} + D_i)$ and $K_{i+1/2} = \frac{1}{2}(K_{i+1} + K_i)$

Eq. (2.14) can alternatively be written in terms of nodal values as

$$\frac{du_i}{dt} = \frac{1}{2(\Delta z)^2}\left[(D_{i-1} + D_i)u_{i-1} - (D_{i-1} + 2D_i + D_{i+1})u_i + (D_i + D_{i+1})u_{i+1}\right]$$

$$+ \frac{g}{2\Delta z}(K_{i-1} - K_{i+1}) \qquad i = 1,2,\ldots,N-1 \qquad (2.15)$$

*Boundary Conditions*

The boundary conditions represented by Eq. (2.10a) and (2.11a) lead to the trivial cases

$$\frac{du_o}{dt} = \frac{du_N}{dt} = 0$$

so that Eq. (2.15) represents a system of N-1 ordinary differential equations in N-1 unknowns.

The *derivative boundary conditions* represented by (2.10b) and (2.11b) can be treated in several ways. Remson, Hornberger and Molz (1971) suggest that one considers the flow region in the vicinity of z = 0 to be extended slightly outside the domain. Using an imaginary node $z_{-1}$, condition (2.10b) may be approximated by

$$\frac{u_1(t) - u_{-1}(t)}{2\Delta z} = \frac{gK_o - q_o(t)}{D_o}$$

This procedure, however, increases the total nodal values by 2, one for each end, and this is not very desirable from computational viewpoints particularly in cases of changing boundary conditions, i.e., from one of specified flux to that of specified pressure head and vice versa. Furthermore, as will be shown later, the finite element approximation requires no such use of imaginary nodes. The following more direct approximation is, therefore, used for the derivative boundary condition.

At z = 0, the R.H.S. of Eq. (2.8) is approximated by the forward difference, i.e.

$$\frac{du_o}{dt} = \frac{1}{(\Delta z/2)} \{[D \frac{\partial u}{\partial z} - gK]_{z_{1/2}} - [D \frac{\partial u}{\partial z} - gK]_{z_o} \}$$

Making use of (2.10b) and simplifying, the above equation yields

$$\frac{du_o}{dt} = \frac{1}{(\Delta z)^2} [-(D_o + D_1)u_o + (D_o + D_1)u_1] + \frac{1}{\Delta z} [2q_o - g(K_o + K_1)] \tag{2.16}$$

Similarly, at $z_N$ we obtain, by backward difference,

$$\frac{du_N}{dt} = \frac{1}{(\Delta z)^2} [(D_{N-1} + D_N)u_{N-1} - (D_{N-1} + D_N)u_N] - \frac{1}{\Delta z} [2q_L - g(K_{N-1}+K_N)] \tag{2.17}$$

*Complete Approximation*

Introducing the solution vector

$$u(t) = [u_o(t)\ u_1(t) \ldots u_N(t)]^T \tag{2.18}$$

one can combine (2.15), (2.16) and (2.17) into a vector equation

$$\{\frac{du(t)}{dt}\} = [D(u)]\{u(t)\} + [F]\{K(u)\} + \{Q(t)\} \tag{2.19}$$

where

$$[D] = \frac{1}{2(\Delta z)^2} \begin{bmatrix} b_o & c_o & 0 & \ldots & 0 \\ a_1 & b_1 & c_1 & 0 & \ldots & 0 \\ 0 \ldots 0 & a_i & b_i & c_i & 0 & 0 \\ 0 & \ldots & 0 & a_N & b_N \end{bmatrix} \tag{2.20a}$$

where $b_o = -c_o = -2(D_o+D_1)$ ; $a_N = -b_N = 2(D_{N-1}+D_N)$

$$\left.\begin{aligned} a_i &= (D_{i-1}+D_i) \\ b_i &= -(D_{i-1}+2D_i+D_{i+1}) \\ c_i &= (D_i+D_{i+1}) \end{aligned}\right\} \quad i = 1,2,\ldots,N-1 \tag{2.20b}$$

$$[F] = \frac{g}{2\Delta z}\begin{bmatrix} -2 & -2 & 0 & \cdots & 0 \\ 1 & 0 & -1 & 0 \cdots & 0 \\ & & & & \\ & & & & \\ 0 & \cdots & 0 & 1 & 0 & -1 \\ 0 & \cdots & \cdots & 0 & 2 & 2 \end{bmatrix} \tag{2.20c}$$

$$\{K\} = [K_o \quad K_1 \quad \cdots \quad K_i \quad \cdots \quad K_N]^T \tag{2.20d}$$

$$\{Q\} = [2q_o/\Delta z \quad 0 \quad \cdots \quad 0 \quad -2q_L/\Delta z]^T \tag{2.20e}$$

The system of equations represented by (2.19) with their members defined by (2.18) and (2.20) as it stands constitutes the approximation to the problem with derivative boundary conditions which easily transforms to that of specified pressure head by letting $du_o/dt$ and $du_N/dt$ vanish.

(iii) Approximation to the h-Based Equation

The 1-dimensional pressure-based equation can be written with variable u in place of h as follows

$$C(u)\frac{\partial u}{\partial t} = \frac{\partial}{\partial z}\left[K(u)\frac{\partial u}{\partial z} - gK(u)\right] \tag{2.21}$$

The initial and boundary conditions are as given in Eq. (2.9) through to (2.11) but with conductivity, K replacing the diffusivity term D.

Following the same procedure as in (ii) we obtain for the derivative boundary problem, the vector equation

$$[A(u)]\{\frac{du}{dt}\} = [D(u)]\{u\} + [F]\{K(u)\} + \{Q(t)\} \tag{2.22}$$

where

$$[A(u)] = \begin{bmatrix} C_o & 0 & \cdots & 0 \\ 0 & C_1 & 0 \cdots & 0 \\ . & . & . \; . \; . & . \\ 0 & \cdots & 0 \; C_i \; 0 & 0 \\ 0 & \cdots & 0 & C_N \end{bmatrix} \tag{2.23a}$$

[D(u)] of the same form as in (2.20a) but with its elements defined by

$$b_o = -c_o = -2(K_o+K_1) \; ; \; a_N = -b_N = 2(K_{N-1}+K_N) \; ;$$

$$a_i = K_{i-1}+K_i \; ; \; b_i = -(K_{i-1}+2K_i+K_{i+1}) \; ; \; c_i = K_i+K_{i+1}, \qquad (2.23b)$$

$$i = 1,2,\ldots,N-1$$

and {u}, [F], {K} and {Q} as defined previously in (ii). Transformation to the problem in which $u_o$ is specified is effected in the same manner as in (ii).

(iv) Kirchoff's Transformation

In unsaturated soils suction gradients as well as their rates of change following entry of water or evaporation can be very high especially in heavy-textured soils. Direct application of the pressure-based equation to problems in which initial suctions are high often leads to erroneous results or if an iterative procedure (section 2.4) is employed the solution will often oscillate and fail to converge (Verma and Brutsaert, 1970). This instability is caused by the non-linear coefficient and the high pressure head gradient at the wetting front. Remedies are a decrease in mesh spacing and a severe limitation on the size of the time steps. Alternatively, various authors (Rubin, 1968 ; Raats and Gardner, 1974 ; Haverkamp et al., 1977) overcame the problem by using the Kirchoff integral transformation whereby a new variable, v is defined according to

$$v = v(h) \triangleq \int_{h_{max}}^{h} K(p)dp \qquad (2.24)$$

where $h_{max}$ is the maximum pressure head allowed. Using Leibnitz's rule the above equation becomes

$$\frac{dv}{dh} = K(h)$$

and by making use of the relationships

$$\frac{\partial h}{\partial t} = \frac{\partial v}{\partial t} \cdot \frac{1}{dv/dh} \qquad \text{and} \qquad \frac{\partial h}{\partial z} = \frac{\partial v}{\partial z} \cdot \frac{1}{dv/dh}$$

Eq. (2.1) transforms into

$$F(v)\,\frac{\partial v}{\partial t} = \frac{\partial^2 v}{\partial z^2} - G(v)\,\frac{\partial v}{\partial z} \qquad (2.25)$$

where $F(v) = \frac{C(h)}{K(h)}$ and $G(v) = \frac{g}{K(h)}\,\frac{dK(h)}{dh}$

Equation (2.25) is now solved using the finite difference spatial approximation to give

$$F(v_i)\frac{dv}{dt} = \frac{1}{(\Delta z)^2}[v_{i-1} - 2v_i + v_{i+1}] - \frac{G}{2\Delta z}(v_i)[v_{i+1} - v_{i-1}]$$

By invoking the derivative boundary conditions we obtain in vector form

$$[A(v)]\{\frac{dv}{dt}\} = [D(v)]\{v\} + \{Q(t)\} \tag{2.26}$$

where

$$\{v\} = [v_o \quad v_1 \ldots\ldots v_N]^T \tag{2.27a}$$

$$[A(v)] = \begin{bmatrix} F(v_o) & 0 & \ldots\ldots & 0 \\ 0 & F(v_1) & 0 \ldots & 0 \\ 0 & \ldots\ldots & F(v_i) & 0 \\ 0 & \ldots\ldots & 0 & F(v_N) \end{bmatrix} \tag{2.27b}$$

$$[D(v)] = \frac{1}{(\Delta z)^2}\begin{bmatrix} -2 & 2 & 0 & \ldots\ldots\ldots & 0 \\ 1+\frac{\Delta z G(v_1)}{2} & -2 & 1-\frac{\Delta z G(v_1)}{2} & 0 \ldots\ldots & 0 \\ 0 & 1+\frac{\Delta z G(v_i)}{2} & -2 & 1-\frac{\Delta z G(v_i)}{2} \ldots & 0 \\ \vdots & & & & \vdots \\ 0 & \ldots\ldots\ldots\ldots\ldots & 0 & 2 & -2 \end{bmatrix} \tag{2.27c}$$

$$\{Q(t)\} = \begin{bmatrix} -\{\frac{2}{\Delta z} + G(v_o)\}(gK_o - q_o) \\ \vdots \\ 0 \\ \vdots \\ \{\frac{2}{\Delta z} - G(v_N)\}(gK_N - q_L) \end{bmatrix} \tag{2.27d}$$

2.2.b. Finite Element Method

The finite element method is a quite recent development. However, due to the tremendous interest in the method especially in structural dynamics as well as fluid dynamics many good textbooks are available, among which are Huebner (1975) and Zienkiewicz (1971).

(i) Theory

While the finite difference discretization gives a pointwise approximation to the governing equation the finite element method gives a piecewise approximation to the governing equation. The basic premise of the

finite element method is that a solution region can be approximated by replacing it with an assemblage of discrete elements. The non-steady problem represented by equation (2.8) can be discretized by the method of weighted residuals in conjunction with finite element discretization. In this section the general method of weighted residuals is outlined and one particular technique called the Galerkin's method is used to derive the finite element approximation.

Briefly, the method of weighted residuals involves two basic steps. The first step is to assume the general functional behaviour of the dependent field variable in some way so as to satisfy the given differential equation and boundary conditions. Substitution of this approximation into the original differential equation and boundary conditions then results in some error called a residual. This residual is required to vanish in some average sense over the entire solution domain. The second step is to solve the equation (or equations) resulting from the first step and thereby specialize the general functional form to a particular function, which then becomes the approximate solution sought.

Suppose it is desired to find an approximate functional representation for a field variable u governed by the differential equation

$$L(u) = 0 \tag{2.28}$$

in the domain D with the boundary conditions prescribed on the surface boundary S. The method of weighted residuals is now applied in two steps as follows.

First, the unknown exact solution u is approximated by $u^*$, expressed as

$$u \approx u^* = [\psi]\{u\} = \sum_{i=1}^{n} \psi_i u_i$$

where $[\psi] = [\psi(z_i)]$ are prescribed functions of coordinates (basis functions) and $\{u\} = \{u(t)\}$ are either the unknown parameters or unknown functions of one of the independent variables t. The set of n functions $[\psi]$ are usually chosen to satisfy the global boundary conditions.

Substitution of $u^*$ into (2.28) gives

$$L(u^*) = R \neq 0$$

where R is the residual of the approximation. The method of weighted residuals seeks to determine the unknowns $u_i$ which minimize R in the entire solution domain. This is accomplished by forming a weighted average of the residual which is required to vanish over the solution domain. Thus, by choosing n linearly independent weighting functions, $W_i$ and then insisting that if

$$\int_D [L(u^*)]\ W_i\ dD = \int_D RW_i\ dD = 0 \qquad i = 1,2,\ldots,n \tag{2.29}$$

then $R \approx 0$ in some sense. The next step is to solve (2.29) for the approximate solution sought.

There is a wide choice of weighting functions or criteria that can be used in (2.29), each leading to a particular weighted residual technique. The most common is the Galerkin criterion in which the weighting functions are chosen to be the same as the approximating functions $\psi_i$. Thus, Galerkin criterion can be written as :

$$\int_D R\ \psi_i\ dD = 0 \qquad i = 1,2,\ldots,n \tag{2.30}$$

As Eq. (2.30) holds for any point in the solution domain, it also holds for any collection of points defining an arbitrary subdomain or *element* of the whole domain. A local approximation analogous to (2.30) and valid for one element at a time can, therefore, be written

$$\int_{D^e} [L(u^e)]\ \psi_i^e\ dD^e = 0 \qquad i = 1,2,\ldots,m \tag{2.31}$$

where the superscript e restricts the range to one element and m is the number of unknown parameters assigned to the element and is equal to the number of nodes in the element. The element relations can then be assembled by summing over all elements (total, NE).

$$\sum_{e=1}^{NE} \int_{D^e} [L(u^e)]\ \psi_i^e\ dD^e = 0 \tag{2.32}$$

to yield the global relations for the domain D.

(ii) Approximation to the θ-Based Equation

The 1-dimensional Richards' Eq. (2.8) can be written as

$$L(u) = \frac{\partial u}{\partial t} - \frac{\partial}{\partial z}\ [D\ \frac{\partial u}{\partial z} - gK] = 0 \tag{2.33}$$

As in the case of the finite difference method we apply on [0,L], here considered as consisting of only 1 element, a grid of N+1 points or nodes ; we assume for convenience they are equidistant (but unlike the FD method, this restriction may be lifted without changing much of the following results).

Following the procedure described earlier the exact solution $u(z,t)$ is approximated by $u^*(z,t)$ given by

$$u^*(z,t) = \sum_{i=o}^{N} \psi_i(z) u_i(t)$$

In addition, $D(u)$ and $K(u)$ are approximated by $D^*(z,t)$ and $K^*(z,t)$ respectively, having the same form as $u^*$,

$$D^*(z,t) = \sum_{i=o}^{N} \psi_i(z) D_i(t)$$

and

$$K^*(z,t) = \sum_{i=o}^{N} \psi_i(z) K_i(t)$$

We now define the simplest linear "roof" coordinate function or basis function $\psi_i(z)$ as

$$\psi_i(z) = 1 - \frac{|z-z_i|}{\Delta z} \qquad \text{for } |z-z_i| \leq \Delta z$$

and

$$\psi_i(z) = 0 \qquad \text{for } |z-z_i| > \Delta z$$

The function is illustrated in Fig. 2.1(a)&(b).

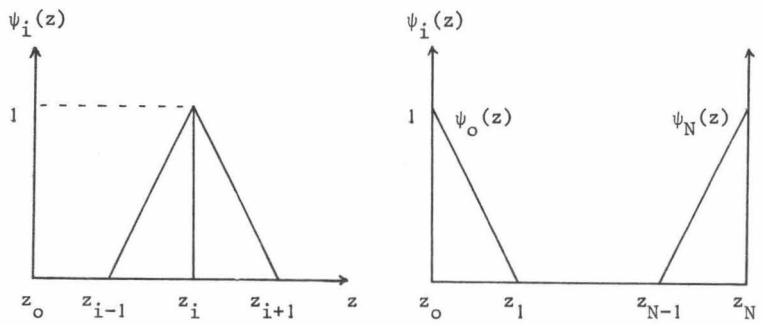


Fig. 2.1(a) Linear basis function in interior region,
(b) Linear basis function at the boundaries.

The Galerkin criterion (2.31) when applied to (2.33) yields

$$\int_{z_o}^{z_N} \psi_m \left[\frac{\partial u}{\partial t} - \frac{\partial}{\partial z}\left(D^*\frac{\partial u^*}{\partial z} - gK^*\right)\right] dz = 0 \qquad m = 0,1,\ldots,N \qquad (2.34)$$

Considering each component separately (evaluation of the component integrals are given in Appendix I ; only the final results are shown here) we obtain

$$\int_{z_o}^{z_N} \psi_m \frac{\partial u^*}{\partial t}\, dz = \begin{cases} \frac{\Delta z}{6}\left[2\frac{du_o}{dt} + \frac{du_1}{dt}\right] & m = 0 \\ \frac{\Delta z}{6}\left[\frac{du_{m-1}}{dt} + 4\frac{du_m}{dt} + \frac{du_{m+1}}{dt}\right] & m = 1,2,\ldots,N-1 \\ \frac{\Delta z}{6}\left[\frac{du_{N-1}}{dt} + 2\frac{du_N}{dt}\right] & m = N \end{cases}$$

The second term in the integral of Eq. (2.34) is first integrated by parts to give

$$\int_{z_o}^{z_N} \psi_m \frac{\partial}{\partial z}\left(D^*\frac{\partial u^*}{\partial z}\right)dz = \psi_m D^*\frac{\partial u^*}{\partial z}\Big|_{z_o}^{z_N} - \int_{z_o}^{z_N} \frac{d\psi_m}{dz} D^*\frac{\partial u^*}{\partial z}\, dz \qquad (2.34a)$$

the components in turn evaluated separately to yield

$$\psi_m D^*\frac{\partial u^*}{\partial z}\Big|_{z_o}^{z_N} = \begin{cases} q_o - gK_o & m = 0 \\ 0 & m = 1,2,\ldots,N-1 \\ gK_N - q_L & m = N \end{cases}$$

and

$$\int_{z_o}^{z_N} \frac{d\psi_m}{dz} D^*\frac{\partial u^*}{\partial z}\, dz = \begin{cases} \frac{1}{2\Delta z}\left[(D_o + D_1)u_o - (D_o + D_1)u_1\right] & m = 0 \\ \frac{-1}{2\Delta z}\left[(D_{m-1}+D_m)u_{m-1} - (D_{m-1}+2D_m+D_{m+1})u_m + (D_m+D_{m+1})u_{m+1}\right] & m = 1,2,\ldots,N-1 \\ \frac{-1}{2\Delta z}\left[(D_{N-1}+D_N)u_{N-1} - (D_{N-1}+D_N)u_N\right] & m = N \end{cases}$$

The last term in the integral of Eq. (2.34) results in

$$\int_{z_o}^{z_N} g\psi \frac{\partial K^*}{\partial z}\, dz = \begin{cases} -\frac{g}{2}[K_o - K_1] & m = 0 \\ -\frac{g}{2}[K_{m-1} - K_{m+1}] & m = 1,2,\ldots,N-1 \\ -\frac{g}{2}[K_{N-1} - K_N] & m = N \end{cases}$$

Substituting these results back into (2.34) and rearranging we obtain the vector equation of the form (2.22), where

$$[A] = \frac{1}{6}\begin{bmatrix} 2 & 1 & 0 & \cdots & 0 \\ 1 & 4 & 1 & 0 \cdots & 0 \\ 0 & \cdot & \cdot & \cdot & \\ & & \cdot & \cdot & \cdot \quad 0 \\ 0 \cdots & 0 & 1 & 4 & 1 \\ 0 & \cdots & 0 & 1 & 2 \end{bmatrix} \qquad (2.35a)$$

$[D(u)]$ is of the same form as in (2.20a) with its elements defined by

$$b_o = -c_o = -(D_o+D_1)\ ;\ a_N = -b_N = D_{N-1}+D_N$$

$$\text{and}\quad a_i = D_{i-1}+D_i\ ;\ b_i = -(D_{i-1}+2D_i+D_{i+1})\ ;\ c_i = D_i+D_{i+1}, \qquad (2.35b)$$

$$i = 1,2,\ldots,N-1$$

$$[F] = \frac{g}{2\Delta z}\begin{bmatrix} 0 & -1 & 0 & \cdots & 0 \\ 1 & 0 & -1 & 0 \cdots & 0 \\ 0 & \cdot & \cdot & \cdot & \\ & & \cdot & \cdot & \cdot \quad 0 \\ 0 \cdots & 0 & 1 & 0 & -1 \\ 0 & \cdots & 0 & 1 & 0 \end{bmatrix} \qquad (2.35c)$$

$$\{Q\} = [\, q_o/2\Delta z \quad 0 \cdots 0 \quad -q_L/2\Delta z \,]^T \qquad (2.35d)$$

and $\{u\}$ and $\{K\}$ as previously defined by (2.18) and (2.20d) respectively.

Equation (2.22) so defined represents the derivative boundary problem. The approximation for the problem in which $u_o$ is specified, is obtained by setting $du_o/dt$ and $du_N/dt$ equal to zero, that is, by reducing all the elements in the $1^{st}$ and $(N+1)$th rows of $[D]$, $[F]$ and $\{Q\}$ to zeros, followed by appropriate adjustments of the corresponding rows of the $[A]$ matrix.

(iii) Approximation to the h-Based Equation

The derivation for the case of the pressure-based equation, rewritten as

$$L(u) = C \frac{\partial u}{\partial t} - \frac{\partial}{\partial z}\left[K \frac{\partial u}{\partial z} - gK\right] = 0$$

proceeds in the same manner as for the θ-based equation. An additional assumption is

$$C \approx C^*(z,t) = \sum_{i=o}^{N} \psi_i(z) C_i(t)$$

requiring the evaluation of the integral

$$I = \int_{z_o}^{z_N} \psi_m \, C^* \frac{\partial u}{\partial t} \, dz \, , \qquad m = 0,1,\ldots,N$$

which yields

$$I = \begin{cases} \frac{\Delta z}{12}\left[(3C_o + C_1)\frac{du_o}{dt} + (C_o + C_1)\frac{du_1}{dt}\right] & m = 0 \\ \frac{\Delta z}{12}\left[(C_{m-1}+C_m)\frac{du_{m-1}}{dt} + (C_{m-1}+6C_m+C_{m+1})\frac{du_m}{dt} + (C_m+C_{m+1})\frac{du_{m+1}}{dt}\right] & m = 1,2,\ldots,N-1 \\ \frac{\Delta z}{12}\left[(C_{N-1}+C_N)\frac{du_{N-1}}{dt} + (C_{N-1}+3C_N)\frac{du_N}{dt}\right] & m = N \end{cases}$$

Evaluation of the other integrals is identical to that in (ii) with K replacing D. The final approximation can again be put into the form (2.22) with {u}, [F], {K} and {Q} for the derivative boundary problem defined by (2.18), (2.35c), (2.20d) and (2.35d) respectively. The [A] matrix, in this case, sometimes referred to as the capacity matrix is given by

$$[A(u)] = \frac{1}{12}\begin{bmatrix} bb_o & cc_o & 0 & \cdots & 0 \\ aa_1 & bb_1 & cc_1 & 0 & 0 \\ 0 & aa_i & bb_i & cc_i & 0 \\ \cdot & \cdots & \cdot & \cdot & \cdot \\ 0 & \cdots & 0 & aa_N & bb_N \end{bmatrix} \qquad (2.36)$$

where $bb_o = 3C_o + C_1$ ; $cc_o = C_o + C_1$ ;

$$aa_i = C_{i-1} + C_i \; ; \; bb_i = C_{i-1} + 6C_i + C_{i+1} \; ; \; cc_i = C_i + C_{i+1} \; , \quad i = 1,2,\ldots,N-1$$

$$aa_N = C_{N-1} + C_N \; ; \; bb_N = C_{N-1} + 3C_N$$

The matrix [D], also known as the conductance (or stiffness) matrix is analogous to that of the θ-based equation but with the elements expressed in terms of K instead of D thus

$$b_o = -c_o = -(K_o + K_1) \; ; \; a_N = -b_N = K_{N-1} + K_N \; ;$$

$$a_i = K_{i-1} + K_i \; ; \; b_i = -(K_{i-1} + 2K_i + K_{i+1}) \; ; \; c_i = K_i + K_{i+1}, \quad i = 1,2,\ldots,N-1 \qquad (2.37)$$

2.2.c. Discussion

From the preceding derivations it is seen that the treatment of boundary conditions in the finite element method is more exact than in the finite difference. The integration by parts (Eq. 2.34a) enables the incorporation of the natural boundary conditions, namely, those of specified flux, whereas in the finite difference case such boundary conditions have to be approximated by the forward or backward difference scheme or by the addition of imaginary nodes.

The coefficient matrices of the vector {u(t)} for a given equation (the θ-based or the h-based) are identical in both approximation methods except for the boundary nodes. However, the coefficient matrices of the time derivative of {u(t)} are quite different. Whilst that obtained by finite difference is the identity matrix (for the θ-based equation) or a diagonal matrix (for the h-based equation), the ones derived using the finite element method are tridiagonal. The latter can be considered as some kind of averaging operator which can prove useful in defining sharp wetting fronts such as observed during flows in fine-textured soils, on the one hand, or be a source of numerical problems on the other (Neuman and Narasimhan, 1977).

The significance of these differences will be appreciated in Chapter 5 when numerical results are presented.

## 2.3. TIME DISCRETIZATION

There is a variety of classical finite difference methods for the approximation of a system of ordinary differential equations of the initial value kind. In principle, all of these are applicable to the integration in time or time marching of the partial differential equation

$$\frac{\partial u}{\partial t} = X(u) \quad ; \quad u = u(x,t)$$

where X is a differential operator, once it has been reduced to a system of ODE's of the form

$$[A] \{\frac{du}{dt}\} = \tilde{X}\{u\}$$

where $\tilde{X}(.)$ is an approximation of X(.) obtained by finite difference or finite element methods.

By discretizing the time domain into a sequence of finite intervals, and replacing the time derivative of u by finite difference, the general integration method can be expressed as

$$[A] \frac{\{u\}^{j+1} - \{u\}^j}{\Delta t^j} = \nu \tilde{X}\{u\}^{j+1} + (1-\nu)\tilde{X}\{u\}^j$$

or

$$[[A] - \Delta t^j \nu \tilde{X}]\{u\}^{j+1} = [[A] + \Delta t^j (1-\nu)\tilde{X}]\{u\}^j \qquad (2.38)$$

where $\Delta t^j = t^{j+1} - t^j$ is the j-th time step and $\nu$ is a factor such that $0 \leqslant \nu \leqslant 1$. A value of $\nu = 0$ corresponds to the Euler explicit method with truncation error $O(\Delta t) + O(\Delta x)^2$ while $\nu = 1$ corresponds to the Euler implicit method, also with truncation error of the same order. The Crank-Nicolson central time difference scheme is obtained by setting $\nu = 0.5$ when the truncation error is reduced to $O(\Delta t)^2 + O(\Delta x)^4$.

Explicit methods of time marching of which Euler's explicit method is a paradigm are easily applied to the system of ODE which are obtained in the case of spatial approximation by finite difference where [A] is the identity matrix so that

$$\{u\}^{j+1} = \{u\}^j + \Delta t^j \tilde{X}\{u\}^j$$

But they require the solution of systems of linear algebraic equations in the case of finite elements because the equations become

$$\{u\}^{j+1} = \{u\}^{j} + \Delta t^{j} \tilde{X} [A]^{-1} \{u\}^{j}$$

Explicit methods which have the advantage of simplicity with spatial finite difference, therefore, lose some of their advantage with finite element approximation. Implicit methods, on the other hand, always involve solution of systems of linear algebraic equations, and their improved numerical stability justify their use with finite element method more so than in the case of finite difference method of spatial approximation. Hence, implicit methods will be used in this study, and in particular, the Crank-Nicolson scheme. An added advantage of the latter scheme is that with the smaller truncation error, the faster will be the rate of convergence of the difference equations to the partial differential equation.

*Note* : *Convergence* refers to the condition of the difference between the approximate solution and the true one, at a given point and time instant as the mesh becomes finer and finer. A difference scheme is said to be convergent if this difference approaches zero as $\Delta z$, $\Delta t \to 0$. A difference scheme is also said to be *stable* if the errors are not amplified, i.e., are bound in some sense, for a given combination of $\Delta t$ and $\Delta z$, as computation marches forward and $t \to \infty$.

## 2.4. QUASILINEARIZATION AND SOLUTION OF DIFFERENCE EQUATION

The difference equations (2.38) are nonlinear since either the coefficient matrix on the L.H.S. or the R.H.S. vector or both depend upon the solution $\{u\}^{j+1}$. Linearization may be accomplished by one of several methods among which are

- iteration
- predictor-corrector sequence
- explicit evaluation (extrapolation)

As the emphasis in this thesis is directed towards differences in space discretization, only one linearization method will be used and that is by iteration, which is rather flexible and easy to apply.

In Eq. (2.38) the coefficients are evaluated at the j-th and (j+1)-th time levels. For highly nonlinear problems such as Richards' equation for unsaturated flow, it is preferable to evaluate the coefficients at the time $t^{j+1/2} = t^{j} + \Delta t^{j/2}$, a form of under-relaxation which helps to improve the rate of convergence (Neuman et al., 1975). Taking this into consideration, the final difference equation for the solution of the

system of equations (2.22) emerging after the appropriate substitution for $\tilde{X}$ in (2.38) is

$$[T]\{u\}^{j+1} = \{R\} \tag{2.39}$$

where [T] is a tridiagonal matrix given by

$$[T] = [A]^{j+1/2} - \Delta t^{j}\nu\,[D(u)]^{j+1/2}$$

and $$\{R\} = [[A]^{j+1/2} + \Delta t^{j}(1-\nu)[D(u)]^{j+1/2}]\{u\}^{j}$$

$$+ \Delta t^{j}\{[F]\{K(u)\}^{j+1/2} + \{Q(t)\}^{j+1/2}\}$$

The system of equations (2.39) can be solved by a highly efficient algorithm based on the decomposition of the tridiagonal matrix [T] into a lower [L] and an upper [U] matrix (refer to Appendix II).

The iterative process may be started with an initial guess

$$\{u\}^{j+1} = \{u\}^{j} + c(\{u\}^{j} - \{u\}^{j-1}) \tag{2.40}$$

where c is a constant having a value $0 < c \leqslant 1$. The values of $\{u\}^{j+1/2}$ needed in order to evaluate the coefficients are then obtained from the relationship

$$\{u\}^{j+1/2} = \frac{\{u\}^{j+1} + \{u\}^{j}}{2}$$

After each iteration the most recent value of $\{u\}^{j+1}$ are substituted into the above equation to obtain improved estimates of $\{u\}^{j+1/2}$. The coefficients are reevaluated and the system of equations are again solved for improved values of $\{u\}^{j+1}$. The iterative process continues until a satisfactory degree of convergence is achieved as defined by

$$\max_{i} \left| \frac{u_i^{j+1,k+1} - u_i^{j+1,k}}{u_i^{j+1,k}} \right| \leqslant \varepsilon \tag{2.41}$$

where the superscript k refers to the iteration index and $\varepsilon$, a criterium parameter.

CHAPTER 3

# PHYSICAL CHARACTERIZATION OF THE SOIL

## 3.1. INTRODUCTION

The concepts of hydraulic conductivity, soil water diffusivity and moisture characteristic are inherent to flow problems in the laboratory and in the field. These moisture dependent or pressure head dependent properties appear explicitly in Richards' Eq.(2.1) and (2.2) and are, therefore, parameters which must be identified in our flow model.

In the context of system modeling the measurements that must be made in the identification process must come from the same system that the model is intended to represent, that is, given $y = f(x,p)$, then $p = g(y,x)$. The ideal situation as demanded by this condition would be to have a vertical flow system whereby the state variables, namely, water content and pressure head and other quantities of interest such as flux and wetting depth can be measured directly and subsequently used to evaluate $D(\theta)$, $C(\theta)$ and/or $K(\theta)$. This approach has been adopted by Watson (1966), Vachaud and Thony (1971) and Rogers and Klute (1971) for drainage, infiltration and/or redistribution in sand columns. In the case of infiltration into air dry soil, however, direct measurement of pressure head is not possible. From theoretical as well as technical considerations one simply does not install tensiometers into soils having suction heads greater than 800 cm water. This constraint leads to indirect methods of determining D, C and or K.

From the relationship expressed by Eq.(1.12) it is clear that only two of the above-named properties have to be identified directly while the third can be deduced from the knowledge of these two. The moisture characteristic $\theta(h)$ is perhaps the easiest to determine experimentally thus leaving a choice between the measurement of either K or D.

There are a number of methods available for determination of $K(\theta)$ and $D(\theta)$. A comprehensive review is given by Klute (1972). Since the soil being studied is clay, direct measurement of $K(\theta)$ over the whole range of $\theta$ from

air dry to saturation would be difficult and prone to large error. Therefore, measurement of $D(\theta)$ is preferred. As the study is primarily concerned with infiltration process rather than drainage, hysteresis is avoided and the properties are determined for the wetting process only.

## 3.2. MATERIALS (The Soil)

The soils used in the study were from the Bungor Series (Typic Paleudult) of clay texture, taken from two sites on the same slope in the campus of the University of Malaysia at Serdang. The first profile, hence called Profile 1 was taken from the bottom of the slope while the second (Profile 2) was taken from a higher elevation. Only the top four horizons of each profile were considered in the study. The profile descriptions are given in Appendix III . Particle size distribution and some of the chemical properties are given in Table 3.1. The fraction used for the study was < 0,5 mm. The bulk densities used throughout the experiments were 1.03 $g.cm^{-3}$ for all horizons of Profile 1 and 0.935 $g.cm^{-3}$ for all horizons of Profile 2.

## 3.3. MOISTURE CHARACTERISTIC (ABSORPTION CURVE)

### 3.3.a. Theory

There is no single method available which can provide us with the $\theta$-h relationship for the complete moisture range from air dry to saturation either for the wetting (absorption) or for the drying (desorption) process. A combination of different methods have to be used, each yielding $\theta$-h relationship within a limited pressure head range. For suction heads (negative of pressure heads) ranging from 1 to 240 cm water (pF 0-2.31) the hanging water column method was used, that is, by allowing air-dry samples to wet at a given suction until equilibrium is reached. For pF > 4.2 the relative humidity method was used whereby the soil was allowed to equilibrate in a closed atmosphere of saturated salt solutions.

The wet portion of the absorption curve between 1 and approximately 15 cm $H_2O$ may have some limitations due to instability in this region resulting from possible air entrapment and slight swelling. A capillary rise method which resembles the system for horizontal and vertical infiltration was therefore used for $\theta$-h relationship in this wet range. The underlying principle is simply that when water is allowed to rise in a vertical soil column an approximately steady state is reached whereby the hydraulic gradient is zero everywhere in the capillary fringe region.

Table 3.1. Characteristics of different horizons of the two profiles of Bungor Series.

| Horizon designation - Code | Depth cm | Mechanical Analysis (%) | | | | Air dry moisture content by weight (%) | Physico-chemical Analysis | | | |
|---|---|---|---|---|---|---|---|---|---|---|
| | | Coarse sand > 200μ | Fine sand 20-200μ | Silt 2-20μ | Clay 0-2μ | | Humus % | $CaCO_3$ % | pH $H_2O$ | pH KCl |
| PROFILE SE 1/1 | | | | | | | | | | |
| $A_p$ - $P_1H_1$ | 0- 12 | 24.6 | 18.8 | 4.2 | 52.4 | 0.010 | 1.86 | 0.0 | 4.5 | 4.0 |
| $B_1$ - $P_1H_2$ | 12- 30 | 24.8 | 17.5 | 3.8 | 53.9 | 0.010 | 1.07 | 0.0 | 4.7 | 4.1 |
| $B_{2t}$ - $P_1H_3$ | 30- 86 | 21.8 | 15.5 | 3.8 | 58.9 | 0.012 | 0.63 | 0.0 | 4.8 | 4.2 |
| $IIC_1$ - $P_1H_4$ | 86-140 | 38.7 | 10.8 | 5.0 | 45.5 | 0.018 | 0.0 | 0.0 | 5.0 | 4.3 |
| PROFILE SE 1/2 | | | | | | | | | | |
| $A_p$ - $P_2H_1$ | 0- 15 | 15.7 | 15.0 | 9.2 | 60.1 | 0.025 | 6.02 | 0.0 | 4.6 | 3.8 |
| $B_1$ - $P_2H_2$ | 15- 31 | 13.7 | 11.1 | 8.9 | 66.1 | 0.029 | 2.65 | 0.0 | 4.0 | 3.9 |
| $B_{2t}$ - $P_2H_3$ | 31- 62 | 14.5 | 10.9 | 9.5 | 65.1 | 0.035 | 1.66 | 0.0 | 4.9 | 4.0 |
| $IIB_{31cn}$ - $P_2H_4$ | 62-120 | 16.3 | 11.0 | 12.8 | 59.9 | 0.035 | 1.03 | 0.0 | 4.9 | 4.0 |

This means that the suction head is numerically equal to the gravitational potential, the latter simply being the height from the free water source.

3.3.b. Method

(i) Hanging Water Column Method

The experimental set-up consisted of several units of the apparatus shown in Fig. 3.1.

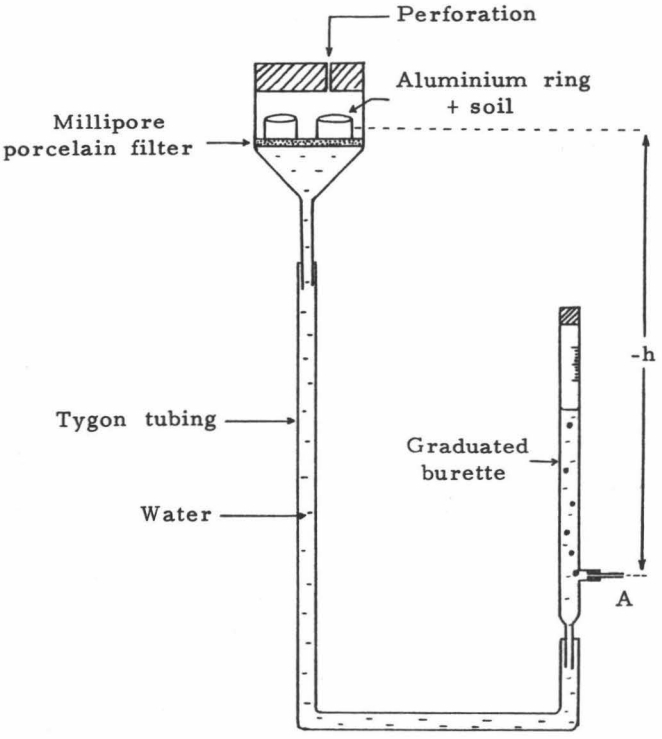


Fig. 3.1 Schematic diagram of apparatus for pF-absorption determination by the "Hanging water column method".

Four aluminium rings were placed on the glass-fritted plate and the desired suction head (-h) was applied before placing the soil samples. This was accomplished by lowering the outlet tube A, a distance -h from the centre of the aluminium rings. Known amounts of air dry samples were packed into the rings to the desired bulk density, namely, 1.03 for samples of Profile 1 and 0.935 for samples of Profile 2. The soil then absorbed water until equilibrium was reached as indicated by unchanging meniscus level in the graduated burette. This situation was attained after approximately 48 hours

for the higher suctions of 150-240 cm and up to 1 week for the lowest suction of 3 cm. The water content of the wet samples were then determined gravimetrically, i.e., by weighing the wet samples, oven drying at 105°C for 20 hours and finally reweighing the oven dry samples. The loss in weight divided by the oven dry weight gave the gravimetric water content which was then converted to the volumetric water content by multiplying with the corresponding bulk density.

(ii) Relative Humidity Method

The saturated solutions used to control the relative humidity are given in Table 3.2. The pF value was obtained from the relationship

$$pF = \log \left[ - \frac{RT}{Mg} \ln r \right] = \log \left[ -10\ 833\ T \log r \right]$$

where R is the universal gas constant, T the absolute temperature in degrees Kelvin, M the molecular weight of water, g the acceleration due to gravity and r the relative humidity.

Table 3.2. Saturated salt solutions and their relative humidity (after O'Brien, 1948).

| Saturated salt solution | Relative Humidity at 20°C | pF |
|---|---|---|
| Ammonium oxalate $(NH_4)_2C_2O_4$ | 0.988 | 4.22 |
| Potassium sulphate $K_2SO_4$ | 0.971 | 4.61 |
| Sodium sulphate $Na_2SO_4$ | 0.930 | 5.00 |
| Potassium chromate $K_2CrO_4$ | 0.880 | 5.25 |
| Sodium chloride NaCl | 0.750 | 5.58 |

As the bulk density has negligible influence on $\theta$ - h relationship at low water content, unconfined samples were used. The soil samples were placed in glass vials and suspended in closed Erlenmeyer flasks each containing one of the saturated salt solutions mentioned above. The flasks were kept in a water bath maintained at 20 $\pm$ 1°C. The vials were weighed on alternate days until constant weight after which the gravimetric water content was determined. In order to ensure that the flasks were at the required humidity, the air in the flasks were evacuated after each weighing of the vials.

(iii) Capillary Rise Method

The capillary rise column (infiltration column) was constructed from

perspex rings with an internal diameter of 3.2 cm and length 1 cm. The rings were fitted tightly together using a transparent adhesive tape. One end of the column was connected to a small chamber C having a water inlet and an outlet. The latter was for air evacuation at the start of the experiment. A sintered glass disc 3 mm thick and of negligible impedance at one end of the chamber served as a mechanical screen for preventing any disturbance of the soil surface at the water source.

Known amounts of air dry soil (< 0.5 mm fraction) were filled into the perspex column by gentle tapping. The mean bulk density could then be calculated from the known soil mass and dimensions of the soil column. In all cases the length of the soil column used was 15 cm. A cotton wool plug was also placed at the free end of the column. The apparatus was then assembled as shown in Fig. 3.2 by connecting the chamber C to a "Mariotte burette" which supplied water at constant zero pressure head. All pinchclips $S_1$, $S_2$, $S_3$ and $S_4$ were initially closed.

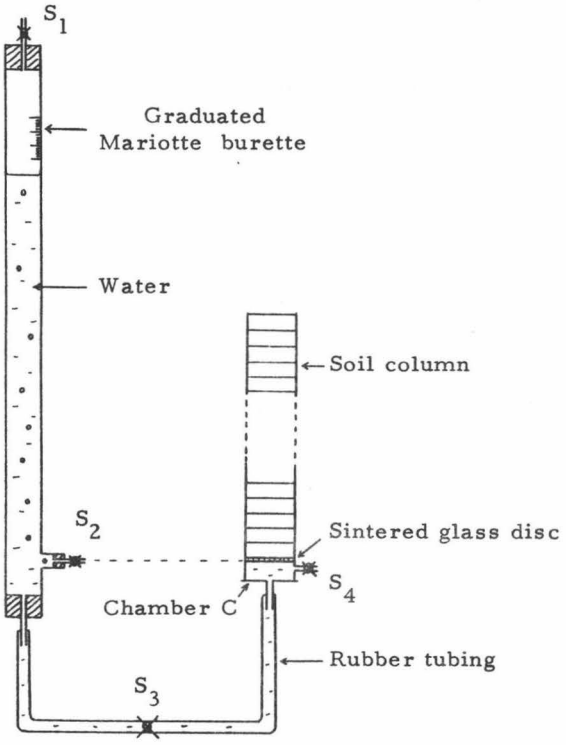


Fig. 3.2 Schematic diagram of apparatus for pF-absorption determination by the "Capillary rise" method.

Flow was initiated as follows. Pinchclip $S_3$ was first opened and water was allowed to enter the soil column by opening pinchclips $S_1$ and $S_4$ simultaneously. As soon as C was full and water started flowing out via $S_4$ both $S_1$ and $S_4$ were closed simultaneously. Pinchclip $S_2$ was then opened carefully so that air at the top of the Mariotte burette attained atmospheric pressure. The capillary rise was timed from the moment C was completely full. The burette reading and position of the wetting front were recorded at frequent intervals.

When the water front was within 1 or 2 mm from the top of the soil column the cotton wool plug was removed and replaced by a sheet of parafilm to prevent evaporation and to allow steady state to be reached sooner. Steady state here refers to the condition whereby fluxes at both ends of the soil are zero or negligible. (Note that if evaporation were allowed the system would assume a steady state that is governed by the atmospheric condition ; fluxes at the top and bottom would be non-zero meaning that the hydraulic gradient is finite and hence our analysis fails). When the rate of absorption became negligible, in this case, less than 0.01 times the saturated conductivity, the experiment was stopped by closing $S_3$. The tube was disconnected and the soil column divided into 1 cm sections by cutting through the joints with a razor blade. The gravimetric water content was determined by oven drying and converted to volumetric water content. The latter corresponds to a suction head equal to the height of the section from the water source.

The criterion used for the attainment of zero hydraulic gradient was as follows. Allowing for a tolerance of 1% (i.e. a 0.01 cm per cm error in suction head value) the maximum flux allowed is, from Darcy's Law, 1% of the saturated conductivity. For $P_1H_1$ for instance, with $K_s \approx 0.077$ cm/min. (from section 3.6) the criterion is approximately 0.023 cm per 30 minutes.

### 3.3.c. Results and Discussion

A comparison among the maximum volumetric water contents or the saturation values $\theta_s$, obtained by absorption from the hanging water column, the capillary rise method and by the horizontal infiltration (from section 3.4) is shown in Table 3.3.

The saturation values obtained by absorption from the hanging water column are clearly higher than the corresponding values from capillary rise and horizontal infiltration with the difference between the two latter methods being negligible. However, the difference between the $\theta$ values from the hanging water column method (unpublished results) and from the capillary

rise method decreases as the suction increases from zero, so that, at approximately 12 to 15 cm suction the corresponding values virtually coincide with each other.

Table 3.3. Saturation values obtained from absorption from the hanging water column, the capillary rise method and the horizontal infiltration.

| Soil | $\theta_s$ $cm^3$ $cm^{-3}$ | | |
|---|---|---|---|
| | Hanging Water Column | Capillary Rise | Horiz. Infiltration |
| $P_1H_1$ | 0.57 | 0.54 | 0.54 |
| $P_1H_2$ | 0.58 | 0.55 | 0.55 |
| $P_1H_3$ | 0.62 | 0.56 | 0.56 |
| $P_1H_4$ | 0.61 | 0.57 | 0.57 |
| $P_2H_1$ | 0.63 | 0.59 | 0.59 |
| $P_2H_2$ | 0.64 | 0.57 | 0.565 |
| $P_2H_3$ | 0.65 | 0.57 | 0.57 |
| $P_2H_4$ | 0.64 | 0.57 | 0.565 |

The above findings can be attributed to the initial mode of water entry, the subsequent absorption process and the instability of the soil matrix at high water contents. Absorption from the hanging water column was initiated slowly because of the high impedance of the millipore filter as well as the fact that the filter was initially under suction. For the capillary rise and horizontal infiltration methods, however, initial water entry was rapid by virtue of the experimental set-up and the negligible impedance of the sintered glass. The latter resulted in greater air entrapment and hence lower $\theta$ values at comparable suctions. Furthermore, because of the slow absorption process and negligible overburden pressure in the former method, a slight degree of swelling is inevitable especially since the clay soils also contain organic matter. Consequently, the true bulk density decreased accompanied by an increase in water content.

Since the purpose of determining the moisture characteristic is for utilisation in Richards' equation for ponded and rain infiltration, both processes involving free and rapid water entry, it is, therefore, decided to use results obtained from the capillary rise method for the $\theta$-h relation-

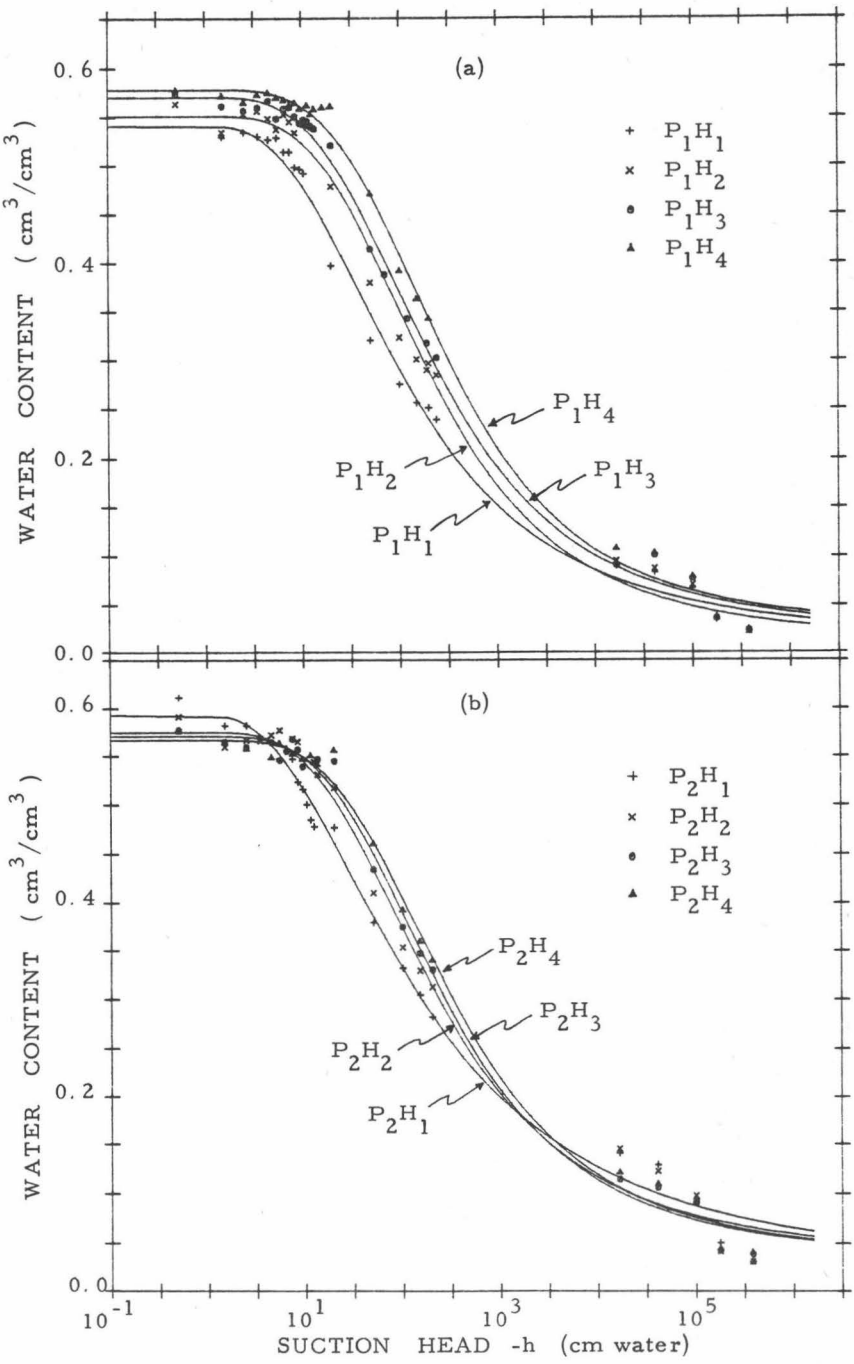


Fig. 3.3 Relationships between water content and suction head for the different horizons of (a) Profile 1 (b) Profile 2.

ship in the suction range of 0 to 15 cm water. These results are combined with those from the hanging water column for suctions between 15 and 240 cm water, and those from the relative humidity method, to yield the water content-suction relationships or pF-curves for the various soil horizons (Fig. 3.3(a) & (b)). The solid curves drawn through the experimental points are all of the form

$$\theta = \frac{\alpha(\theta_s - \theta_r)}{\alpha + (\ln|h|)^{\beta}} + \theta_r$$

where $\theta_s$ and $\theta_r$ are the saturation and residual or air dry water contents and $\alpha$ and $\beta$ are parameters determined by non-linear least square fitting.

## 3.4. SOIL WATER DIFFUSIVITY

### 3.4.a. Theory

Soil water diffusivity, $D(\theta)$, was measured according to the method of Bruce and Klute (1956) with slight modifications in the method of analysis. The method is based on the "constant head" absorption by a horizontal semi-infinite medium with a uniform density and constant initial water content. Mathematically the system can be expressed as

$$\frac{\partial\theta}{\partial t} = \frac{\partial}{\partial x}\left[(D(\theta)\ \frac{\partial\theta}{\partial x}\right] \qquad (3.1)$$

i.e., Richards' equation, with the gravity component omitted, subject to conditions

$$\theta(x,o) = \theta_i \qquad (3.2a)$$

$$\theta(\infty,t) = \theta_i \qquad (3.2b)$$

$$\theta(o,t) = \theta_c \qquad (3.2c)$$

The water content $\theta_c$ is that of the front end of the absorbing soil column and is slightly less than the saturation value.

The non-linear partial differential equation (3.1) can be linearized by applying the Boltzmann transformation

$$\phi(\theta) = xt^{-1/2} \qquad (3.3)$$

This leads to

$$-\frac{\phi}{2}\frac{d\theta}{d\phi} = \frac{d}{d\phi}\left[D(\theta)\ \frac{d\theta}{d\phi}\right] \qquad (3.4)$$

with boundary conditions

$$\theta(\phi = \infty) = \theta_i \tag{3.5a}$$

$$\theta(\phi = 0) = \theta_c \tag{3.5b}$$

Upon integration between limits $\theta_i$ and $\theta$, Eq. (3.4) yields

$$\int_{\theta_i}^{\theta} \phi \, d\theta = -2D(\theta)\frac{d\theta}{d\phi} \tag{3.6}$$

Note that the integration yields the term $D(\theta_i)\,[\,d\theta/d\phi\,]_{\theta=\theta_i}$ to be added on to the right side of Eq.(3.6) but this term vanishes because condition (3.5a) implies $d\theta/d\phi = 0$ at $\theta = \theta_i$. Rearranging (3.6) yields the diffusivity

$$D(\theta) = -\frac{1}{2}\frac{d\phi}{d\theta}\int_{\theta_i}^{\theta} \phi \, d\theta \tag{3.7}$$

Bruce and Klute (1956) applied Eq.(3.6) to measurements of $\theta(x)$ at a fixed time t which may be written as

$$D(\theta_x) = -\frac{1}{2t}\left(\frac{dx}{d\theta}\right)_{\theta_x}\int_{\theta_i}^{\theta_x} x \, d\theta \tag{3.8}$$

However, taking into account certain experimental difficulties Eq. (3.7) appears to be more appropriate. The reasons are, firstly, if measurement of water content is by the $\gamma$-ray attenuation technique (Verplancke, 1973) the resulting $\theta(x)$ or water content profile is not for a single time instant. This is because a finite time elapses from the start of the measurement at a position just a head of the water source, until the wetting front is reached (the time interval between successive $\gamma$-ray readings is approximately 20 seconds). The above time lapse can easily be accounted for by direct use of Eq. (3.7) where the x-values are transformed to $\phi$ using Eq. (3.3) with t being the actual time of measurement at the given position. The second reason follows from the fact that it is quite impossible to obtain a perfectly homogeneous packing, i.e., a constant bulk density throughout the semi-infinite medium. Analysis based on a single moisture profile is thus inadequate. By employing several measured moisture profiles use of Eq. (3.8), however leads to an equivalent number of diffusivity functions which is undesirable. Equation (3.7), on the other hand, enables us to obtain a so-called "mean" diffusivity function from several moisture profiles since the Boltzmann transformation implies that all $\phi(\theta)$ curves determined from $\theta(x)$ profiles at different times should coalesce into a single curve identifiable as the unique $\phi(\theta)$.

From the preceding discussion the following method of analysis is suggested.

(i) Several moisture profiles (at least 3) during horizontal infiltration are obtained, preferably at short, intermediate and large times.

(ii) The x-values for each $\theta$ versus x profile are transformed into $\phi$ values using actual t values, that is to say, by adding 20 seconds to the starting measurement time for every cm increment in x if the measurement is made using $\gamma$-ray attenuation method, or the time at which infiltration is stopped in the case of direct gravimetric determination.

(iii) A single plot of $\phi$ against $\theta$ is prepared and a smooth monotonically decreasing curve is drawn through the points.

(iv) $D(\theta)$ is then computed by the discretization of Eq. (3.7)

$$D(\theta_m) = -\frac{1}{2}\frac{\phi_{m+1} - \phi_{m-1}}{\theta_{m+1} - \theta_{m-1}} \sum_{j=1}^{m} \frac{1}{2}(\phi_j + \phi_{j-1})\,\Delta\theta_j \qquad (3.9)$$

where

$$\Delta\theta_j = \theta_j - \theta_{j-1}$$

3.4.b. Method

Infiltration columns were prepared in the same manner as for the capillary rise experiment, however, this time, with longer soil columns. The apparatus was set up as shown in Fig. 3.4 and water was allowed to enter the horizontal soil column at a constant zero pressure head (preliminary trials using two samples, $P_1H_1$ and $P_2H_1$, with water supplied at pressure heads of +2, 0, -2, -7 and -12 cm favoured the use of 0 cm head for obtaining good linear fits between position of wetting front, x, and square root of time). During infiltration the total amount of water absorbed and position of wetting front were recorded at different times. Infiltration was stopped when the wetting front had reached a certain desired position. The soil column was immediately sectioned and water contents determined gravimetrically.

Three such horizontal infiltrations were carried out on samples from each horizon terminating when the wetting front had advanced to approximately 14,17 and 20 cm respectively. At the end of each determination graphs of x versus $t^{1/2}$ and total infiltration, Q versus $t^{1/2}$ were prepared. The slopes of the best fitting lines yield the penetrability $\lambda$ (cm/min$^{1/2}$) and sorptivity S (cm/min$^{1/2}$) respectively. For each horizon the three $\theta$ versus x profiles were transformed into $\phi$ and plotted together from which the diffusivity was computed according to Eq. (3.9). The water content interval $\Delta\theta_j$ was fixed at 0.01 so as to yield tabulated $D(\theta)$ values at inter-

vals of 0.01 $cm^3/cm^3$ volumetric water content.

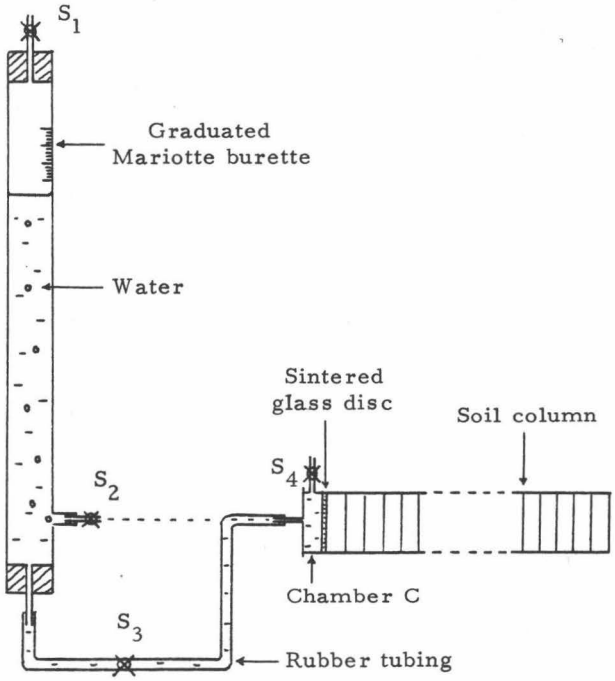


Fig. 3.4 Schematic diagram of apparatus for horizontal infiltration measurements.

3.4.c. Results and Discussion

(i) Penetrability and Sorptivity

In every case the plots of x against $t^{1/2}$ and Q against $t^{1/2}$ show excellent linear fits with $R^2$ greater than 0.99. However, due to experimental error mainly in the initiation of infiltration none of the lines passes through the origin as to be expected from theory. Tables 3.4(a) and 3.4(b) summarize the results of regression analyses for penetrability, $\lambda$ and sorptivity, S, respectively. In all cases $\lambda$ and S as well as the intercepts represent means of three determinations (regression lines); individual functional relationships are presented in Appendix V.

The mean penetrabilities of $P_1H_3$ and $P_1H_4$ are not significantly different from each other and so are the mean sorptivities of $P_1H_1$ and $P_1H_2$, $P_1H_3$ and $P_1H_4$, and $P_2H_3$ and $P_2H_4$ not significantly different fom one another (see Appendix VI). There does, however, appear to be a trend of decreasing penetrability and sorptivity with depth in Profile 1 and the reverse in Profile 2. This behaviour is probably due to an increase in clay content with depth in Profile 1 and a decrease in organic matter content

Table 3.4(a). Results of linear regression analysis on horizontal infiltration measurements into air dry soils for penetrability $\lambda$.

| Soil horizon | x versus $t^{1/2}$ plot | | | | $\phi$-$\theta$ curve |
|---|---|---|---|---|---|
| | Penetrability $\lambda$ (cm/min$^{1/2}$) | $s_\lambda$ | Intercept $a_\lambda$ (cm) | $s_{a_\lambda}$ | Penetrability $\lambda'$ (cm/min$^{1/2}$) |
| Profile 1 | | | | | |
| $P_1H_1$ | 2.094 | 0.056 | 0.406 | 0.054 | 2.130 |
| $P_1H_2$ | 1.967 | 0.035 | 0.324 | 0.078 | 1.981 |
| $P_1H_3$ | 1.767 | 0.066 | 0.240 | 0.035 | 1.787 |
| $P_1H_4$ | 1.676 | 0.068 | 0.323 | 0.077 | 1.702 |
| Profile 2 | | | | | |
| $P_2H_1$ | 1.039 | 0.050 | 0.902 | 0.083 | 1.103 |
| $P_2H_2$ | 1.163 | 0.033 | 0.821 | 0.123 | 1.225 |
| $P_2H_3$ | 1.319 | 0.071 | 0.503 | 0.077 | 1.377 |
| $P_2H_4$ | 1.444 | 0.022 | 0.115 | 0.016 | 1.444 |

Table 3.4(b). Results of linear regression analysis on horizontal infiltration measurements into air dry soils for sorptivity S.

| Soil horizon | Q versus $t^{1/2}$ plot | | | | $\phi$-$\theta$ curve |
|---|---|---|---|---|---|
| | Sorptivity S (cm/min$^{1/2}$) | $s_S$ | Intercept $a_S$ (cm) | $s_{a_S}$ | Sorptivity S' (cm/min$^{1/2}$) |
| Profile 1 | | | | | |
| $P_1H_1$ | 1.020 | 0.038 | 0.170 | 0.035 | 1.040 |
| $P_1H_2$ | 1.006 | 0.041 | -0.062 | 0.104 | 1.001 |
| $P_1H_3$ | 0.912 | 0.040 | -0.112 | 0.040 | 0.924 |
| $P_1H_4$ | 0.862 | 0.036 | -0.057 | 0.082 | 0.883 |
| Profile 2 | | | | | |
| $P_2H_1$ | 0.527 | 0.042 | -0.018 | 0.131 | 0.550 |
| $P_2H_2$ | 0.614 | 0.013 | 0.036 | 0.050 | 0.613 |
| $P_2H_3$ | 0.703 | 0.047 | -0.096 | 0.079 | 0.692 |
| $P_2H_4$ | 0.745 | 0.038 | -0.011 | 0.043 | 0.729 |

with depth in Profile 2. In general the organic matter content in Profile 2 is higher than in Profile 1 and this has prevented the attainment of higher bulk densities during column packing of samples from this profile. An added consequence is that all horizons of Profile 1 are more penetrable as well as more sorptive than the horizons of Profile 2 inspite of their higher bulk densities. In every case the bulk density of the prepared soil columns are very much lower than the corresponding value from undisturbed cores (Maene, personal communication). Thus, the penetrability and sorptivity obtained on these disturbed samples are expected to be much higher than their corresponding values in the field.

(ii) The Unique $\phi$-$\theta$ Relationship

The resulting $\phi$-$\theta$ curves for the various horizons obtained from horizontal infiltration experiments are shown in Fig. 3.5.

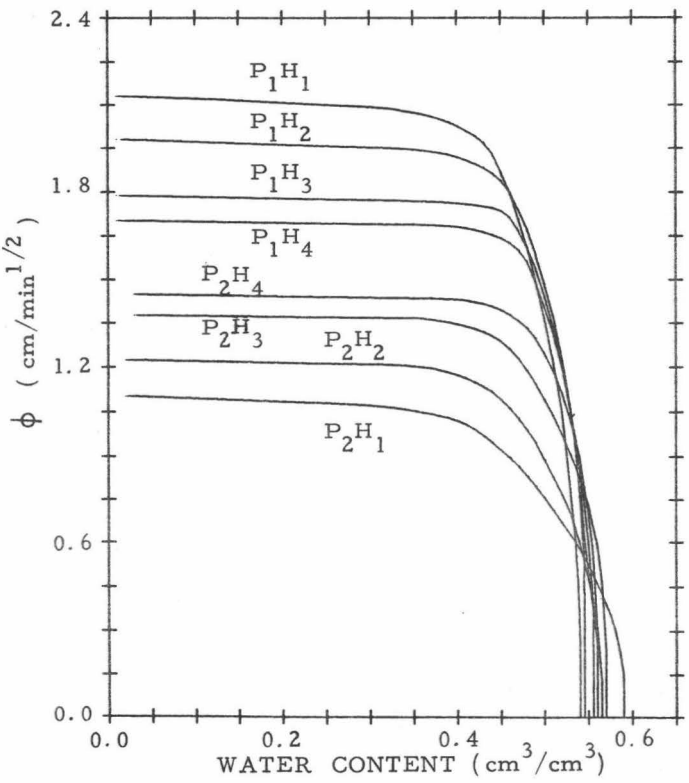


Fig. 3.5 Relationship between the Boltzmann transformation variable $\phi$ and water content for various horizons of the two soil profiles.

Fig. 3.6, in addition, illustrate the scatter of points around the unique $\phi$ versus $\theta$ curves for $P_1H_1$ and $P_2H_1$, these being typical of the scatter among the 8 soil horizons. It is evident that the $\phi$-$\theta$ distributions at different times can be adequately described by a unique curve thereby giving validity to the Boltzmann transformation method employed as well as the applicability of Darcy's Law for describing unsaturated flow in these soils.

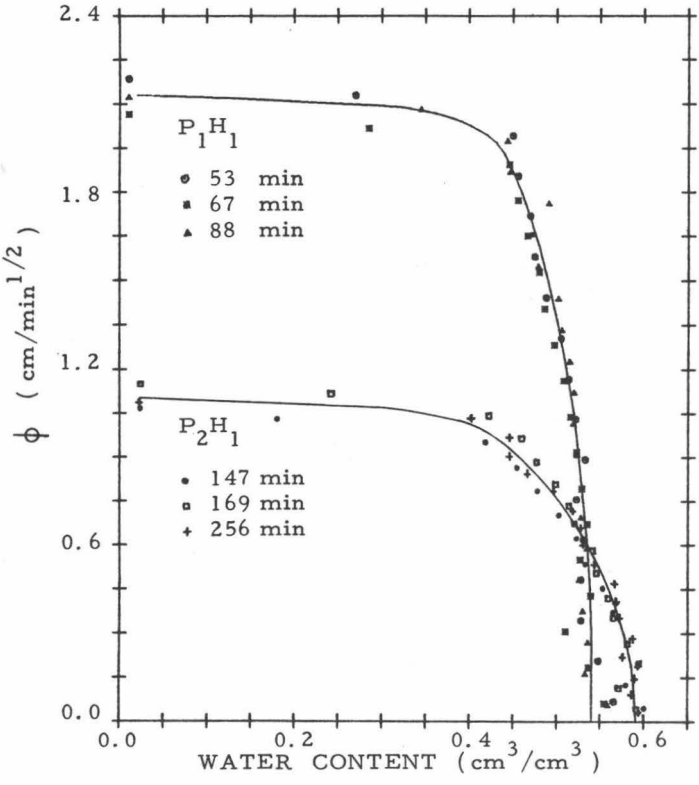


Fig. 3.6 Plots of the Boltzmann transformation against water content at different times for horizons $P_1H_1$ and $P_2H_1$.

The values of $\phi$ at $\theta = \theta_n$ should be the same as the corresponding penetrabilities calculated in the preceding section (i). This follows from the fact that the equation $x = \lambda t^{1/2} + a_\lambda$ suggests that the penetrability $\lambda$ is the value of $\phi$ at the water content of the wetting front, in this case, the air dry water content. Similarly, from the relationship (Philip, 1957a)

$$Q = t^{1/2} \int_{\theta_n}^{\theta_s} \phi \, d\theta$$

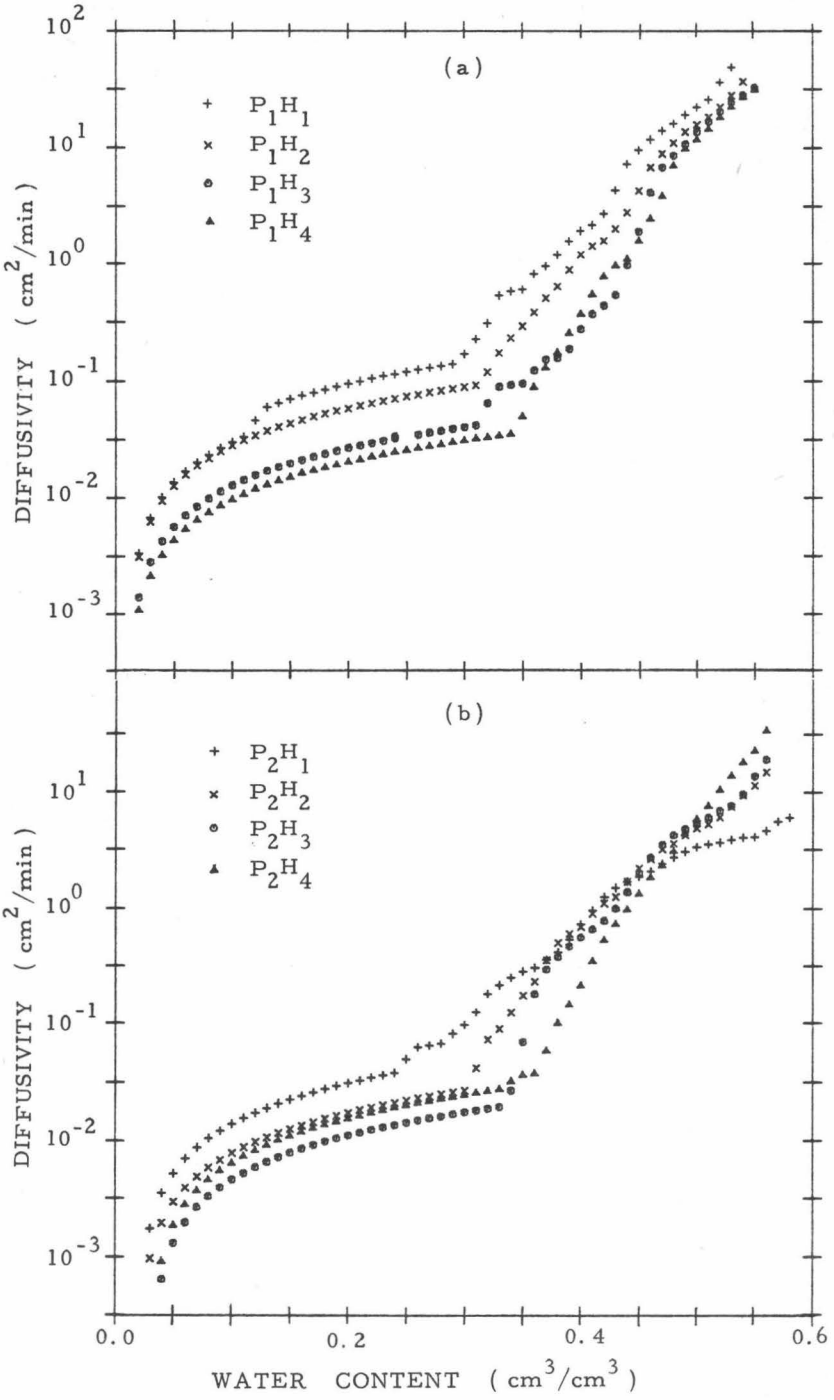


Fig. 3.7 Soil water diffusivity versus water content relationships for the various soil horizons: (a) Profile 1 and (b) Profile 2.

where Q is the total infiltration at time t, and the experimental relationship $Q = St^{1/2} + a_s$, it follows that the area bounded by the $\phi$-$\theta$ curve between $\theta_s$ and $\theta_n$ should be equal to the sorptivity determined earlier. Both assertions are confirmed by the results shown in Tables 3.4(a) & (b) in which there appears to be fair agreement between penetrability and sorptivity measured from horizontal infiltration and those ($\lambda'$ and S' respectively) obtained from the unique $\phi$-$\theta$ curve.

(iii) Diffusivity

Results of the diffusivity calculations are presented in Fig. 3.7(a) & (b) for the different horizons of Profile 1 and 2 respectively. Differences between horizons of the same profile are not large with the maximum diffusivities being of the same order of magnitude. While there is some overlapping at the low- and mid-range water contents, the diffusivities at the high water contents are greater in horizons of Profile 1 than in Profile 2. This accounts for the larger penetrabilities and sorptivities in the former since the rate of water movement is dictated almost entirely by the hydraulic characteristics at the high water contents.

The resulting diffusivity functions all appear to obey exponential relationships at approximately 50% saturation and more. In the next chapter some analytical models will be fitted to these results.

## 3.5. SATURATED HYDRAULIC CONDUCTIVITY

### 3.5.a. Theory

In principle a knowledge of the diffusivity and specific water capacity in the $\theta$ or h range of interest is sufficient to solve Richards' equation. Nevertheless, a glance at the $\phi$-$\theta$ curve (Fig. 3.5) reveals that $d\phi/d\theta \to \infty$ as $\theta \to \theta_s$. Consequently, diffusivity at $\theta_s$ cannot be determined with a reasonable degree of certainty. It has to be obtained by extrapolation using diffusivities just below $\theta_s$ or by predicting from a diffusivity model fitted to experimental points. Alternatively, if the specific water capacity has a finite (non-zero) value at or near saturation caused by occluded air the diffusivity at saturation can be calculated from a knowledge of saturated conductivity $K_s$. The latter can be determined by one of the many standard methods available in the literature (Childs and Poulovassilis, 1960 ; Childs, 1969 ; Klute, 1972).

In this particular study where interest is on quantitative description of water flow, the saturated conductivity is determined from measurements of flux at large times during vertical infiltration at constant pressure

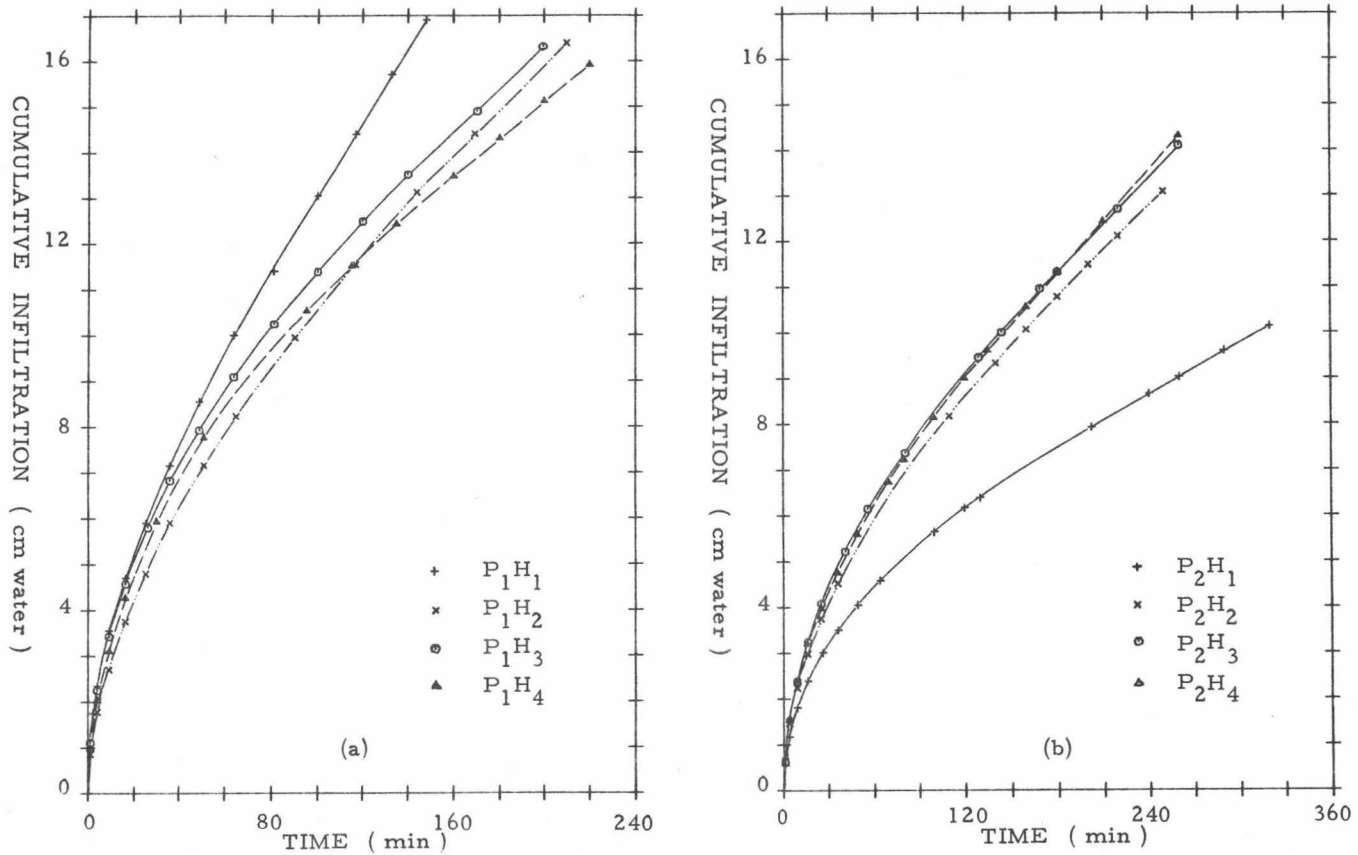


Fig. 3.8 Cumulative infiltration versus time during vertical infiltration into air dry soil for the various horizons of (a) Profile 1 (b) Profile 2 .

head (Youngs, 1964). The method is based on the fact that at large times the moisture profile assumes a constant shape. During this "constant profile" stage, hydraulic gradient at and near the surface is unity implying a constant flux at the surface (infiltration rate) equal to the conductivity at the corresponding moisture content and suction head. The cumulative infiltration versus time will approach a linear dependence on time and the slope will be the conductivity in question. If the constant head applied is zero, then the conductivity is essentially that of saturation.

3.5.b. Method

The experimental set up was the same as that for horizontal infiltration and capillary rise experiments except for the following. First, the infiltration column was constructed from a single piece of perpex glass tubing having the same cross-section as the rings for horizontal and capillary rise columns. Secondly, water was allowed to infiltrate from the top of the column (capillary rise experiment inverted) at zero suction. During the flow process cumulative infiltration and position of wetting front were recorded at frequent intervals. The experiment was stopped when a constant infiltration rate was attained and this persisted for at least 1 hour. A plot of cumulative infiltration versus time was then prepared, the slope of the asymptote giving the value of the saturated conductivity.

3.5.c. Results and Discussion

The results of the vertical infiltration are presented in Fig. 3.8(a) and Fig. 3.8(b) in terms of cumulative infiltration against time for one series of determination (Replicate 1) on horizons of Profile 1 and Profile 2 respectively. The respective saturated conductivities are determined from the gradients of the linear parts of the plots and are given in Table 3.5.

The saturated conductivities obtained vary with depth in the same manner as did the penetrabilities and sorptivities. In relative terms the variation is not great. All of them are within the same order of magnitude, the difference between the highest and lowest values being less than twice within a given profile and less than four times among all horizons studied. This is readily understood from the fact that there are only minor textural differences between the horizons. The apparent influence of organic matter on saturated conductivity can also be readily seen from the fact that horizons $P_2H_1$ and $P_2H_2$ with higher organic matter contents than others are also the least permeable.

Table 3.5. Saturated conductivities of various horizons of Profiles 1 and 2 as measured by the infinite time flux during vertical infiltration.

| Soil horizon | Saturated conductivity ($10^{-2}$ cm/min) | | |
|---|---|---|---|
| | Replicate I | Replicate II | Mean |
| Profile 1 | | | |
| $P_1H_1$ | 8.3664 | 7.0020 | 7.6842 |
| $P_1H_2$ | 4.7059 | 4.9414 | 4.8237 |
| $P_1H_3$ | 4.2105 | 4.5000 | 4.3553 |
| $P_1H_4$ | 4.1000 | 3.9250 | 4.0125 |
| Profile 2 | | | |
| $P_2H_1$ | 1.8750 | 2.0650 | 1.9700 |
| $P_2H_2$ | 3.2200 | 2.6857 | 2.9529 |
| $P_2H_3$ | 3.4700 | 3.2714 | 3.3707 |
| $P_2H_4$ | 3.7700 | 3.5143 | 3.6422 |

CHAPTER 4

# STRUCTURE IDENTIFICATION OF HYDRAULIC PROPERTIES

## 4.1. INTRODUCTION

For almost any flow condition Richards' equation can be solved with the aid of computers and certain numerical approximations. Comparisons of numerical solutions with known semi-analytical solutions and experimental results for well-defined problems (Hanks and Bowers, 1962 ; Haverkamp et al., 1977) have shown that the accuracy which can be achieved by numerical approximations are excellent, far exceeding that necessary for predictive purposes. Accuracy of prediction apparently is limited not by the complexity of the flow processes but by the poor accuracy of the input data. This is true either in the case of experimental validation of numerical models where reproducibility is difficult to achieve even under controlled laboratory conditions or in the prediction of flow processes in the field with the attendant variability and heterogeneity. Great importance is, therefore, attached to accurate and reliable estimation of the parameters of the Richards' flow equation.

For the computer implementation of numerical solutions of the unsaturated flow problem, tabulated values relating D or K to $\theta$ and/or h in the range of interest are adequate and yield excellent results. However, in terms of storage and computational efficiency, simple empirical formulae are more desirable. Moreover, for derivation of closed analytical solutions, the formula representation of these relationships is a prerequisite.

Since the last three decades many empirical formulae for the hydraulic characteristics have been used. The unknown parameters of the various formulae or structures are generally determined by using some kind of best fitting technique in order to adjust them to the experimentally measured data of each particular soil or class of soils. As most of the structures involved are nonlinear, the least square method, for example, applied to several of them can be a tedious and time consuming operation.

For the same reason of nonlinearity, curve fitting technique based on the minimization of sum squares of deviation can be inadequate unless accompanied by some kind of weighting. Comparisons of goodness of fit among the different structures are at best subjective.

A recent approach to structure identification is that of pattern recognition proposed by Karplus (1972) and Saridis and Hofstadter (1974). Here, structures are considered to be different patterns and identification is regarded as a task of recognizing patterns using experience and current information. Certain details of the procedure have been worked out by Simundich (1975) and these have been extended and modified by Vansteenkiste, Bens and Spriet (1978a). The method suggested by the latter authors is still in its infancy and more exploratory work with various kinds of data and structures is required to establish it as a useful tool in structure characterization. This chapter aims at applying their technique in the identification of simple structures for the soil water characteristic and diffusivity which are to be used in solving Richards' equation.

## 4.2. STRUCTURE IDENTIFICATION BY PATTERN RECOGNITION

### 4.2.a. General Approach

The pattern recognition approach, in simple terms, involves a comparison of the pattern emerging from certain operations on the data set coming from the system to be modelled with an input library of patterns from known "candidate" models. A choice is then made among the candidates as to which structure is best adapted to the data.

The procedure is illustrated in Fig. 4.1. Two stages of operation are distinguished ; first is the training of the classification algorithm (switches in position I) and second is the use of the classifier (switches in position II). In the first stage, a number of candidate models are proposed. A "feature extraction" procedure is performed on artificial data generated from these models. The resulting "feature space" is then classified into partitions corresponding to different models. When the training is complete the classification algorithm or pattern recognizer is coupled to the data being investigated (second stage) and the most suitable model selected. The next step is then to identify the parameters of the chosen model.

### 4.2.b. Feature Extraction

Feature extraction is the most crucial part of the method. Features

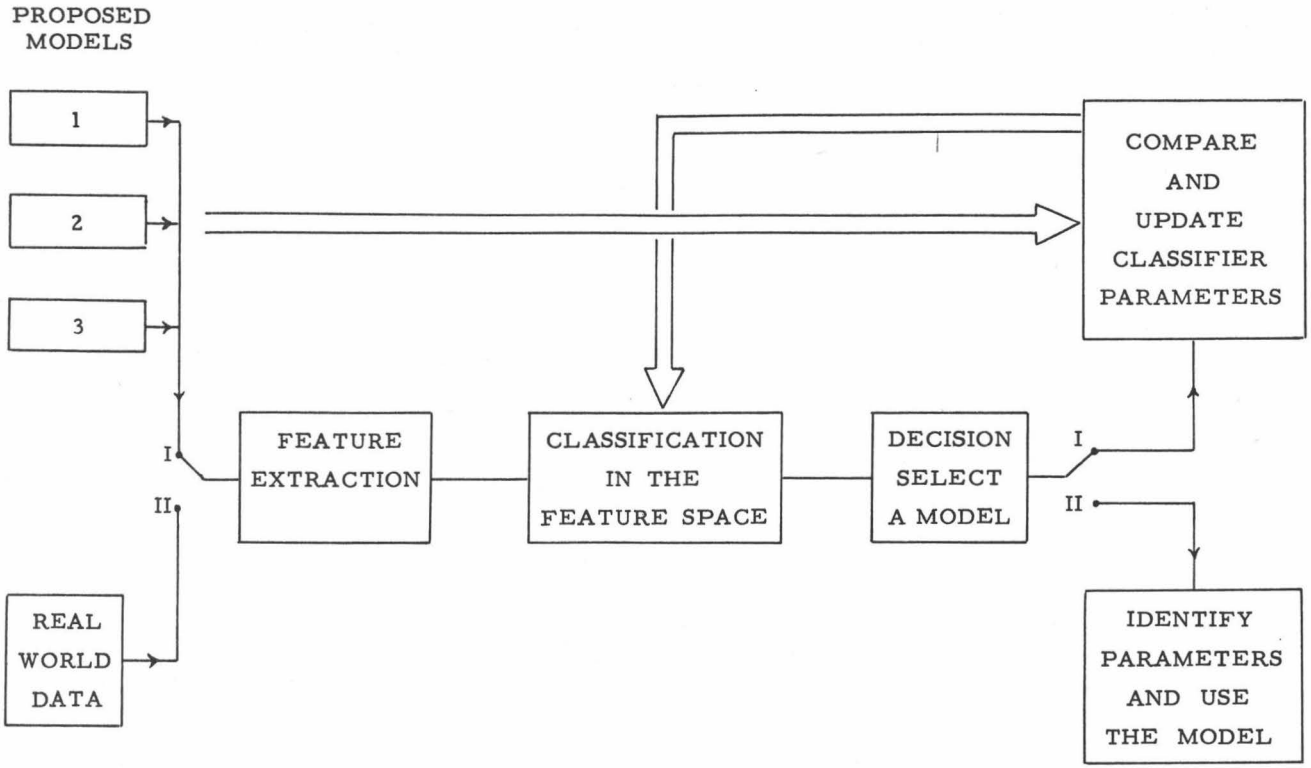


Fig. 4. 1 Structure determination by the pattern recognition approach ( after Vansteenkiste, Bens and Spriet, 1978 a ).

or characteristic expressions have to be defined, on the basis of which a choice among the different models will be made. No hard and fast rules exist in the choice of the features. However, they should be rather insensitive to noise besides having good discriminating properties. Very often one feature per proposed model is used, but sometimes more features can provide better discrimination. The different features form a so-called feature space in which most of the characterization operations are performed.

Consider the data set $D = \{(t_i, x_i) \mid i = 1,2,\ldots,n\}$ coming from the experiment or simulation of the experiment. Feature extraction can be regarded as a mapping of the set $D$ of all possible data sets to a feature space

$$\Theta : D \rightarrow R^k : D \rightarrow f$$

where k is the number of features and f is a point in the feature space. The mapping $\Theta$ can be single valued, i.e., a single point f is the image of a set D (Simundich, 1975), or multiple valued, i.e., more than one point f is the image of D, as in the current approach of Vansteenkiste, Bens and Spriet (1978a). The advantage of the multiple-valued mapping is that a poor or erroneous measurement will not destroy the information present in the other measurements.

4.2.c. Classification of the Feature Space

During the training stage a "classifier" splits up the feature space into partitions in an optimal way, each subset corresponding to a cluster of points and hence to a candidate (proposed) model. To achieve this several simulation runs have to be made with each model. Feature points derived from these simulations are used as input to the classifier, whose parameters are then adjusted iteratively so as to give maximal correspondence between input and output, the latter being the various partitions or subsets of the feature space. It is, thus, evident that the more simulation runs with each of the candidate models and the more diverse these runs are, the better would the classification algorithm be.

*Note* : The discussion and development of the classifier is beyond the scope of this thesis. There are, however, a number of handbooks covering this topic (Nilsson, 1965 ; Young and Calvert, 1974). Kanal (1974) provides an excellent survey of the different methods available while Vansteenkiste, Bens and Spriet (1978) discuss the various

problems of choosing a classifier algorithm. The latter authors emphasized that where it is deemed fit, as in a two or three-dimensional feature space, visual classification can be the most convenient method.

## 4.3. STRUCTURE CHARACTERIZATION OF THE SOIL WATER CHARACTERISTIC

### 4.3.a. Candidate Models

In most instances the soil water characteristic or the θ-h relationship yields an S-shaped curve, although it is not uncommon to find a relationship which exhibits two or more points of inflection. Some of the empirical relationships that have been used are listed in Table 4.1. These form the candidate models in the structure identification.

Table 4.1. Some empirical formulae used to represent the water content-pressure head relationship.

| Formula | | Source |
|---|---|---|
| Model 1 : $S = \dfrac{\alpha}{\alpha + (\ln\lvert h\rvert)^{\beta}}$ | (4.1) | Haverkamp et al. (1977) |
| Model 2 : $S = \dfrac{\delta}{\delta + \lvert h\rvert^{\gamma}}$ | (4.2) | Haverkamp et al. (1977) |
| Model 3 : $S = \begin{cases} \left(\dfrac{h_a}{h}\right)^{\lambda} & , h < h_a \\ 1 & , h \geqslant h_a \end{cases}$ | (4.3) | Brooks and Corey (1964) |

S is the dimensionless water content given by $S = (\theta - \theta_r)/(\theta_s - \theta_r)$ where $\theta_s$ and $\theta_r$ are the saturation and residual water contents respectively.

### 4.3.b. Feature Extraction

An examination of the candidate models reveals little except that the θ-h curve tends to be rather flat at the low and high ends. Although the first derivative has an important physical significance (this being the specific water capacity), it offers no immediate help in the characterization process. We thus resort to the parameters of the models for deriving features, since in the ideal cases, these parameters are invariant for each model respectively. Their variability would be a measure of deviation from the model under consideration. In the present identification process only one parameter per proposed model is used to derive features.

Feature 1 :

As h is negative, operations are made easier by using suction head $\psi = -h$, so that Model 1 now reads

$$S = \frac{\alpha}{\alpha + (\ln \psi)^{\beta}} \tag{4.4}$$

Differentiating with respect to $\psi$ we obtain

$$\frac{dS}{d\psi} = -\frac{S^2 \beta}{\alpha \psi} (\ln \psi)^{\beta-1} \tag{4.5}$$

Elimination of $\alpha$ from (4.4) and substituting it in (4.5) yields

$$\beta = -\frac{dS}{d\psi} \frac{\psi \ln \psi}{S(1-S)}$$

or

$$\beta = -\frac{dS}{dh} \frac{h \ln|h|}{S(1-S)} \tag{4.6}$$

Thus, for any point in the data set $\beta$ may be obtained by the use of Eq. (4.6) and the central difference approximation $dS/dh = (S_{i+1} - S_{i-1})/2\Delta h$. Now, two random points, A and B with coordinates $(h_A, S_A)$ and $(h_B, S_B)$ respectively, are taken from the data set (simulated or experimental) and feature 1 or the first coordinate of the point corresponding to the chosen (A,B)-tuple is computed according to

$$f_1 = \frac{\beta_A}{\beta_B} \tag{4.7}$$

Hence, $f_1$ provides us with a measure of the variability of parameter $\beta$. The procedure is repeated for different (A,B)-tuples providing a set of values corresponding to the projections on one of the axis of the feature space.

Feature 2 :

The second feature is obtained by resorting to Model 2. Again, differentiating S with respect to h or $\psi$ and solving for $\gamma$ yields

$$\gamma = \frac{-h}{S(1-S)} \frac{dS}{dh} \tag{4.8}$$

Following the same procedure as with the first, the second feature, $f_2$, is found by taking the ratio of the $\gamma$'s at the same two points, A and B used earlier. Thus,

$$f_2 = \frac{\gamma_A}{\gamma_B} \tag{4.9}$$

Feature 3 :

Model 3 is now used to derive feature 3 or the third component of the point in the feature space. Differentiating and solving for $\lambda$ yield

$$\lambda = -\frac{h}{S} \cdot \frac{dS}{dh} \quad , \quad h < h_a \tag{4.10}$$

Feature 3 is then calculated using points A and B

$$f_3 = \frac{\lambda_A}{\lambda_B} \quad , \quad h < h_a \tag{4.11}$$

Complications arise for $h > h_a$ because now the function has a constant value (i.e., equal to 1) and, therefore, $\lambda$ is imaginary. One way of overcoming this dilemma is to define an alternative feature $f'_3$ specific to this region according to

$$f'_3 = S_A/S_B \quad , \quad h \geq h_a \tag{4.11a}$$

*Note* : If the absolute value of any feature is greater than unity, then the ratio is inverted, i.e., its reciprocal is taken instead. The reason for taking ratios for all features is thus clear, that is, to reduce them all to the same scale of -1 to +1.

Since computation of the second set of parameters involves very little extra effort, three more features can be easily defined. These are

$$f_4 = \frac{\alpha_A}{\alpha_B} \quad , \quad f_5 = \frac{\delta_A}{\delta_B} \quad , \quad f_6 = \frac{h_{a_A}}{h_{a_B}} \tag{4.12}$$

4.3.c. Training

The feature extraction procedure just described is performed on each model using simulated data. For each model and for a simulation run, two random points A and B are taken and the features $f_1$, $f_2$ and $f_3$ or $f'_3$ computed according to the procedure outlined. This gives a point in the feature space belonging to the given model. The procedure is repeated for as many points as desired (the more points the better), after which more simulations are performed and feature points computed likewise. In this study 5 simulation runs per model are carried out. The parameter values used for the different models are shown in Table 4.2. To make the training more realistic a 2% of full scale random error (hence 0.01 $cm^3/cm^3$ water content) is introduced to the simulated data.

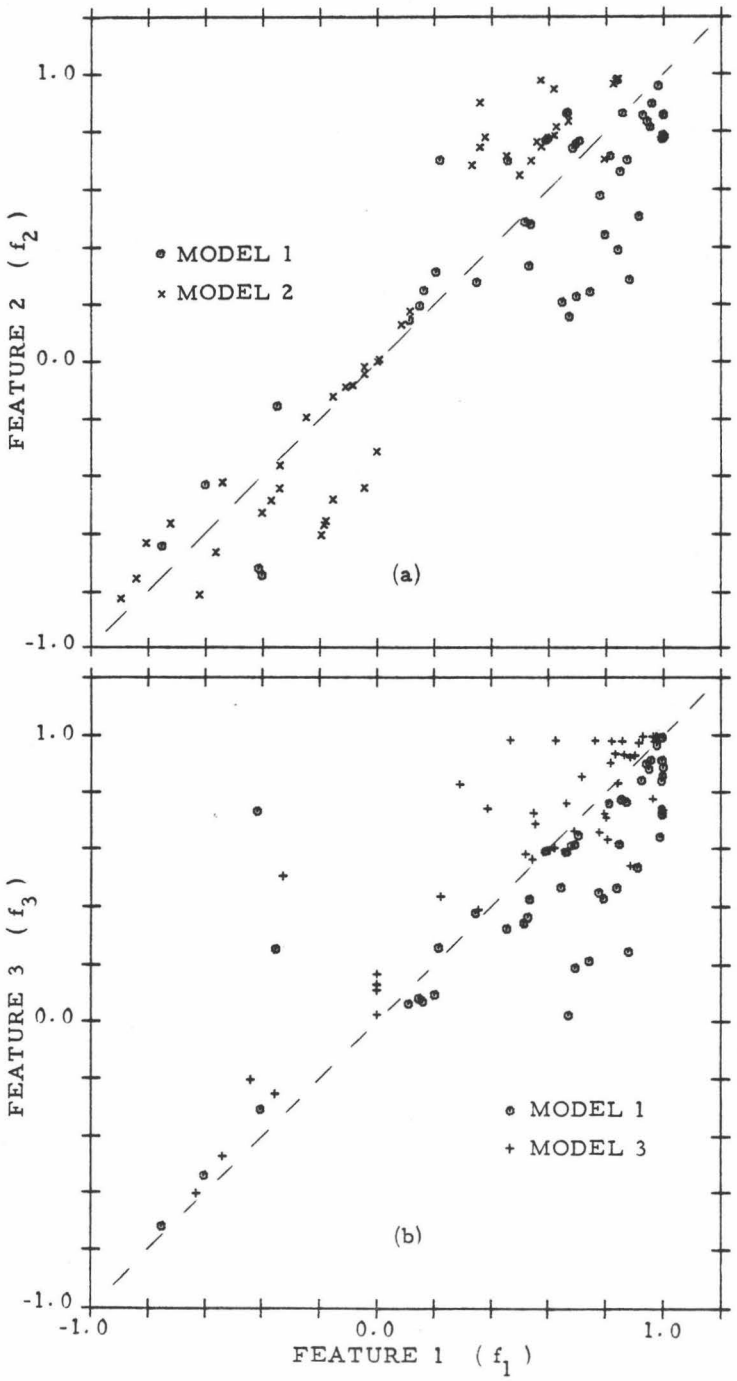


Fig. 4.2 Feature space of the various candidate models for the soil water characteristic : (a) Model 1 and Model 2 , (b) Model 1 and Model 3 .

Table 4.2. Parameter values used to generate data needed in the classification of the feature space for the different models.

| Simulation run | Model 1 | | Model 2 | | Model 3 | |
|---|---|---|---|---|---|---|
| | $\alpha$ | $\beta$ | $\delta$ | $\gamma$ | $h_a$ | $\lambda$ |
| 1 | 50 | 2.4 | $1x10^2$ | 2.2 | - 5 | 0.21 |
| 2 | 100 | 2.6 | $5x10^1$ | 3.0 | - 10 | 0.23 |
| 3 | 250 | 3.2 | $1x10^3$ | 3.4 | - 25 | 0.30 |
| 4 | 500 | 3.8 | $1x10^4$ | 2.8 | - 50 | 0.28 |
| 5 | 1,000 | 3.6 | $1x10^6$ | 2.5 | -100 | 0.32 |

For convenience and ease of visual comparison the features are now plotted two by two. Figures 4.2(a) & (b) show feature points for Model 1 and Model 2 in the $f_1$-$f_2$ feature space, and for Models 1 and 3 in the $f_1$-$f_3$ feature space, respectively. Some overlapping of feature points is observed. This is due to the contamination of the 2% error. Had no error been introduced one would expect to obtain two narrow bands of clusters, one along the line $f_1 = 1$, consisting of points from Model 1 and the other along the line $f_2 = 1$ or $f_3 = 1$ for feature points from Model 2 or Model 3, respectively. Nevertheless, in these cases the feature space can still be seen to be split into two subsets by an approximately 45% line extending from the proximity of the origin.

4.3.d. Identification of the structure for the soil water characteristic

The water content versus pressure head data from each soil horizon are now subjected to the feature extraction procedure. Note that in order to reduce the water content to the dimensionless S, the maximum and residual water contents must be known. The former are assumed to be the same as those obtained by capillary rise (Section 3.3), while for the latter the air dry values are used. In addition to these, an estimate of $h_a$ is also necessary due to reasons stated earlier. This is obtained by inspecting the data and locating the approximate pressure head at which an abrupt fall of water content to values significantly below saturation occurs.

Plots of $f_2$ against $f_1$ and $f_3$ against $f_1$ are then prepared for each soil. In all cases the choice between Model 1 and Model 2 can be readily made since most of the feature points fall in the space belonging to Model 1. However, discrimination between Model 1 and Model 3 is rather difficult in most of the test cases. Figures 4.3 (a) through (d) illustrate some of the features of the analysis. Figures 4.3 (a) & (b) clearly indi-

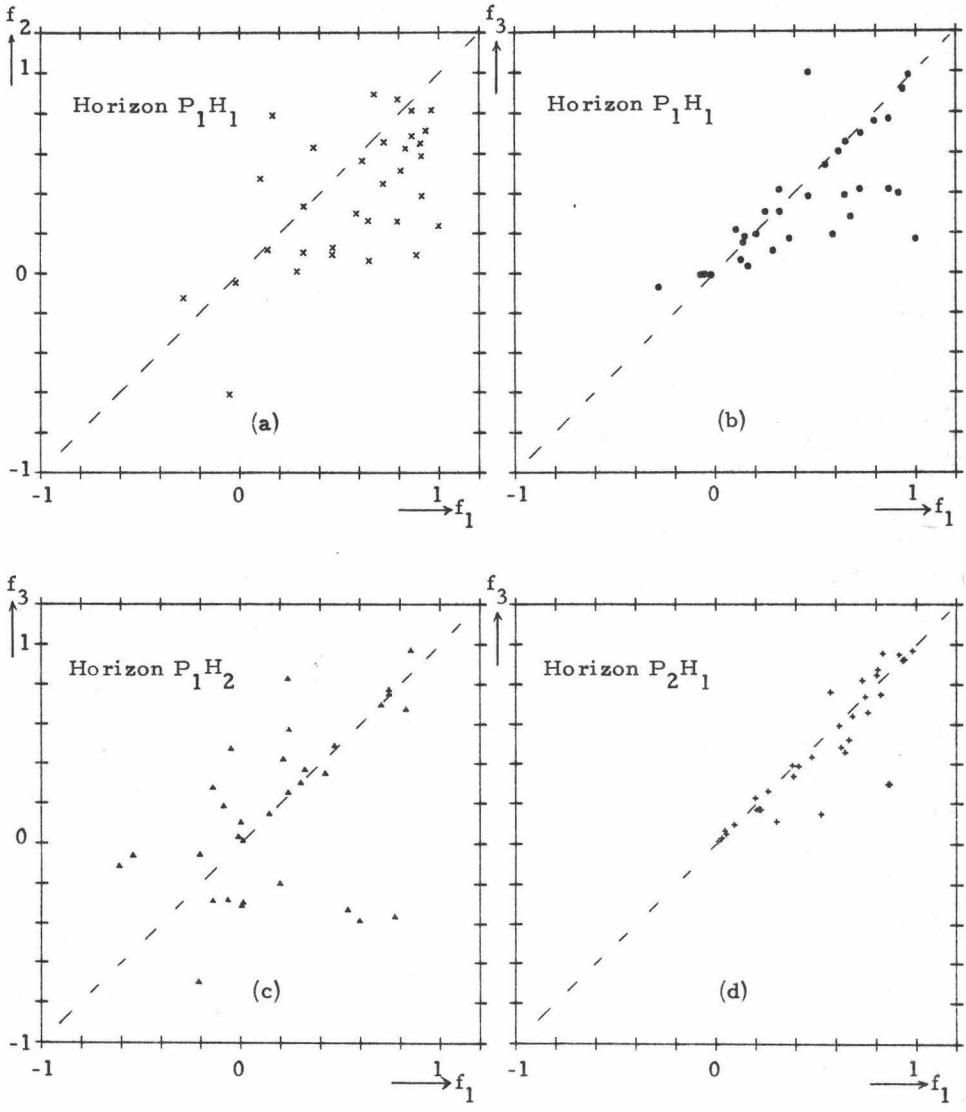


Fig. 4. 3 Feature space containing feature points for various test cases in the structure identification of the soil water characteristic.

Table 4.3. Results of parameter identification of Model 1, 2 and 3 by the least squares method.

| Soil Horizon | $\theta_s$ | $\theta_r$ | Model 1 | | | Model 2 | | | Model 3 | | |
|---|---|---|---|---|---|---|---|---|---|---|---|
| | | | $\alpha$ | $\beta$ | SSDx10$^2$ | $\delta$ | $\gamma$ | SSDx10$^2$ | $h_a$ | $\lambda$ | SSDx10$^2$ |
| PROFILE 1 | | | | | | | | | | | |
| $P_1H_1$ | 0.54 | 0.01 | 75.61 | 2.764 | 1.796 | 85.5 | 0.932 | 9.169 | - 6.03 | 0.242 | 1.123 |
| $P_1H_2$ | 0.55 | 0.01 | 321.3 | 3.429 | 2.327 | 176.2 | 0.986 | 8.701 | -12.05 | 0.249 | 1.252 |
| $P_1H_3$ | 0.57 | 0.02 | 289.3 | 3.342 | 1.314 | 135.3 | 0.925 | 5.978 | -15.05 | 0.263 | 2.843 |
| $P_1H_4$ | 0.575 | 0.025 | 667.0 | 3.718 | 1.313 | 154.4 | 0.895 | 5.220 | -22.40 | 0.249 | 2.144 |
| PROFILE 2 | | | | | | | | | | | |
| $P_2H_1$ | 0.59 | 0.02 | 45.65 | 2.389 | 1.923 | 32.4 | 0.700 | 9.484 | - 4.87 | 0.209 | 2.225 |
| $P_2H_2$ | 0.57 | 0.03 | 236.3 | 3.242 | 2.817 | 111.6 | 0.898 | 9.056 | - 9.90 | 0.235 | 2.617 |
| $P_2H_3$ | 0.57 | 0.03 | 394.1 | 3.477 | 1.488 | 105.6 | 0.843 | 5.633 | -17.70 | 0.271 | 2.580 |
| $P_2H_4$ | 0.565 | 0.03 | 551.2 | 3.596 | 1.474 | 98.6 | 0.790 | 5.745 | -23.35 | 0.274 | 2.078 |

SSD = Sum of squares of deviation = $\sum_{i=1}^{n} (S_i - S_i^m)^2$ where superscript m refers to measured value.

cate the superiority of Model 1 to the other two. Figure 4.3(c), on the other hand, appears slightly favour Model 3 to Model 1, while Fig.4.3(d) indicates the opposite; in both cases, the distinction is not very convincing. Overall, the asymptotic model (Model 1) fits best data from three soil horizons, namely, $P_1H_1$, $P_2H_1$ and $P_2H_4$ while the Brooks and Corey model (Model 3) is best for two horizons, $P_1H_2$ and $P_2H_2$. For horizons $P_1H_3$, $P_1H_4$ and $P_2H_3$, both models 1 and 3 are equally adapted. However, in view of the fact that the soils are texturally similar, one should expect a predominance of one particular model. Further attempts at classification using features 4 and 6 fail to resolve the ambiguity.

The lack of success can be attributed in part,to the inadequacy of the chosen features in discriminating the suitable model; the importance of finding suitable features has already been emphasized earlier. A certain degree of experience and insight is necessary in deriving good features for classification. Another reason is that the present identification has been performed in only two dimensions using one feature per model. By increasing the number of features it should be possible to obtain a more convincing result.

4.3.e. Parameter Identification

Least squares parameter identification is performed with all the three models so as to provide a comparison between the least squares technique and the pattern recognition approach. Results of the least squares fit are presented in Table 4.3. The sum of squares of deviations (SSD) for Model 2 are markedly higher than those of either Model 1 or Model 3, thus in accord with the pattern recognition results. As with the pattern recognition method, there is no complete dominance of a particular model. One significant feature, however, emerges and that is, the least squares method and the pattern recognition technique can give conflicting results as observed in the case of horizon $P_1H_1$. The most obvious reason for this is that a few bad observations can increase the SSD significantly, yet these same observations will have little impact on the overall pattern from the whole data set in the pattern recognition approach. This augers well for the latter technique.

## 4.4. STRUCTURE CHARACTERIZATION OF THE SOIL WATER DIFFUSIVITY

### 4.4.a. Candidate Models

Early work with diffusivity (Childs and Collis-George, 1950; Klute, 1952) left the functional form of $D(\theta)$ completely general. An exponential function of the form $D(\theta) = \alpha.\exp(\beta\theta)$ was suggested by Gardner and Mayhugh (1958), which since then has been widely used. This can also be written as

$$D(\theta) = D_{min}\, e^{\beta(\theta-\theta_{min})} \qquad (4.13)$$

Ahuja and Swartzendruber (1972) suggested a power function of the form

$$D(\theta) = \frac{a\theta^n}{(\theta_s - \theta)^{n/5}} \qquad (4.14)$$

which yields infinite diffusivity at saturation.

A third model is proposed herein. From the commonly used relationship $K = K_s S^n$ where K is conductivity and subscript s refers to saturation, and the Brooks and Corey model (Eq.4.3) for $h < h_a$, from which the above conductivity relationsh. p is derived, we obtain via Eq.(1.12), a diffusivity structure of the form

$$D(\theta) = b\left(\frac{\theta - \theta_r}{\theta_s - \theta_r}\right)^m \qquad (4.15)$$

where $b = -\frac{K_s h_a}{\lambda(\theta_s - \theta_r)}$ and $m = n - 1 - \frac{1}{\lambda}$

Equation (4.15) is also a power function but unlike (4.14), the diffusivity at saturation is finite and equal to b.

The three models represented by (4.13), (4.14) and (4.15), hereby called Model 1, Model 2 and Model 3 respectively, are now considered as the candidate models for the diffusivity functions of the soils under investigation.

4.4.b. Feature Extraction

In contrast to the method employed for the soil water characteristic, here both parameters of each model are used to derive a single feature per model. The feature is defined as the sum of the ratios of each parameter evaluated for a random pair of points from the data set. Thus,

$$\text{Feature 1, } f_1 = \frac{\beta_A}{\beta_B} + \frac{D_{minA}}{D_{minB}}$$

$$\text{Feature 2, } f_2 = \frac{n_A}{n_B} + \frac{s_A}{s_B}$$

and $$\text{Feature 3, } f_3 = \frac{m_A}{m_B} + \frac{b_A}{b_B}$$

The various parameters for points A and B are computed in the same manner as described in section 4.3. These are

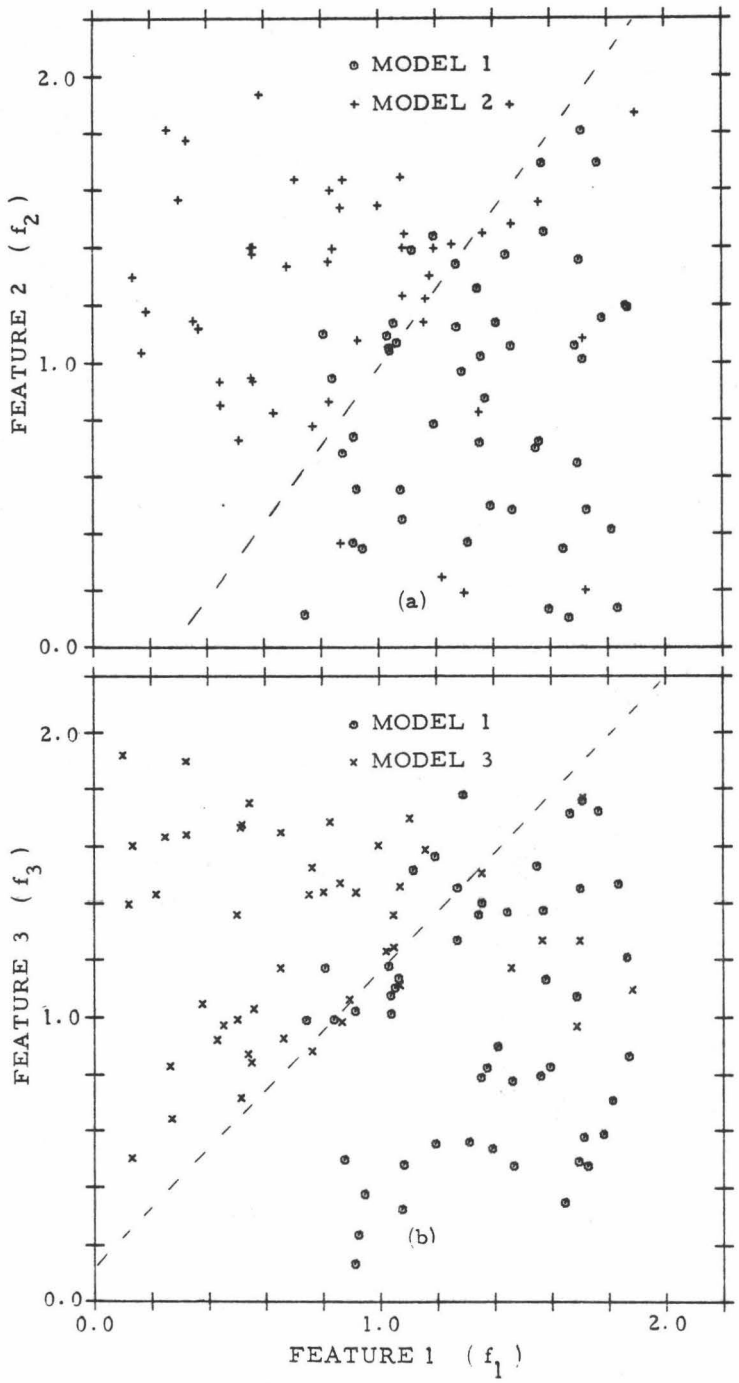


Fig. 4.4 Feature space of the various candidate models for the soil water diffusivity : (a) Model 1 and Model 2 , (b) Model 1 and Model 3 .

$$\beta = \{\frac{1}{D(\theta-\theta_r)} \frac{dD}{d\theta}\}^{1/2} \quad , \quad D_{min} = D\, e^{-\beta(\theta-\theta_r)}$$

$$n = \frac{5\theta}{D} \left(\frac{\theta_s - \theta}{5\theta_s - 4\theta}\right) \frac{dD}{d\theta} \quad , \quad a = \frac{D(\theta_s-\theta)^{n/5}}{\theta^n}$$

$$m = \frac{\theta-\theta_r}{D} \frac{dD}{d\theta} \quad , \quad b = D\left(\frac{\theta-\theta_r}{\theta-\theta_r}\right)^{-m}$$

Whenever the ratio between parameter values at the two points exceeds unity, its reciprocal is taken instead. In this way, all the features remain within the limits of -2 and +2.

4.4.c. Training

Five simulation runs are performed with different combinations of parameter values. Since error in the D(θ) determination is rather large, a 10% relative error is added randomly to the simulated data. The parameter values used for the different simulation runs are indicated in Table 4.4.

Table 4.4. Parameter values used to generate data needed in the classification of the feature space for the different diffusivity models.

| Simulation | Model 1 | | Model 2 | | Model 3 | |
|---|---|---|---|---|---|---|
| run | $D_{min}$ | β | a | n | b | m |
| 1 | $1x10^{-4}$ | 60.0 | 15.0 | 2.0 | 5.0 | -6.0 |
| 2 | $1x10^{-5}$ | 50.0 | 12.0 | 4.0 | 0.0001 | 4.0 |
| 3 | $1x10^{-6}$ | 30.0 | 4.0 | 3.5 | 0.01 | 10.0 |
| 4 | $1x10^{-7}$ | 20.0 | 1.0 | 4.0 | 0.1 | 7.0 |
| 5 | $1x10^{-8}$ | 40.0 | 8.0 | 3.0 | 1.0 | -2.0 |

Figures 4.4 (a) & (b) show the plots of feature points for the classification between Model 1 and Model 2 and between Model 1 and Model 3. Again some overlapping is observed, nevertheless, the splitting of the feature space into two subsets corresponding to the respective models is quite evident.

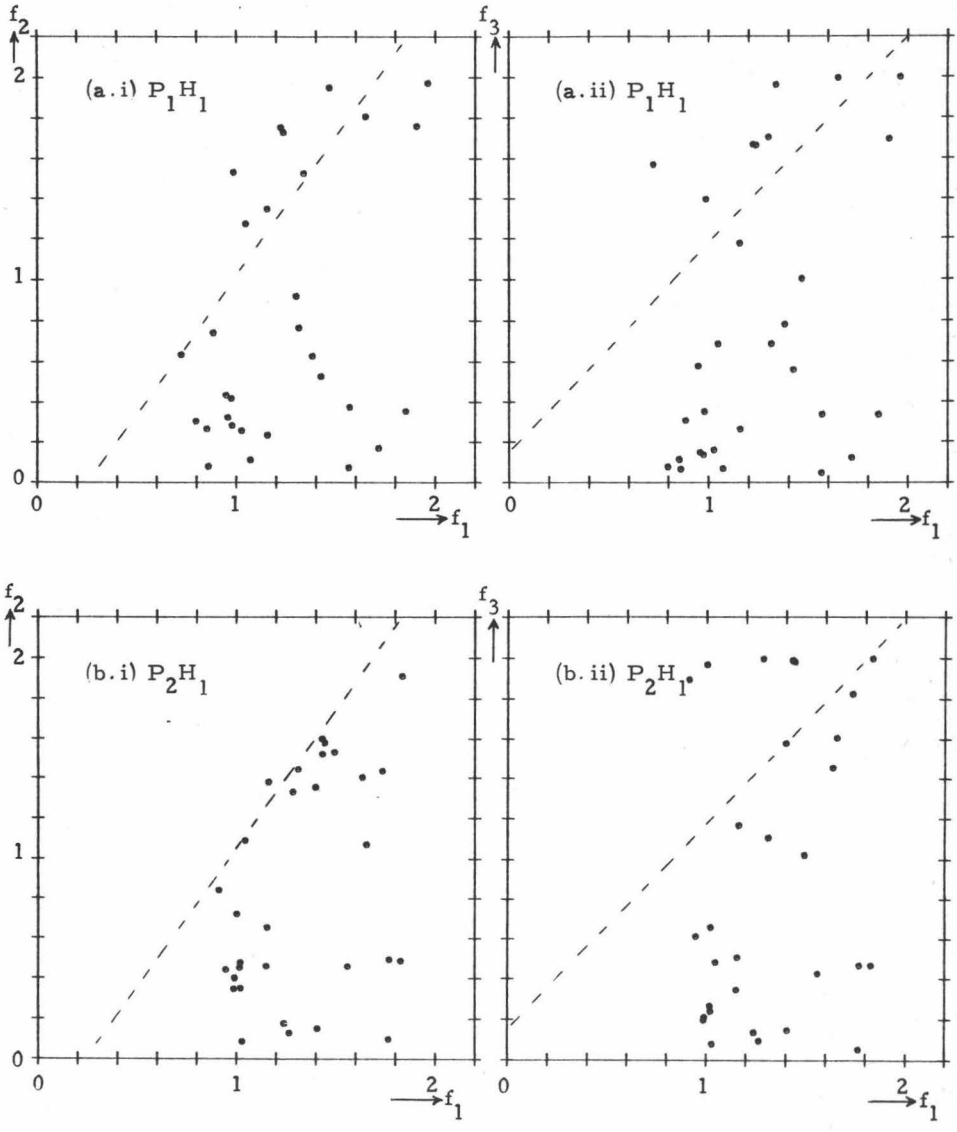


Fig. 4.5 Feature space containing feature points for various test cases in the structure identification of soil water diffusivity.

Table 4.5. Soil water diffusivity $D(\theta)$, expressed as a unique and piecewise exponential function. R is the correlation coefficient for the lineair regression $\ln D = \ln D_{min} - \beta(\theta - \theta_{min})$.

| Soil Horizon | Unique Function: Diffusivity function ($cm^2$/min) | R | Piecewise Function: Diffusivity function ($cm^2$/min) | R |
|---|---|---|---|---|
| PROFILE 1 | | | | |
| $P_1H_1$ | $D = 2.928 \times 10^{-3} \exp[11.473(\theta-0.01)]$ | 0.975 | $D = \begin{cases} 2.468 \times 10^{-3} \exp[13.345(\theta-0.01)], & 0.01 < \theta < 0.356 \\ 7.186 \times 10^{-5} \exp[23.553(\theta-0.01)], & 0.356 < \theta \leq 0.54 \end{cases}$ | 0.945<br>0.996 |
| $P_1H_2$ | $D = 1.157 \times 10^{-3} \exp[15.311(\theta-0.01)]$ | 0.960 | $D = \begin{cases} 2.750 \times 10^{-3} \exp[4.761(\theta-0.01)], & 0.01 < \theta < 0.335 \\ 1.459 \times 10^{-5} \exp[25.881(\theta-0.01)], & 0.335 < \theta \leq 0.55 \end{cases}$ | 0.923<br>0.998 |
| $P_1H_3$ | $D = 4.389 \times 10^{-4} \exp[16.081(\theta-0.02)]$ | 0.940 | $D = \begin{cases} 1.086 \times 10^{-3} \exp[11.288(\theta-0.02)], & 0.02 < \theta < 0.352 \\ 6.354 \times 10^{-6} \exp[26.310(\theta-0.02)], & 0.352 < \theta < 0.57 \end{cases}$ | 0.927<br>0.973 |
| $P_1H_4$ | $D = 3.074 \times 10^{-4} \exp[16.592(\theta-0.02)]$ | 0.940 | $D = \begin{cases} 7.972 \times 10^{-4} \exp[11.747(\theta-0.02)], & 0.02 < \theta < 0.352 \\ 4.689 \times 10^{-6} \exp[26.779(\theta-0.02)], & 0.352 < \theta < 0.56 \end{cases}$ | 0.929<br>0.976 |
| PROFILE 2 | | | | |
| $P_2H_1$ | $D = 9.467 \times 10^{-4} \exp[14.054(\theta-0.02)]$ | 0.991 | - | |
| $P_2H_2$ | $D = 3.277 \times 10^{-4} \exp[16.780(\theta-0.02)]$ | 0.936 | $D = \begin{cases} 6.096 \times 10^{-4} \exp[14.012(\theta-0.02)], & 0.02 < \theta < 0.357 \\ 4.718 \times 10^{-5} \exp[21.600(\theta-0.02)], & 0.357 < \theta < 0.57 \end{cases}$ | 0.934<br>0.989 |
| $P_2H_3$ | $D = 1.765 \times 10^{-4} \exp[18.235(\theta-0.03)]$ | 0.963 | $D = \begin{cases} 5.198 \times 10^{-4} \exp[10.869(\theta-0.03)], & 0.03 < \theta < 0.32 \\ 4.321 \times 10^{-6} \exp[27.408(\theta-0.03)], & 0.32 < \theta < 0.57 \end{cases}$ | 0.926<br>0.981 |
| $P_2H_4$ | $D = 2.730 \times 10^{-4} \exp[16.692(\theta-0.03)]$ | 0.942 | $D = \begin{cases} 7.802 \times 10^{-4} \exp[10.111(\theta-0.03)], & 0.03 < \theta < 0.356 \\ 9.024 \times 10^{-7} \exp[30.744(\theta-0.03)], & 0.356 < \theta < 0.57 \end{cases}$ | 0.924<br>0.993 |

4.4.d. Identification of the Structure for Soil Water Diffusivity

Using data from each horizon, features are calculated according to Eq. (4.16) and (4.17) and plots of feature points, $f_1$-$f_2$ and $f_1$-$f_3$ are prepared. Figures 4.5 (a) and (b) illustrate, respectively, the plots obtained with $P_1H_1$ and $P_2H_1$. From these figures it is clear that the exponential function fits the data best. A similar trend is also observed with all other horizons.

4.4.e. The Diffusivity Function

Diffusivity functions (Model 1) are fitted to the data from the various horizons. Even though high correlation coefficients are obtained in all cases it is found that the derived functions underpredict the $D(\theta)$ values at and near saturation by as much as 30%. Obviously, this is going to have an effect on the solution of Richards' equation. Therefore, a piecewise (2-parts) exponential function is fitted to each of the $D(\theta)$-$\theta$ relationships, except in the case of soil $P_2H_1$ where a unique function is found adequate. The results for the eight soil horizons are presented in Table 4.5.

## 4.5. DISCUSSION AND CONCLUSION

The pattern recognition approach has been applied to the structure characterization of two soil properties, namely, the soil moisture characteristic and the soil water diffusivity. While the method was able to elineate the most suitable model for the diffusivity (i.e. an exponential function) from three possible candidate models, classification in a two-dimensional feature space achieved limited success in the structure identification of the soil moisture characteristic. Two of the candidates, an asymptotic model (Model 1) and the Brooks and Corey model (Model 3) were equally adapted to the data. Better discrimination could probably be obtained by using better and/or more features, the latter entailing classification in multi-dimensional space.

The training stage of the procedure admittedly entails heavy computations, however, once this stage is complete, processing of each data set requires minimal effort. In fact, it took less than 0.5 hour of computation time on the CDC 1700 (32K) to process the diffusivity data and to plot the graphs of $f_1$- $f_2$ and $f_1$- $f_3$ for all the 8 test cases. Together with the fact that the technique can give different results from the least squares method leads to the conclusion that the pattern recognition approach provides us with a useful technique in the identification of model structures of poorly defined systems.

CHAPTER 5

# EVALUATION OF NUMERICAL METHODS FOR SOLVING RICHARDS' EQUATION

## 5.1 INTRODUCTION

Simulation studies on unsaturated and partly saturated soil water flow have been dominated by the finite difference methodology. The ready acceptance of the finite difference method is primarily due to the ease of this approach in handling one-dimensional and two-dimensional problems of regular geometry, which constitute the main areas of interest in unsaturated and partly saturated flow.

In dealing with non-uniform systems of complex geometry and unusual boundary conditions, however, the finite difference approach becomes rather difficult to apply. The way prescribed flux boundaries are handled often leads to a non-symmetric matrix, which is a disadvantage if the equations are to be solved simultaneously at all nodes by means of a direct method such as the Gaussian elimination scheme.

The finite element method does not recognize such problems as associated with the finite difference method. Indications of the flexibility in varying the size of elements and in treating prescribed flux boundaries can be seen from the mathematical derivations in Chapter 2 even for the simple one-dimensional case. Hence, in recent years the Rayleigh-Ritz and Galerkin finite element methods have found growing acceptance and applications in the field of hydrology and groundwater flow (Guymon et al., 1970; Fang and Wang, 1972; Pinder and Frind, 1972; Smith et al., 1973). Similar progress, unfortunately, has not occurred in unsaturated soil water flow.

A recent finite element analysis of two-dimensional flow in soils considering water uptake by plant roots (Feddes et al., 1975), while providing evidence of the flexibility of the finite element approach, however, yielded poorer results than the finite difference method. A more fundamental look at the finite element approach is, therefore, necessary before considering the possibility of extending it to complex unsaturated

flow problems.

In this chapter, apart from the need to validate Richards' model for the soil under study, a critical examination is made of the finite element and finite difference approximation methods when applied to flow in one dimension. The assessment is based not only on accuracy, but also on programming ease and usage of computer time in conjuction with both forms of Richards' model, i.e., the $\theta$-based and h-based equation.

It was also seen in the previous chapter that the moisture characteristic curve can be represented equally well by two models (Eq.4.1 and 4.3). The merits of both models will be examined in reference to the infiltration process.

## 5.2 METHOD

The two forms of Richards' model were solved by the finite difference and finite element methods for the two cases of ponded infiltration and rain infiltration (specified flux). Philip's quasianalytical solution for the $\theta$-based equation was also obtained for the case of ponded infiltration into air dry soil. The idea was to provide some indication of the magnitude of the computational and numerical approximation errors involved.

Due to some difficulty in time marching in the case of the h-based equation for the air dry initial condition, the Kirchoff transformation has been applied and the resulting equation solved by the finite difference method. The finite element approximation has been omitted in the latter for reasons that will be apparent later. A list of models and discretization methods used is given in Table 5.1

Table 5.1 Various forms of Richards' equation and the spatial approximations used in the numerical simulation.

| Equation | Spatial discretization | Abbreviation |
|---|---|---|
| $\theta$-based (Eq.2.2) | Finite difference | $\theta$-FD |
| | Finite element | $\theta$-FE |
| h-based (Eq.2.1) | Finite difference | h-FD |
| | Finite element | h-FE |
| h-based (Kirchoff transformation Eq.2.25) | Finite difference | v-FD |

## 5.2.a Computer Programs and Numerical Considerations

For convenience three main programs with associated subroutines were prepared for the θ-, h- and v-equations respectively. The choice between the finite difference and finite element method as well as that of the integration sheme (factor $\nu$) were made by relevant input parameters. Each program consists of a main line with a series of subroutines for various operations. The simulation aspect of the problem, i.e., changing boundary conditions, water balance, etc., were also incorporated at this stage of the study so that the sensitivity of the different algorithms could be examined. The bases of the solution process have been discussed in Chapter 2. Details of the program organization are shown in Fig.5.1, and for the sake of completeness the important steps in the computational procedure are described below.

### (i) Input

The input consists of the soil hydraulic properties in tabulated or formula form, the initial and boundary conditions, the parameter which specifies finite difference or finite element method, the integration factor $\nu$, the size of the distance step $\Delta z$, the initial time step, the convergence parameter $\varepsilon$,etc. Unless otherwise stated, a value of $\nu$=0.5 corresponding to the Crank-Nicolson scheme was used in all computations.

### (ii) Trial Nodal Values

For time t=0, the initial values of {u} are taken to be the trial nodal values. At succeeding time steps the trial values are given by Eq. (2.40) where the constant c is assigned the value of 0.7 .

### (iii) Boundary Conditions

In ponded infiltration problems, treatment of the boundary at z=0 is straightforward, that is, by setting $u_o^j = u_o$ for all j. By taking L large enough so that the soil is effectively semi-infinite we can set $u_L^j = u_L$ for all j. The case of finite L should pose no extra difficulty. In physical terms, however, it would be more appropriate to consider this case as one in which flux is specified, hence requiring some specification of $q_L$.

For rain or specified flux infiltration, the derivative boundary condition applies so long as the soil surface remains unsaturated. Assuming no structural changes, the surface would remain so provided rain intensity $q_o$ is less than the saturated conductivity of the soil. For $q_o$ exceeding the saturated conductivity the surface condition must be tested for

the occurrence of ponding or runoff. Ponding occurs when both the following conditions are met: a) $q_o \geqslant$ potential infiltration rate, and b) $\theta_o^j \geqslant \theta_{sat}$. Concurrently, the boundary condition is changed to $\theta_o^j = \theta_{sat}$ or $h_o^j = 0$ for all j. If, however, the soil surface has a capacity to detain water to a maximum effective depth, DETCAP, then $h_o^{j+1}$ is estimated according to the equation

$$h_o^{j+1} = \text{DETAIN} + \Delta t^j (q_o - \text{RATEIN})$$

where DETAIN is the depth of detained or ponded water at time $t^j$ and RATEIN is the infiltration rate.

Although the phenomena of redistribution and evaporation are not directly related to the present study these are readily handled and have been included in the subroutine FORM. Hysteresis, however, is neglected. The boundary at z=0 becomes an evaporating surface with simultaneous redistribution of the soil water as soon as both DETAIN and rain intensity become zero. If the potential flux upwards from the soil surface, which is numerically equal to the infiltration rate RATEIN, is less than the potential evaporation rate (PEV) due to atmospheric demand, then evaporation equals RATEIN. Otherwise, evaporation equals PEV.

(iv) Convergence Test

Convergence is achieved when the relative error between successive iterations is less than a specified parameter value (Eq.2.41). In the $\theta$- and h- equations the value of $\varepsilon$=0.002 is used in all computations.

For the v-FD model the relative error term defined by Eq.(2.41) is found to be unsatisfactory because v approximates an increasing exponential function of $\theta$. The change of v is very small at low $\theta$ values and increases as $\theta$ increases towards saturation. Thus $\varepsilon$ will be too large when the soil is relatively dry and too small when the soil becomes wet. The former results in a poor approximation. For example, at the beginning of infiltration only 1 iteration is sufficient for convergence but later when the upper part of the soil is sufficiently wet a larger number of iterations is required and usually the solutions fail to converge. To overcome this, a scaled or weighted error term is defined and the test is as follows.

$$\max_i \frac{| v_i^{j+1,k+1} - v_i^{j+1,k} |}{(\theta_i^j)^3} \leqslant \varepsilon$$

A much smaller value $\varepsilon$=0.0005 is specified in this case.

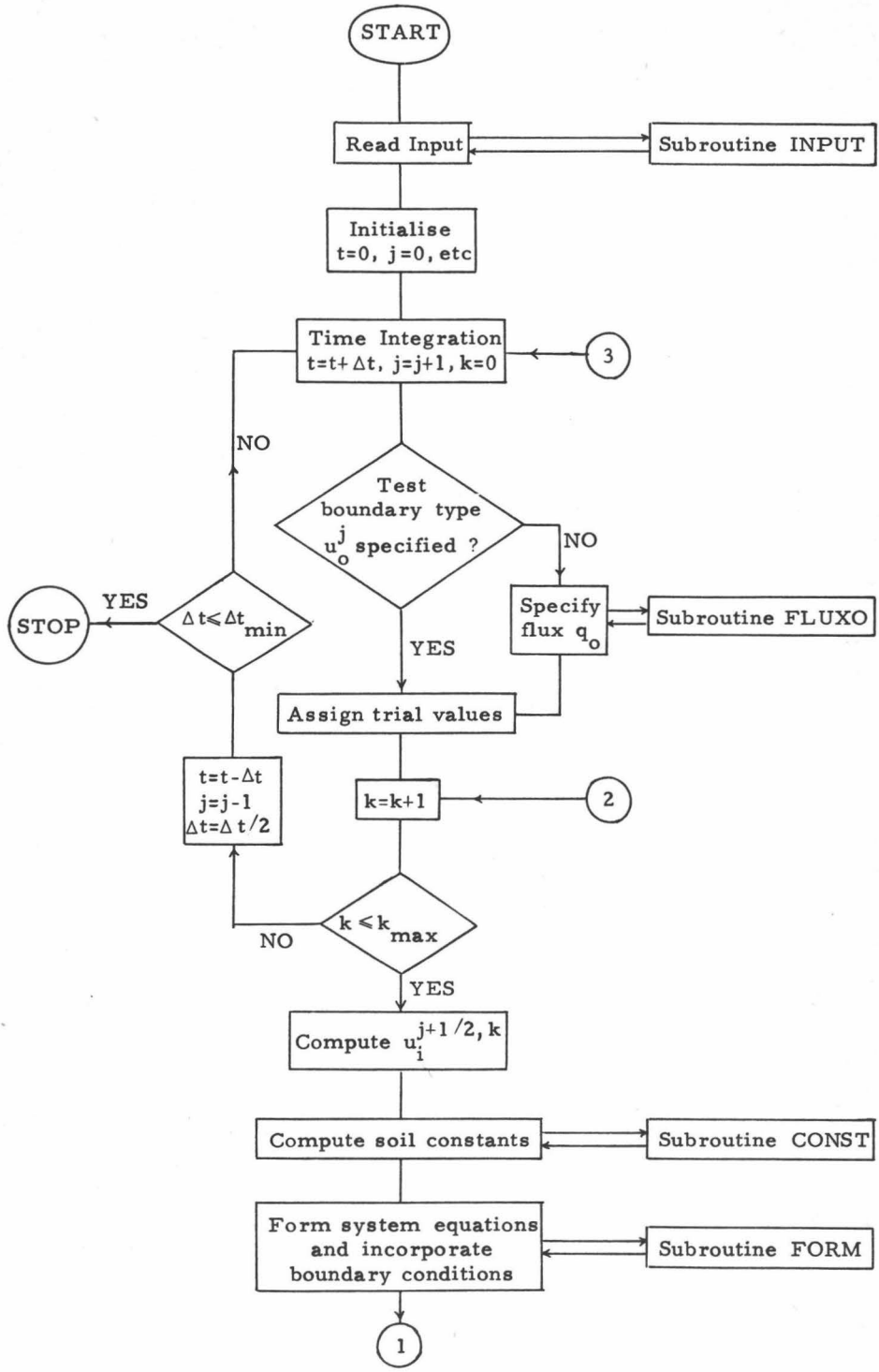
START
Read Input
Subroutine INPUT
Initialise
t=0, j=0, etc
Time Integration
t=t+Δt, j=j+1, k=0
3
NO
Test
boundary type
$u_o^j$ specified ?
NO
YES
Specify
flux $q_o$
Subroutine FLUXO
STOP
YES
Δt≤Δt min
Assign trial values
t=t-Δt
j=j-1
Δt=Δt/2
k=k+1
2
k ≤ k max
NO
YES
Compute $u_i^{j+1/2,k}$
Compute soil constants
Subroutine CONST
Form system equations
and incorporate
boundary conditions
Subroutine FORM
1

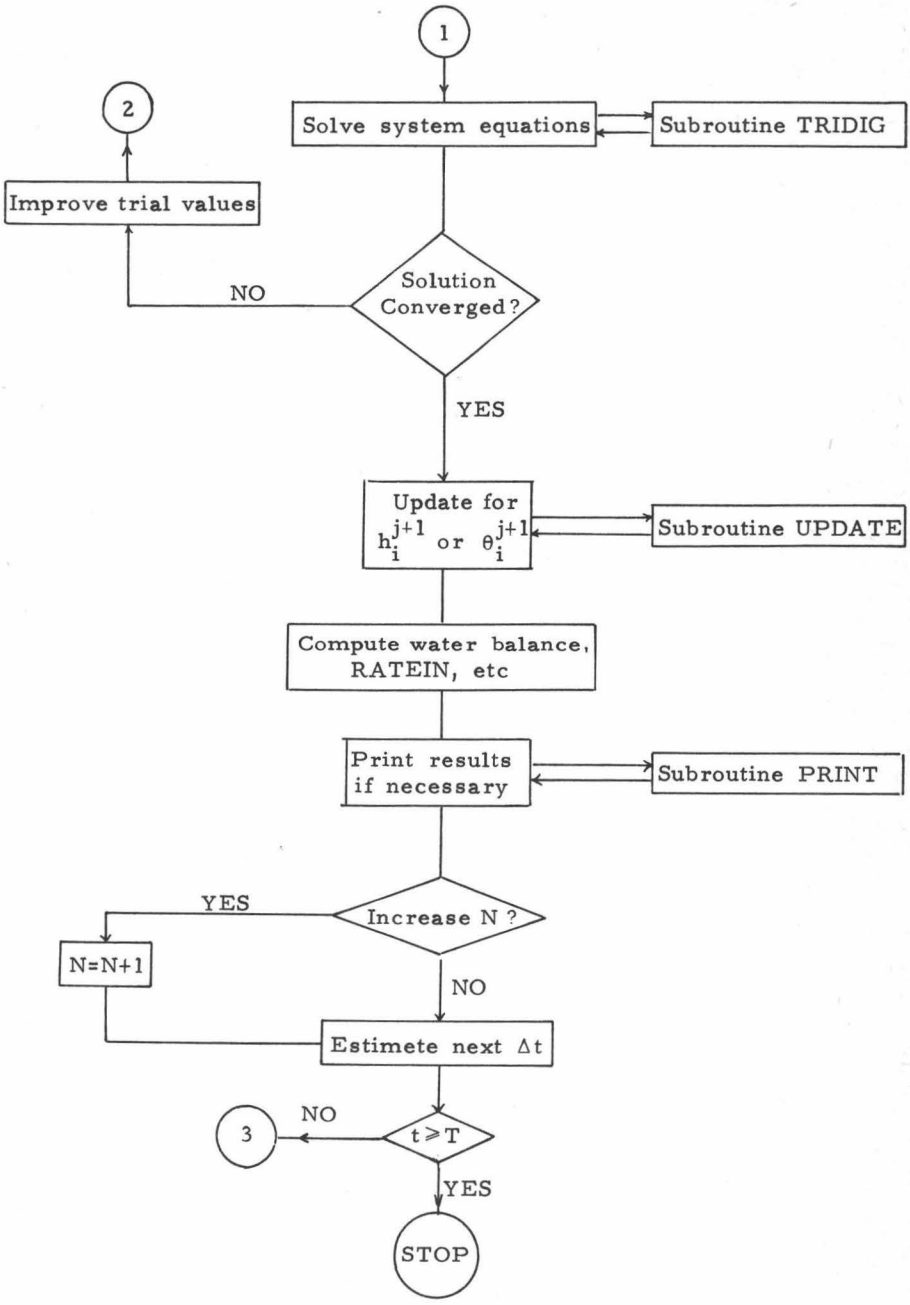


Fig. 5. 1 Flow chart for solving Richards' equation by finite element or finite difference approximation.

(v) Water Balance

The total amount of water in the soil profile is calculated by the trapezoidal rule and the difference between the amounts at time $t^j$ and at the start gives the cumulative infiltration (QCUM) assuming no net drainage from the profile. Infiltration rate, RATEIN is calculated according to Darcy's Law approximated by

$$\text{RATEIN} = 0.5(K_o^{j+1/2} + K_l^{j+1/2})(h_l^{j+1/2} - h_o^{j+1/2} - g\Delta z)/\Delta z$$

where $h_i^{j+1/2} = 0.5(h_i^{j+1} + h_i^j)$. This same value of RATEIN is assigned to the potential infiltration rate when testing the boundary condition at the succeeding time step.

For rain infiltration, the amount of water detained after the surface layer is saturated assuming a non-zero detention capacity, is simply the difference between total amount of rain that has fallen and the cumulative infiltration.

(vi) Adjustment of Time Step-size

There is no objective criterion based on rigorous mathematical treatment available for varying the time step-size in the implicit scheme adopted for this study. The scheme is unconditionally stable for linear problems (Richtmeyer and Morton, 1967). In the case of nonlinear problems, however, this unconditional stability does not always hold and it is necessary to base the time increment on the condition $(\Delta t/\Delta z^2) \leq 1/D_{max}$, where $D_{max}$ is the maximum diffusivity. This leads to a constant $\Delta t$ for ponded infiltration problems since $D_{max}$ in this case is constant. If $\Delta z$ were set at 1 cm then $\Delta t$ would be of the order of 3 seconds, which is rather unsatisfactory for long simulation runs.

The iterative scheme employed, however, allows some freedom in the choice of $\Delta t$. It is noted that in ponded infiltration the moisture distribution changes rather slowly with time and the infiltration rate decreases almost exponentially in function of time. The time increment is now chosen such that there occurs a constant amount of infiltration during each time step (Hanks and Bowers, 1962; Zaradny, 1978), that is,

$$\Delta t = F.\Delta z/\text{RATEIN}$$

where F is a constant. A few trial runs are made to establish the range of F for "optimal conditions". The range is found to be 0.04 - 0.07 for the $\theta$- and h- equations, and 0.02 - 0.04 for the v-model. For rain infiltration a similar expression is used with $q_o$ replacing RATEIN. However,

smaller values have to be assigned to F in order to obtain a reasonable prediction of ponding time. The values are 0.02 for the $\theta$-model and 0.01 for h- and v- models.

If the iteration cycle does not converge within the maximum number of iterations allowed (MAXIT), in this case 20, the time step-size is halved and the integration step repeated. This procedure is continued until convergence is achieved or $\Delta t$ becomes less than a specified minimum value, $\Delta t_{min}$. Should the latter occur, computation is stopped and repeated using different values of $\varepsilon$ and F.

(vii) Computational Nodes

In order to speed up computation where possible N is initially set at a low value of say, 8. As time integration proceeds N is increased by 1 whenever the water content at the (N-1)th node changes by 0.0001 $cm^3/cm^3$ and subsequently kept constant when the maximum value for N is reached.

5.2.b Experimental Verification

The following experiments were performed in order to verify the results of the numerical simulation for different infiltration problems with soil $P_1H_1$.

(i) Vertical infiltration at zero pressure head into air dry soil.

(ii) Specified flux (rain) infiltration into air dry soil.

(iii) Specified flux (rain) infiltration into soil with initial conditions defined by $h(z,0) = z-60$ cm.

Soil columns were prepared in the same manner as described in Chapter 3 for the capillary rise experiments. For experiment (i) the infiltration procedure was the same as for the determination of saturated conductivity (Section 3.5). Infiltration was stopped at 100 minutes and the soil column immediately divided into sections for determining the moisture profile.

For specified flux infiltration, flux was imposed on the soil surface which was protected by a 3 mm layer of fine sand, by water drops falling from a 3 mm raindrop former or from a burette. The calibration curve for the drop former (copper capillary) in terms of flow rate in mm/hr over a surface area of 8.043 $cm^2$ (this being the cross-sectional area of the soil column) and number of drops per minute as functions of water head $H_w$ over the drop-former are given in Fig.5.2. It is seen that the lowest flux that can be obtained conveniently is approximately 70 mm/hr. Smaller fluxes of 25 and 50 mm/hr (see Section 5.3.a) had to be supplied using a burette.

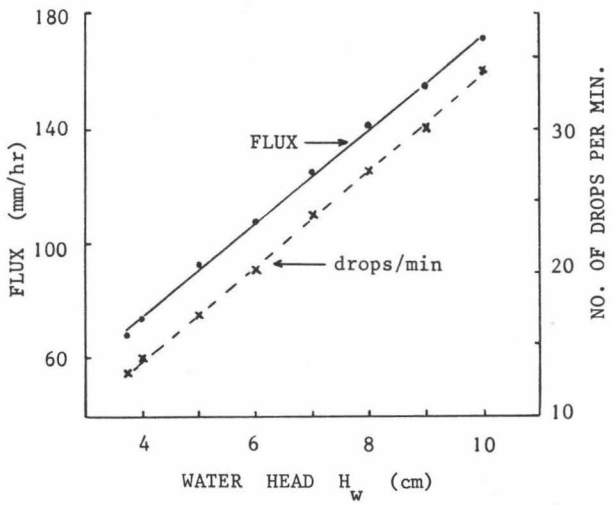


Fig. 5.2 Calibration curves for a 3 mm raindrop former.

For experiment (iii), the wet soil column was prepared by capillary rise into 35 cm length of air dry soil column with water entering the bottom at a pressure head of -25 cm water. When the whole length of the soil column was wet the top was covered to prevent evaporation and the column allowed to equilibrate under gravity. An additional period of 24 hours was found sufficient to attain equilibrium. The cover was then removed and water was supplied to the top of the column at specified flux.

In all experiments the wetting depth was recorded at frequent intervals and the time of occurrence of ponding, i.e., when the soil surface became saturated and completely covered by a thin film of water, was also noted. Experiment (ii) was stopped after 36 minutes while experiment (iii) was stopped earlier, at 30 minutes, and the soil columns sectioned for water content determination.

## 5.3 RESULTS AND DISCUSSION

### 5.3.a θ-based Equation - Model Validation and Comparison between FD & FE

The soil hydraulic properties used to derive numerical solutions in this section were all in tabulated form. These consisted of the diffusivity function $D(\theta)$ depicted in Fig.3.7(a) and the moisture characteristic curve $h(\theta)$ obtained by eye fitting through the relevant points in Fig.3.3(a).

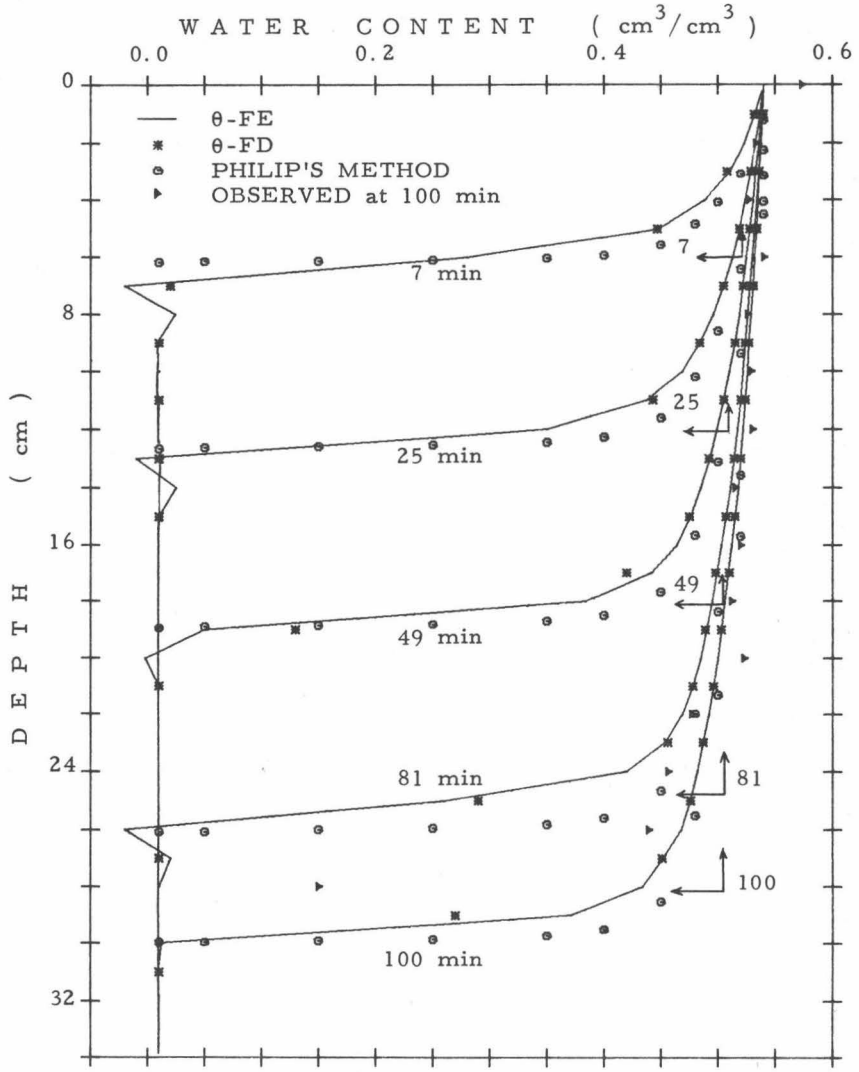


Fig. 5.3 Computed ($\theta$-based equation) and observed water content profiles for infiltration at zero pressure head into air dry soil $P_1H_1$. Horizontal and vertical arrows indicate position of wetting front and mean water content respectively.

(i) Ponded Infiltration

Water content profiles in $P_1H_1$ resulting from infiltration at zero pressure head into air dry soil obtained by the finite difference, finite element and Philip's quasianalytical methods are presented in Fig.5.3. In obtaining Philip's solution only the first three terms of the power series in Eq.(2.5) were considered. The contribution of the third term was of the order of 1.5 cm for t=100 minutes and, hence, the fourth term would be negligible. Also shown are the observed positions of the wetting front and mean water content (the latter is the ratio of total infiltration to the wetting depth) at different times and the measured profile at 100 minutes.

The finite difference and the finite element solutions are almost identical. The averaging operator or the [A] matrix in the finite element approximation causes small oscillations in the solution at and beyond the wetting front giving $\theta$ values less than the initial value . However, this does not affect the overall performance of the method.

Both approximation methods show fair agreement with Philip's method indicating that the numerical and computational error associated with either method is small. However, all three methods appear to give overpredictions when compared to experimental results. For example, after 100 minutes, the observed total infiltration is 13.88 cm water while those computed by $\theta$-FD, $\theta$-FE and Philip's method are 14.58, 14.59 and 15.24 cm water respectively. The corresponding wetting fronts are 28.1, 30.0, 30.0 and 30.0 cm respectively. The lack of agreement could be due to one or all three of the following reasons:

- experimental error arising from non-uniform packing and poor initiation of the infiltration,
- error in the computed results due to uncertainties in $D(\theta)$ and $C(\theta)$ functions, and
- the working model is inadequate for describing water flow in this particular soil.

Of these the first two appear to be most probable because of the usually large error associated with such kind of experiments. An indication of the variability in infiltration measurements can be seen from the saturated with variations of up to 10% are in fact less than the maximum variation of about 18% in the latter. We are, therefore, quite justified in accepting Richards' equation and, hence, Darcy's Law as valid descriptions of unsaturated water flow in the soil being investigated.

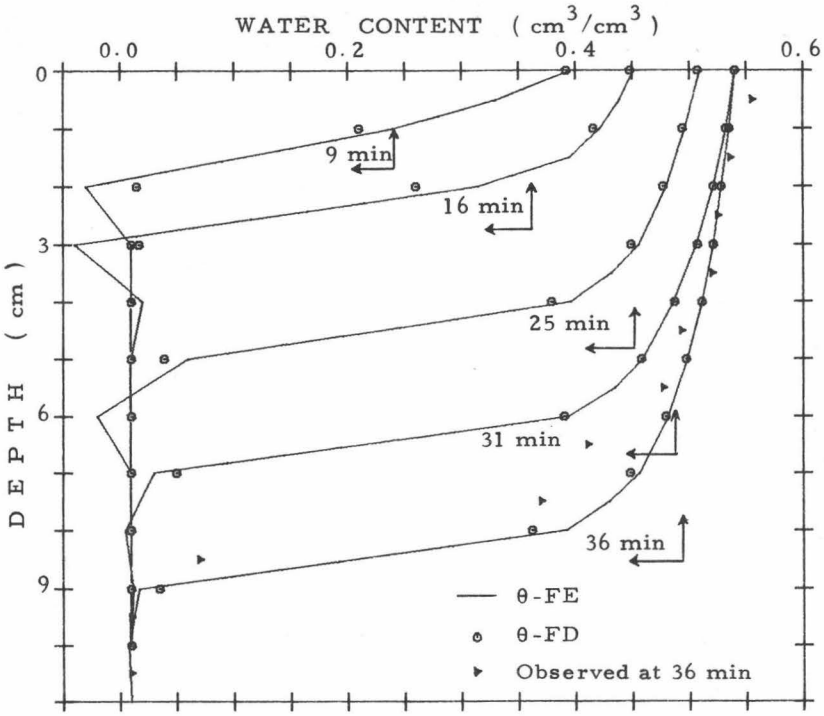


Fig. 5.4 Computed (θ-based equation) and observed water content profiles during infiltration at specified flux into air dry soil $P_1H_1$. Horizontal and vertical arrows indicate position of wetting front and mean water content respectively.

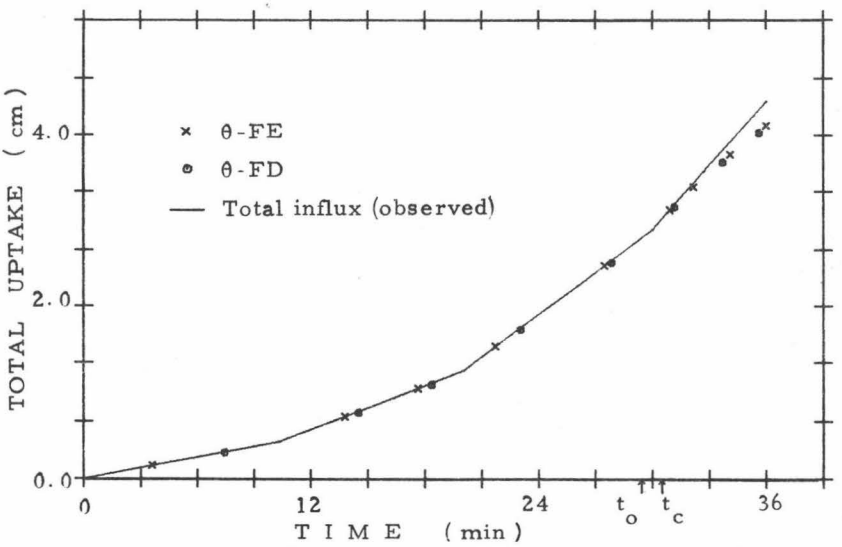


Fig. 5.5 Computed (θ-based equation) and observed total water uptake during infiltration at specified flux into air dry soil $P_1H_1$ ($t_o$ = observed time of ponding; $t_c$ = computed ponding time for both FE and FD methods).

(ii) Rain Infiltration

For investigating the mass balance of the two approximation methods both were run subject to the initial conditions $\theta(z,0)=0.01$ and boundary condition $-(D.d\theta/dz - K)_{z=0} = q_o$, where $q_o$ is given as a step function

$$q_o = \begin{cases} 25 \text{ mm/hr}, & 0 \leq t < 10 \text{ min} \\ 50 \text{ mm/hr}, & 10 \leq t < 20 \text{ min} \\ 100 \text{ mm/hr}, & 20 \leq t < 30 \text{ min} \\ 150 \text{ mm/hr}, & 30 \leq t < 40 \text{ min} \end{cases}$$

Figures 5.4 and 5.5 show respectively the water content profiles and the total infiltration or uptake for different times, obtained by the finite difference and finite element spatial approximation methods as compared to the measured values. Except for early times, the water content profiles in both methods are essentially the same. The profiles at 36 minutes are in satisfactory agreement with the observed inspite of the rather unsophisticated means of supplying water to the soil surface. The computed ponding times in both cases are 30.4 minutes compared to the observed time of 29.2 minutes. The mass balance, defined as the relative error in the computed total infiltration when compared to the actual amount infiltrated is slightly superior in the case of the finite element method, the relative error up to the time of ponding being only 0.33% in comparison to 0.67% for the finite difference. This is to be expected since the treatment of the boundary condition by the former method is more natural and exact. However, even with the finite difference method, the mass balance is more than adequate for predictive purposes.

(iii) Computer Time and Programming Considerations

For similar input and output specifications the running time (compilation + execution) on the Siemens 4004 for a 2 hour ponded infiltration into air dry soil is 45.2 sec for the $\theta$-FD and 60.2 sec for the $\theta$-FE. Although the rate of convergence is the same in both cases, needing on the average, only 2 iterations per time step, the small oscillations in the proximity of the wetting front in the latter method generated a larger number of computational nodes. The difference in computer time would even be greater if the programs were prepared separately in view of the fact that the coefficient matrix as well as the right-hand side vector in the tridiagonal system are easier to calculate in the case of $\theta$-FD.

The above comparisons show that both $\theta$-FD and $\theta$-FE provide excellent approximations for the infiltration process. Since there is only

a marginal difference in accuracy, the finite difference method must be preferred considering its shorter running time and greater ease in programming. In this study, however, a compromise is made whereby, in the numerical solutions to follow, $\theta$-FD will be used for ponded infiltration and $\theta$-FE for rain infiltration.

5.3.b Comparison of Models for Soil Water Characteristic

Two models which appear to characterize the soil water retention curve well are those given by Eq.(4.1) or Model 1 and Eq.(4.3) or Model 3. Richards' Eq.(2.1) and (2.2) were solved numerically using as inputs the soil water capacity C, defined by Eq.(4.1) and (4.3), and the soil water diffusivity as an exponential function of $\theta$. It is noted here that even though the diffusivity function is better represented by a piecewise rather than a single function, preliminary tests with both showed that a single function representing the upper 50% saturation or so yielded results not significantly different from those obtained using a piecewise function. This is in accordance with Hanks and Bowers (1963) who asserted that the infiltration process is largely, if not entirely governed by soil properties at the higher saturation range. Therefore, poor estimation of the parameters at the low moisture range will not materially affect the overall prediction of the flow pattern. A single exponential function function was thus used as the $D(\theta)$ input in this study since this would incur less computation and programming effort.

The initial conditions considered were those of air dryness for the $\theta$-based equation and field capacity, defined by $h(z,0)=-345$ cm for the h-based equation. The boundary conditions were those for ponded infiltration as well as rain infiltration with intensities as defined in Section 5.3.a. Solutions were all obtained using the finite difference approximation except in the case of rain infiltration into air dry soil where the $\theta$-FE was used.

Figure 5.6 depicts the cumulative infiltration into air dry soil obtained via Model 1, Model 3 as well as tabulated values to represent the soil water characteristic curve. With results obtained using tabulated input data as a basis of comparison, Model 3 gives a better prediction of cumulative infiltration during ponded infiltration. For rain infiltration the mass balance are similar in both cases. However, due to a slight difference in the shape of the $\theta$-profiles (not shown here) ponding commences at slightly different times with the different models. The difference is, nevertheless, too small to merit further discussion.

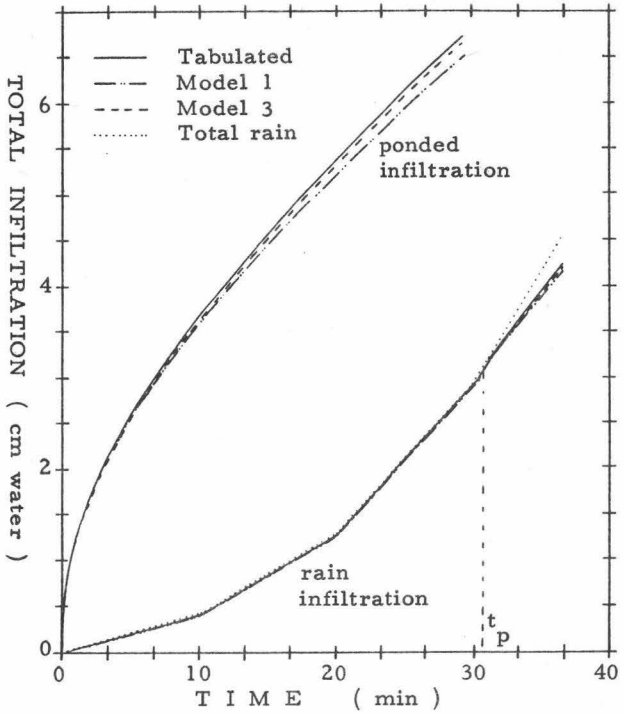


Fig. 5.6 Total infiltration versus time for infiltration into air dry soil $P_1H_1$ computed using the θ-based equation and different models for the soil water characteristic ($t_p$ is the ponding time for all models).

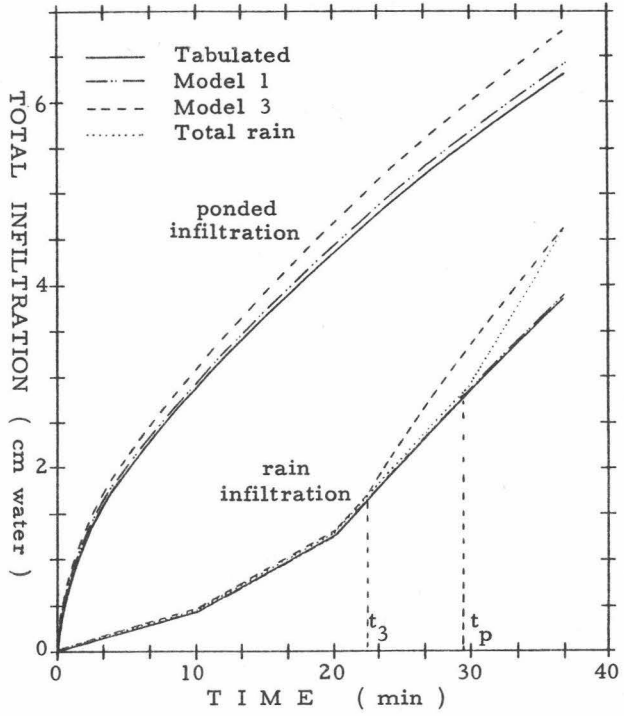


Fig. 5.7 Total infiltration versus time for infiltration into soil $P_1H_1$ at field capacity computed using the h-based equation and different models for the soil water characteristic ($t_3$ is ponding time for Model 3 and $t_p$ for others).

Suffice to say that both models are equally suited for the θ-based equation.

The corresponding results for infiltration into soil at field capacity using the h-based equation are presented in Fig. 5.7. In both types of infiltration, Model 3 is inferior to Model 1. For ponded infiltration, it gives a marked overprediction of cumulative or total infiltration while in the case of rain infiltration, ponding is initiated very much earlier and as a result, the subsequent mass balance is very poor. This is due to the exaggerated influence of the physical properties at and near saturation. In ponded infiltration, saturation of the upper portion of the soil is attained at an early stage because of a substantial negative value of $h_a$. This in turn confers greater permeability (conductivity) to the upper part, thereby, resulting in increased rates of infiltration. The situation during rain infiltration is very much similar. The surface reaches saturation earlier than expected when $h_o = h_a$. The specific water capacity of the surface layer becomes zero at this stage and, concurrently, the boundary condition of prescribed flux changes to one of prescribed pressure head ($h_o$ = 0 cm), and with it an accelerated infiltration. Model 1, on the other hand, has an equivalent $h_a$ of -1 cm. Thus, the error in estimating ponding time is much smaller.

Based on the above results Model 1 would certainly be more preferable for describing wetting processes as is the case in infiltration. Model 3, on the other hand, would be more suited to drying processes such as drainage since it is known that the soil remains saturated as suction is applied to it until a critical value of $h_a$ or air entry value is exceeded. Only then will the soil begin to drain.

Inputs: On the basis of the findings in this section, inputs for all numerical solutions to follow shall consist of the θ - h relationship given by Model 1 and the diffusivity as an exponential function of θ.

5.3.c h-based Equation

For assessing the relative performance of the h-FD, h-FE and the v-FD models, these models were solved for different initial conditions and subject to the boundary conditions of the type defined in Section 5.3.a, translated into pressure head terms. The initial conditions considered were as follows:

I. $h(z,0) = -10^8$ cm (air dry soil)
$\theta(z,0) = 0.0225$ cm$^3$/cm$^3$

II. $h(z,0) = -50000$ cm
$\theta(z,0) = 0.0602$ cm$^3$/cm$^3$

III. $h(z,0) = -15000$ cm (15 bar suction or wilting point)
$\theta(z,0) = 0.0772$ $cm^3/cm^3$

IV. $h(z,0) = -345$ cm (1/3 bar suction or field capacity)
$\theta(z,0) = 0.2034$ $cm^3/cm^3$

V. $h(z,0) = z - 60$ cm (wet soil in equilibrium in the

VI. $h(z,0) = z - 38$ cm presence of a water table)

The depth of the soil, L was chosen large enough so that the medium was effectively semi-infinite in the course of the simulation run. To provide comparisons with θ-models, the θ-FD (for ponded infiltration) and θ-FE (for rain infiltration) models were also solved for the same initial conditions (in the case of air dry condition, solutions have already been obtained in the immediately preceding section). The results are now discussed in terms of stability, mass balance, programming ease and computer time.

(i) Stability

The θ- and v-FD models with implicit time marching show excellent stability properties, allowing for a wide choice of initial time step-size. For example, with $\Delta z$=1 cm, initial time steps varying from 1 to 10 seconds for the θ-models and from 1 to 5 seconds for the v-FD model had negligible consequence on the final results. This, however, was not the case with the h-models. Time marching during ponded infiltration failed after the first time increment of 1 sec in the case of the two driest initial conditions, meaning that the solutions failed to converge within the specified number of iterations inspite of repeatedly reducing the time step-size. To circumvent this problem, small constant step sizes of 0.2 sec and 0.01 sec were used for ponded infiltration with -50000 cm and $-10^8$ cm initial conditions, respectively, during the first 30 time integration steps before invoking the variable time increment criterion discussed in Section 5.2.a. It was necessary to impose this severe restriction because of the large pressure head gradients at the start of the infiltration. After the wetting front had progressed by 1 or 2 cm and the pressure head gradient significantly reduced, the restriction could be removed and time marching proceeded in a normal manner. For rain infiltration, however, where smaller pressure head gradients exist at the start compared to ponded infiltration, initial time steps as large as 5 sec and 2 sec could be used for $h(z,0)=-50000$ cm and $-10^8$ cm, respectively, without encountering stability problems. With wetter initial conditions, the h-models exhibit similar stability properties as the θ- and v-FD models.

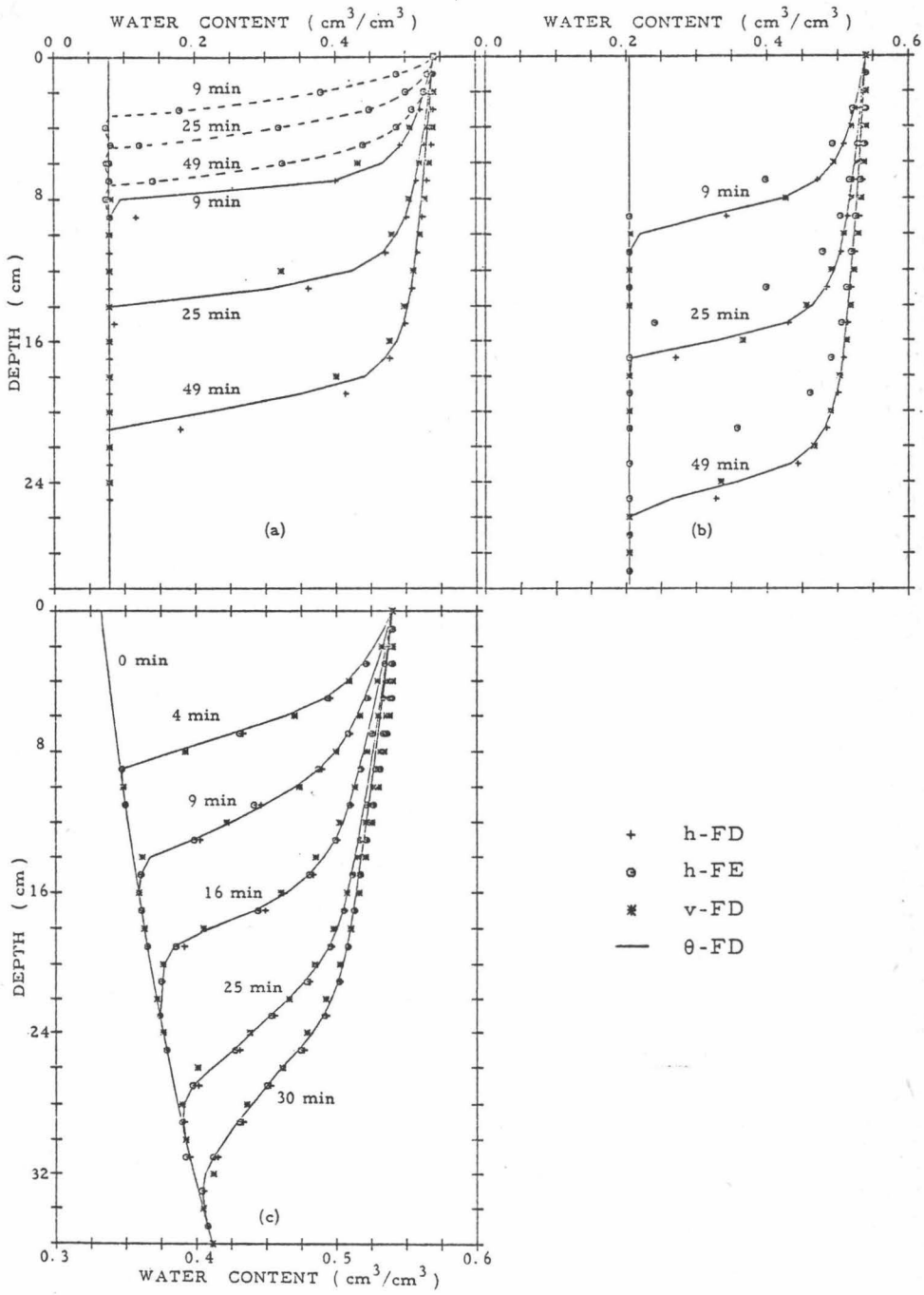


Fig. 5.8 Simulated water content profiles during ponded infiltration into soil $P_1H_1$ at different initial conditions: (a) $h(z,0)=-15000$ cm, (b) $h(z,0)=-345$ cm and (c) $h(z,0)=z-60$ cm.

(ii) Mass Balance

Water content profiles resulting from ponded infiltration into soil $P_1H_1$ at three different initial conditions, obtained using the different models are given in Fig. 5.8, while the corresponding results for rain infiltration are presented in Fig. 5.9. Also shown are experimental results for rain infiltration into soil initially at $h(z,0)=z-60$ cm (Fig. 5.9(c)). Cumulative infiltration and wetting depths at two time instances (30 and 60 minutes for ponded infiltration, and 20 minutes and ponding time for rain infiltration) are shown in Tables 5.2 and 5.3.

A glance at these results reveals, among others, three striking features, namely (a) the excellent performance of the $\theta$-models compared to the others, (b) the inconsistency of the h-FE model, and (c) the relatively poor performance of the h-FD with increasingly dry conditions. The discussion is begun with the first of the three.

*Excellent performance of $\theta$-models:*

The $\theta$-models are seen to provide the best results either for ponded or rain infiltration. The $\theta$-FE consistently yields the best mass balance in the rain infiltration problems while the $\theta$-FD (as well as the $\theta$-FE, previous section) shows fair agreement with experimental results of ponded and rain infiltration into air dry soil. Why this is so is probably due to the lesser degree of non-linearity of Eq.(2.2) as compared to Eq.(2.1), or simply that, relative variations in $\theta$ and $D(\theta)$ are much smaller than the corresponding variations in h and K(h). Acknowledging these facts and lacking in other means of comparison, it is therefore, justified to employ results of the $\theta$-models as bases for the evaluation of the other models.

*Inconsistency of the h-FE model:*

The h-FE model yields very poor results for the drier initial conditions (field capacity and drier), underpredicting cumulative infiltration as well as depth of wetting zone. Predictions, however, improve with wetter initial conditions and are even better than the h-FD and v-FD models as the initial water content approaches saturation.

Because the conductance matrix [D], the coefficient matrix [F] and vectors {K} and {Q} are identical in the h-FD and h-FE models for the case of ponded infiltration, the poor mass balance with the h-FE model must be entirely due to the capacity matrix [A]. We note that in the h-FD model [A] is a diagonal matrix, whereas in the h-FE model it is non-diagonal. There is evidence in the literature suggesting that non-diagonal capacity matrix can lead to conceptual as well as numerical difficulties.

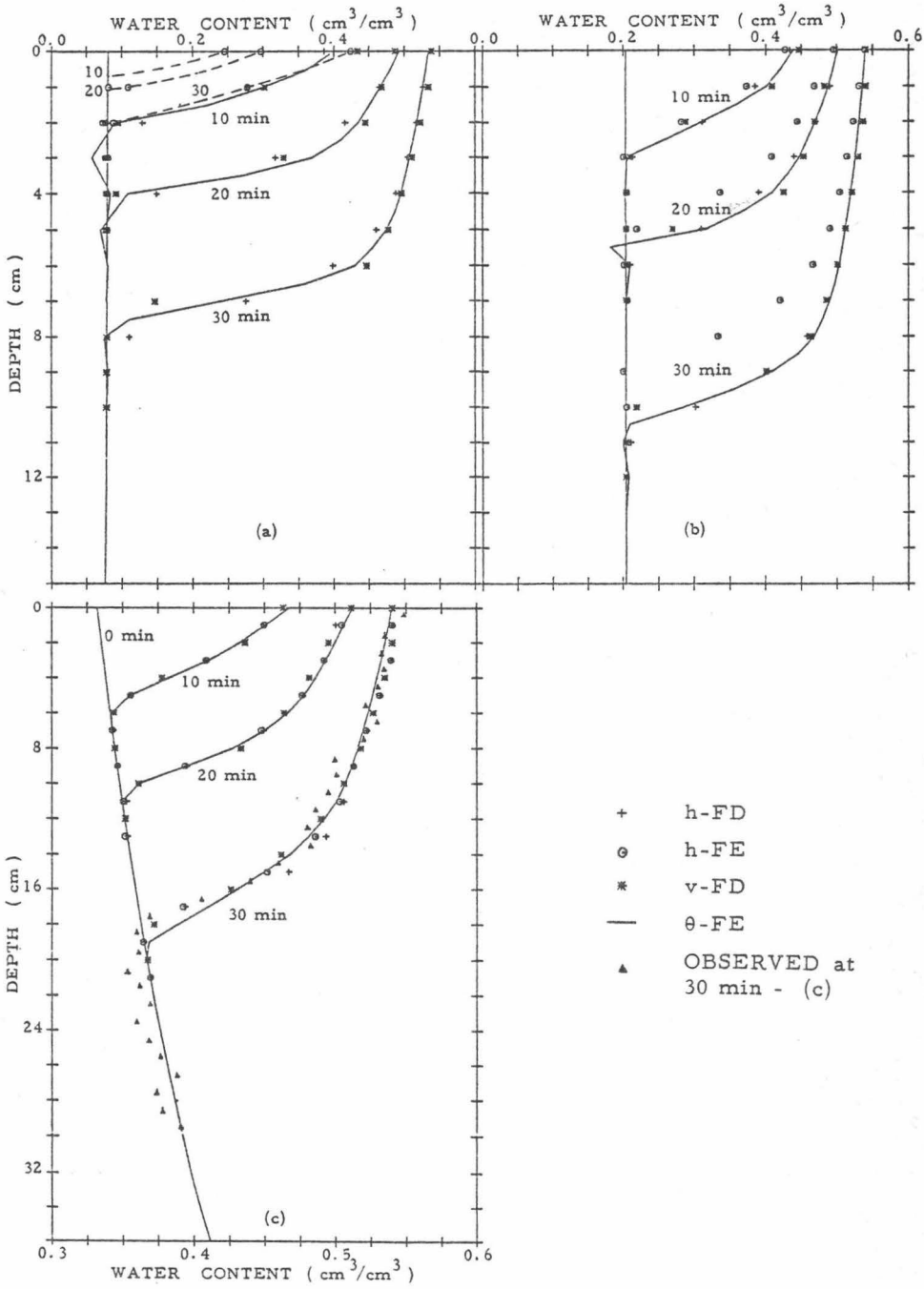


Fig. 5.9 Simulated water content profiles during rain infiltration into soil $P_1H_1$ at different initial conditions: (a) h(z, 0)=-15000 cm, (b) h(z, 0)=-345 cm and (c) h(z, 0)=z-60 cm.

Table 5.2 Comparison between simulation results for ponded infiltration into soil $P_1H_1$ at different initial conditions using different numerical methods.

| Initial condition | Method | Time = 30 min | | Time = 60 min | |
|---|---|---|---|---|---|
| | | Q cm $H_2O$ | WD cm | Q cm $H_2O$ | WD cm |
| | h - FD | 6.9311 | 16.0 | 10.5307 | 23.2 |
| h(z,0) | h - FE | 0.4105 | 1.4 | - | - |
| = - $10^8$ cm | v - FD | 6.4430 | 14.7 | 9.9542 | 22.0 |
| | θ - FD | 6.6110 | 14.6 | 10.1425 | 21.8 |
| | Experiment | 6.755 | 14.0 | 9.885 | 20.9 |
| | h - FD | 6.5468 | 17.0 | 10.0357 | 25.6 |
| h(z,0) | h - FE | 2.0676 | 5.4 | 2.9760 | 7.7 |
| = - 15000 cm | v - FD | 6.0032 | 15.7 | 9.3835 | 24.2 |
| | θ - FD | 6.2014 | 15.7 | 9.9510 | 24.2 |
| | h - FD | 5.6254 | 19.9 | 8.7753 | 30.9 |
| h(z,0) | h - FE | 4.7172 | 17.2 | 7.3630 | 28.0 |
| = - 345 cm | v - FD | 5.4967 | 19.4 | 8.5958 | 30.4 |
| | θ - FD | 5.4326 | 19.2 | 8.4930 | 30.1 |
| | h - FE* | 4.8103 | 17.5 | 7.5103 | 28.5 |
| | h - FD | 4.5830 | 34.7 | - | - |
| h(z,0) | h - FE | 4.5503 | 34.5 | - | - |
| = z - 60 cm | v - FD | 4.4843 | 34.4 | - | - |
| | θ - FD | 4.4814 | 34.5 | - | - |

Q = Cumulative infiltration WD = Wetting depth

h - FE* = Finite element method with capacity matrix diagonalized

Table 5.3. Comparison between simulation results for rain infiltration into soil $P_1H_1$ at different initial conditions using different numerical methods.

| Initial condition | Method | T = 20 min | | | At Ponding | | |
|---|---|---|---|---|---|---|---|
| | | Q cm $H_2O$ | Mass balance error % | WD cm | $T_p$ min | Q cm $H_2O$ | WD cm |
| h(z,0) = $-10^8$ cm | h - FD | 1.2051 | 3.34 | 4.1 | 30.6 | 3.0038 | 8.0 |
| | h - FE | 0.0982 | 92.1 | 1.1 | - | - | - |
| | v - FD | 1.2030 | 3.48 | 4.0 | 30.4 | 2.9333 | 6.5 |
| | θ - FE | 1.2366 | 0.03 | 3.8 | 30.4 | 2.9950 | 6.7 |
| | Experiment | - | - | 3.6 | 29.2 | 2.783 | 6.5 |
| h(z,0) = -50,000 cm | h - FD | 1.2209 | 2.05 | 4.2 | 30.4 | 2.9683 | 8.1 |
| | h - FE | 0.1120 | 91.0 | 1.2 | - | - | - |
| | v - FD | 1.2270 | 1.56 | 4.0 | 30.3 | 2.9300 | 7.3 |
| | θ - FE | 1.2360 | 0.01 | 3.9 | 30.4 | 2.9702 | 7.4 |
| h(z,0) = -15,000 cm | h - FD | 1.2213 | 2.01 | 4.5 | 30.2 | 2.9209 | 8.3 |
| | h - FE | 0.1430 | 88.53 | 1.3 | >40 | - | - |
| | v - FD | 1.2240 | 1.80 | 4.3 | 30.2 | 2.8702 | 8.0 |
| | θ - FE | 1.2366 | 0.03 | 4.3 | 30.3 | 2.9683 | 8.0 |
| h(z,0) = - 345 cm | h - FD | 1.2223 | 1.93 | 5.8 | 28.1 | 2.5837 | 9.4 |
| | h - FE | 1.0801 | 13.34 | 4.9 | 30.1 | 2.3430 | 8.9 |
| | v - FD | 1.2262 | 1.62 | 5.8 | 29.6 | 2.7627 | 9.7 |
| | θ - FE | 1.2358 | 0.03 | 5.8 | 29.3 | 2.7725 | 9.5 |
| | h - FE* | 1.1050 | 10.61 | 5.1 | 29.9 | 2.3912 | 9.0 |
| h(z,0) = z - 60 cm | h - FD | 1.2382 | 0.67 | 11.3 | 22.8 | 1.7027 | 13.0 |
| | h - FE | 1.2523 | 0.43 | 11.2 | 22.9 | 1.7163 | 12.3 |
| | v - FD | 1.2315 | 1.21 | 11.2 | 23.7 | 1.8403 | 13.0 |
| | θ - FE | 1.2361 | 0.01 | 11.2 | 23.2 | 1.7803 | 12.2 |
| | Experiment | - | - | 10.6 | 21.5 | 1.500 | 11.2 |
| h(z,0) = z - 38 cm | h - FD | 1.2411 | 0.42 | 20.0 | 22.0 | 1.5554 | 23.0 |
| | h - FE | 1.2481 | 0.14 | 19.5 | 22.0 | 1.5620 | 22.5 |
| | v - FD | 1.2380 | 0.67 | 19.8 | 22.1 | 1.5605 | 22.8 |
| | θ - FD | 1.2361 | 0.01 | 19.5 | 22.3 | 1.590 | 22.5 |

Q = cumulative infiltration WD = wetting depth

$T_p$ = time of commencement of ponding

h - FE* = Finite element method with capacity matrix diagonalized.

Total rain after 20 minutes = 1.2464 cm (for h- and v-models)

= 1.2362 cm (for θ - FE model)

Neuman and Narasimhan (1977) indicated that a non-diagonal capacity matrix may upset the maintenance of local mass or energy balance, although overall balance over the entire region may still be preserved. They maintained that unrealistic values of {h} could result when there is a sudden and drastic change in {Q} which could be remedied by diagonalizing the [A] matrix as has been done by Emery and Carson (1971). In fact, Neuman et al. (1975) were forced to diagonalize the [A] matrix in dealing with unsaturated and partly saturated flow; otherwise the finite element scheme would not converge.

As can be seen from Tables 5.2 and 5.3, in this study, the overall mass balance has not been conserved. That this inconsistency had not been observed by Neuman and Narasimhan (1977) is probably due to the fact that these authors were dealing with a predominantly saturated flow where changes in {Q} are not anywhere as drastic as in the case of unsaturated flow. As hinted at the beginning of the chapter, evidence of such inconsistency in soil water study first came into view from the results of Feddes et al. (1975) in which the finite element method underpredicted evaporation from the soil surface as compared to the finite difference method and measured evaporation. In addition, within the soil profile, the finite element was again found to underpredict the moisture contents, while the finite difference gave a slight overprediction. The authors attributed the discrepancy partly to the difference in the integration schemes employed and in the treatments of boundary conditions.

In the current investigation, the same integration scheme was used in both cases, this being the central time difference scheme with $\nu=0.5$. The finite difference model did in fact yield a slight overprediction, in the order of 2-4% when the equation for the infiltrating boundary was approximated by backward implicit scheme. An explicit approximation of the boundary condition led to a slight improvement, but this time underpredicting by 1-2%. The latter scheme was subsequently used in all simulation runs.

Diagonalizing the [A] matrix by lumping all the off-diagonal terms with the diagonal terms in the same manner as in Neuman et al. (1975) produced only a slight improvement in the mass balance but still very much inferior to the h-FD and v-FD results (see Tables 5.2 and 5.3 for $h(z,0)=-345$ cm).

The above findings clearly support the earlier claim about the repressive influence of the capacity matrix obtained by the finite element approximation. This effect is expected to be further magnified in two- or

three-dimensional problems in which more nodal specific water capacity terms are contained in the non-zero terms of the capacity matrix. It is for this same reason that the Kirchoff transformation version of the h-FE model has been omitted in this investigation.

*Poor performance of h-FD for dry initial conditions:*

Attention is now focussed on the third important feature and that is, with regards to the performance of the h-FD for dry initial conditions. Fig. 5.8 and Table 5.2 indicate a tendency for the h-FD to overpredict as the initial condition of the soil gets drier. The wetting front becomes more diffuse with increasing dryness (compare the wetting depths for air dry initial condition). This behaviour appears to be in accordance with the results of Feddes et al. (1975) cited earlier. Accumulation of round-off errors with the large negative values of {h} must certainly be the major cause for this behaviour. This could also be the reason why Staple (1966) used the $\theta$-based equation for the initial infiltration into air dry soil before solving for redistribution with the h-based equation. Under these circumstances, the v-FD model provides a convenient alternative. The Kirchoff transformation effectively reduces the degree of non-linearity of the h-based equation, thereby, improving the stability and mass balance.

Turning now to the experimental and simulation results for the initial conditions $h(z,0)=z-60$ cm, it is noted that the observed wetting depths as well as ponding time are generally smaller than those obtained numerically. Several reasons can be advanced for this lack of agreement. First, the initial conditions for the simulation and experiment could have differed markedly from each other by virtue of estimating the initial water contents using Eq.(4.1). Secondly, due to the long equilibration period, a certain degree of structural deterioration was inevitable, which in turn led to a general decrease in permeability. Also, during rain, the surface did not absorb water continuously. Water was supplied in impulses and, hence, the surface was subjected to repeated wetting and drying, a phenomenon which involves hysteresis. This is expected to result in a higher water content at the surface. Finally, non-uniformity in the bulk density throughout the soil column would cause fluctuations in the water content profile.

As a final remark, it is worthwhile to make one fundamental observation regarding rain infiltration and which is not altogether irrelevant to the present discussion. This is the influence of antecedant moisture condition of the soil, whereby, it is observed that the wetter the antecedant soil moisture, the greater is the depth of wetting, but the lower the uptake of rain water before ponding or runoff occurs.

(iv) Computer Time and Programming Considerations

For similar input and output specifications the execution times for the h-models are 20% to 80% longer than those for the θ-models. The average number of iterations needed to achieve convergence is about 3 for the wetter initial conditions (i.e., $h(z,0) < -1000$ cm) and about 5 for the drier conditions. While for a given wetting depth, the number of computational nodes is greater in the h-FE because of oscillations in the neighbourhood of the wetting front, the extra computation time incurred for the large grid size is "artificially" offset by the fact that at any given time the wetting depth is smaller in the case of the h-FE model. Thus, the difference in computation time between h-FE and h-FD is not as great as expected.

The execution time for the v-FD model is comparable to the h-FD model for the wetter initial conditions and shorter than the latter for drier initial conditions inspite of the more involved programming. This is due to its excellent time marching properties which is almost as good as those for the θ-models.

Comparative execution times in seconds for solving a 40-minute rain infiltration into soil $P_1H_1$, initially at field capacity, using the various numerical models (in parenthesis) are 28.4 (θ-FE), 35.5 (h-FD), 47.0 (h-FE) and 42.1 (v-FD). The order of programming ease is as follows (in decreasing order): θ-FD, θ-FE, h-FD, h-FE and v-FD. The v-FD is the most complex due to the inclusion of a new variable, v, while the other variables, θ and h are still needed for intermediate and secondary calculations. At the same time, more storage is also required for the v-FD.

## 5.4 CONCLUSIONS

Five main conclusions can be drawn from this study:

(i) Richards' model for unsaturated water flow is valid for the soil and conditions of the present study.

(ii) In soil water flow studies involving the wetting process, it is preferable to use the asymptotic form (Eq. 4.1) for characterizing the θ-h relationship even though the Brooks and Corey model (Eq. 4.3) may fit the data better.

(iii) The non-diagonal capacity matrix emerging from the finite element spatial approximation, to which we can attribute the excellent results in cases when the soil is near saturation becomes a major source of error when the soil is drier and/or when large pressure head gradients

exist in the flow system. Thus even though the finite element method has been applied with considerable success in groundwater studies, its usage in unsaturated studies should be restricted to predominantly wet conditions. In relatively non-complex problems the simpler finite difference method should certainly be preferred.

(iv) The v-FD model is slightly superior to the h-FD model in cases involving large pressure head gradients such as existing in dry soils, but this advantage no longer holds with wetter soils.

(v) The $\theta$-based equation is superior to the h-based equation, either transformed or untransformed, in practically all computational aspects. It works equally well for the complete range from air dry to saturation, has better accuracy, is easier to program and uses less computer time. Therefore, for problems which can be characterized by the $\theta$-based equation, preference should be given to it rather than the h-based equation as the governing equation of flow.

CHAPTER 6

# SIMULATION OF WATER FLOW IN BUNGOR SERIES

## 6.1 INTRODUCTION

Natural soil is rarely uniform in its properties, but exhibits profile variations of texture, structure, water retentivity and hydraulic conductivity. The same general principles that govern water movement in uniform soils can be applied to layered and heterogeneous soils. However, it is more difficult to predict the flow pattern because of the differences in hydraulic characteristics within the profile.

Laboratory studies such as those by Colman and Bodman (1944), Eagleman and Jamison (1962) and Miller and Gardner (1962) throw light on the physical factors involved in the flow between different textural layers and its overall effect on infiltration rate. Generally, when water, moving in a fine-textured soil encounters a coarse layer, flow is temporarily inhibited until the suction in the coarse layer is low enough to allow for the existence of water meniscus with a large radius of curvature commensurate with the pore sizes within the coarse layer. Such phenomenon can also be explained on the basis of Darcy's Law in that at relatively high suctions flow in coarse soils is practically non-existent due to negligible hydraulic conductivity. The extent of modification of the flow process is to a large measure dependent upon the difference in porosity between the layers.

The fact that hydraulic properties are not only functions of pressure head or water content but also of position precludes the development of rigorous analytical methods for predicting infiltration into layered soils. Thus, quantitative predictions have been based almost entirely on numerical methods (Hanks and Bowers, 1962; Wang and Lakshminarayana, 1968; van Keulen and van Beek, 1971; Reichardt, Nielsen and Biggar, 1972). The work of Hanks and Bowers (1962) indicates infiltration to be governed by flow through the least permeable layer, providing the wetting front has extended well into this layer, whilst that of Reichardt, Nielsen and Biggar (1972)

shows that flow could be enhanced or retarded when water flows into a less permeable layer. These cases exemplify the subtleties involved when textural differences exist, as they always do, in natural soil.

The phenomenon of crusting or surface seal development alters the surface soil in relation to the soil immediately below it. The system can also be viewed as a layered soil with the additional feature that the hydraulic properties of the surface layer is not only a function of h or $\theta$ but also of time. Attempts at describing the influence of seal development on infiltration have been simplified by assuming the surface layer to be saturated at all time (Edwards and Larson, 1969; van Keulen and van Beek, 1971).

This chapter discusses the various methods of assigning heterogeneity in the numerical solution of Richards' equation. The influence of layering sequence on the infiltration process is then examined and the response to rain of the two disturbed profiles of the Bungor Series in relation to erosion problems simulated. As mentioned at the beginning of the thesis, of special interest is the estimation of the time of ponding or runoff, the influence, if any, of the lower horizons on the uptake of rain water and the water balance during rain.

## 6.2 TREATMENT OF HETEROGENEITY

### 6.2.a Governing Equation

In predicting flow in layered soils the Darcian flow theory leads naturally to the use of the h-based equation where h is assumed to vary continuously across the boundary between the layers. While some authors (D'Hollander, 1976; Herudjito, 1977) have employed the $\theta$-based equation with success, use of the latter is generally not recommended. The reason as mentioned in Chapter 1, is that, whilst the solution of Richards' Eq. (2.2) will yield continuous $\theta$-profile across the boundary, in reality, this is not the case as can be expected from energy concepts. Abrupt changes in $\theta$ can occur even under hydrodynamic continuity depending on the water retentivities of the two layers involved. Experimental results of Reichardt, Nielsen and Biggar (1972) illustrate this point, whereby, discontinuity in the water content profiles are observed at interlayer boundaries. The water content in the second layer is distinctly higher or lower than in the first depending on the layering sequence used.

The same circumstance also applies in the case of the Kirchoff transformation of the h-based equation. Continuity condition implied by

the governing differential equation for the transformed variable precludes its usage in layered and heterogeneous soils.

On the basis of these considerations, the h-based equation will be used in this study. The numerical approximation method to be employed is the finite difference since the finite element method has been shown to perform very poorly in relatively dry soils.

### 6.2.b Interlayer Boundary

Layering is handled quite easily by simply assigning different hydraulic properties to the various layers. The treatment of the interlayer boundary is, however, subject to more uncertainty. Hanks and Bowers (1962) specified that the flux leaving one layer is equal to that entering the next. In addition, the conductivity, $K_b$ at the boundary is given by $K_b = 0.5K_1K_2/(K_1+K_2)$, where, $K_1$ and $K_2$ are conductivities at the boundary assuming the soil were homogeneous as layer 1 or layer 2 respectively. Reichardt, Nielsen and Biggar (1972), in providing solutions for horizontal infiltration into layered soils, used the same assumption regarding flux, but estimated $K_b$ according to the equation $K_b = 0.5(K_1+K_2)$.

Another approach is that used by Wang and Lakshminarayana (1968), van Keulen and van Beek (1971) and Bruce and Whisler (1973). Flux conditions at the boundary between layers need not be specified at all. Flow is entirely governed by the heterogeneity of the system which in turn is completely specified in terms of hydraulic properties being functions of pressure head and position. Furthermore, the problem of assigning hydraulic properties at the interlayer boundary is avoided by setting the latter at internodal instead of nodal position in cases where constants are evaluated at nodes and vice versa. In essence though, this leads to the same averaging procedure as that of Reichardt, Nielsen and Biggar (1972).

Confirmation as to the appropriateness of these approaches is difficult because of the fact that comparisons between numerical and experimental results are very scarce, while those available are not fine enough to allow one to make the required assessment. However, some remark can be made in regard to these assumptions. Firstly, the assumption of flux leaving the first layer to be equal to that entering the next is questionable. In physical terms, this implies a steady state condition at the boundary since such a constraint would not allow water to accumulate at this location. Numerically, however, flow across the boundary would be enhanced at the early stages because the top of the second layer is specified to have the same flux as the bottom of the first layer. At

latter stages, on the other hand, flow would be depressed due to the creation of a pseudo steady-state condition at the boundary. This assumption may also be the cause as to why the results of Reichardt, Nielsen and Biggar (1972) generally lag behind the measured profiles in the second layer.

The boundary conductivity given by Hanks and Bowers (1962) is another questionable feature. If the soil were to be homogeneous, i.e., $K_1 = K_2$ then $K_b$ would have a value of $0.25K_1$ when in fact $K_b = K_1$!

Two trial simulation runs are now made. The first uses the assumption of flux equality at the interlayer boundary and with the boundary conductivity given according to Reichardt, Nielsen and Biggar (1972). In the second run, the generalised approach cited last, i.e., the one without flux specification, is used. Results of the first run confirm the earlier claim about the early enhancement and late inhibition of the infiltration rate. The overall effect, however, is small when the results are compared to those from the second simulation run. More important is the numerical difficulty that is encountered with the first run. With the iterative scheme employed, the solutions fail to converge after the wetting front has extended well into the second layer. This apparently, is brought about by the pseudo steady-state condition at the interlayer boundary imposed by the assumption of flux equality. Based on these results, the approach used in the second run will be adopted in the present study.

## 6.3 EFFECT OF LAYERING SEQUENCE ON INFILTRATION

In order to examine the influence of layering sequence on infiltration the two horizons having extreme values of permeability and porosity are chosen, namely, $P_1H_1$ (most permeable and with lowest porosity) and $P_2H_1$ (least permeable and with highest porosity). Ponded infiltration into three soil configurations, all initially air dry, are compared by numerical simulation as well as experimentally. These are: (a) homogeneous $P_2H_1$ , (b) layered soil comprising of 10.5 cm $P_1H_1$ over $P_2H_1$ and (c) layered soil consisting of 10.5 cm $P_2H_1$ over $P_1H_1$.

Simulated pressure head and water content distributions are presented in Fig. 6.1 and 6.2 respectively. Figure 6.3 shows comparisons between simulated and experimental results for total infiltration versus time and the propagation of the wetting fronts.

An interesting feature to be observed is the development of positive pressure heads at the boundary between the two layers, extending upwards

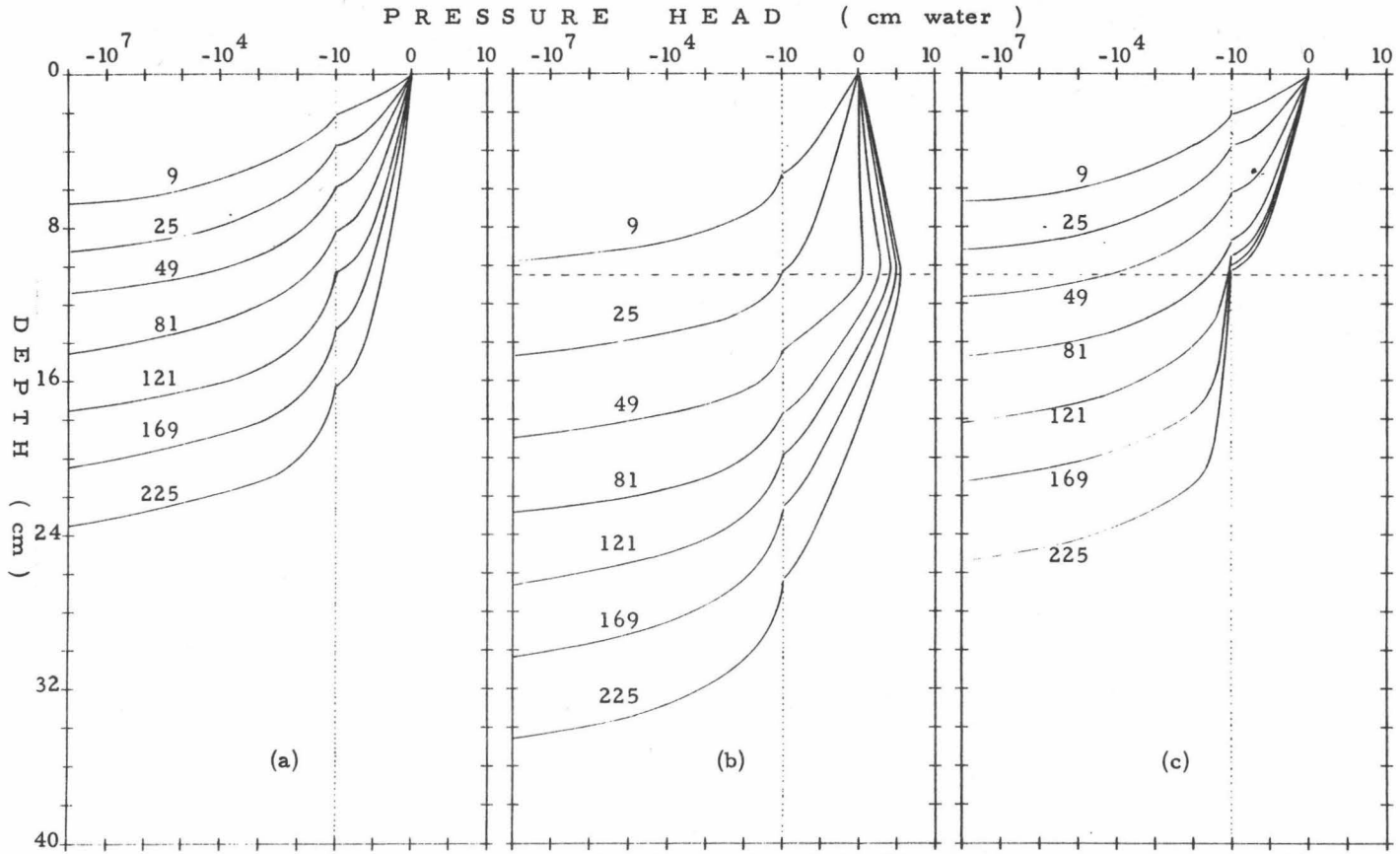


Fig. 6. 1 Pressure head profiles during simulated ponded infiltration into air dry homogeneous and layered soils: (a) Homogeneous $P_2H_1$, (b) 10. 5 cm $P_1H_1$ overlying $P_2H_1$ and (c) 10. 5 cm $P_2H_1$ overlying $P_1H_1$. (Numbers alongside the curves refer to time in minutes).

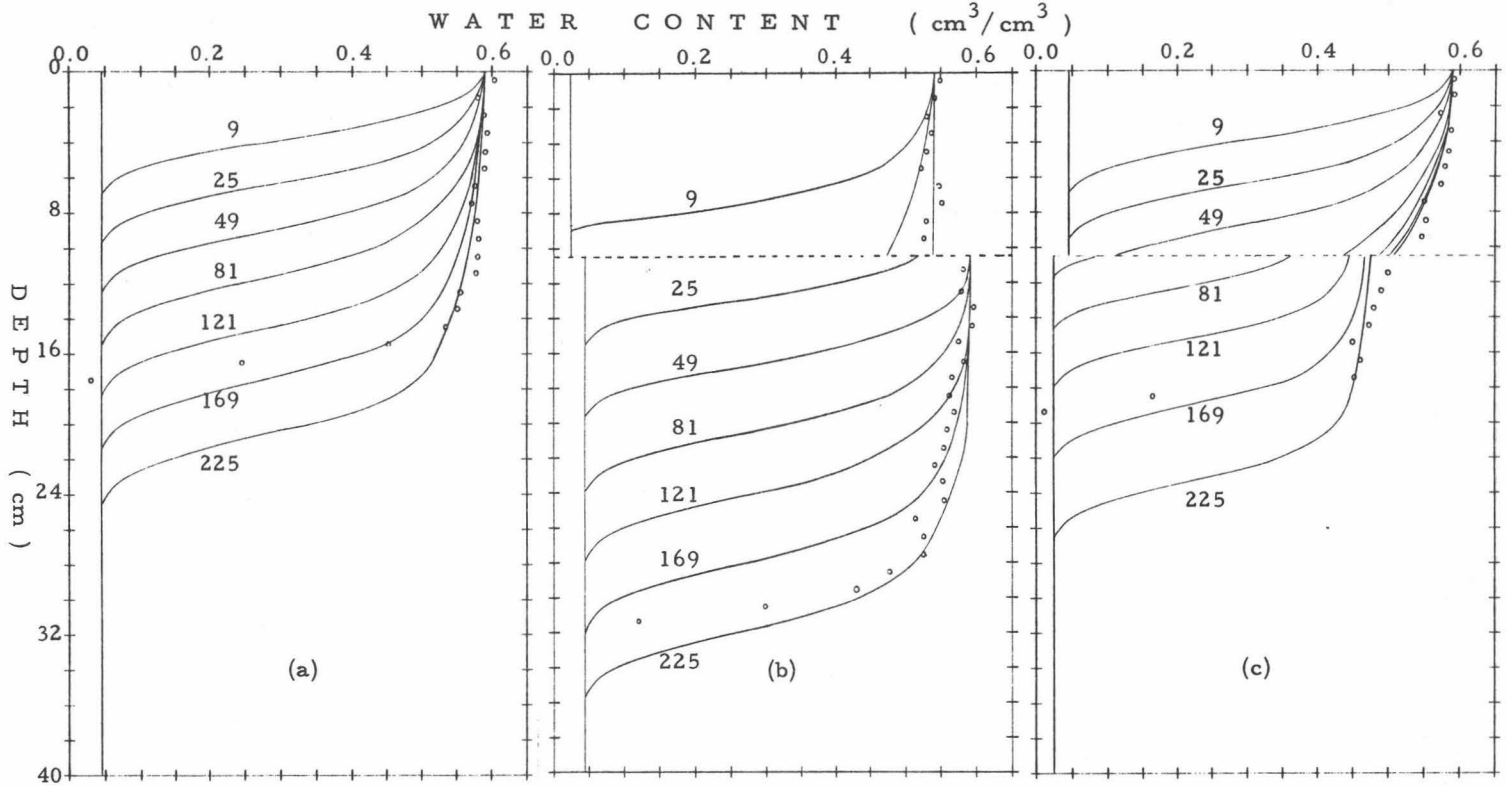


Fig 6.2 Water content profiles during simulated ponded infiltration into air dry homogeneous and layered soils: (a) Homogeneous $P_2H_1$, (b) 10.5 cm $P_1H_1$ overlying $P_2H_1$ and (c) 10.5 cm $P_2H_1$ overlying $P_1H_1$. (Numbers alongside the curves refer to time in minutes; circles indicate observed water content profiles at 225 minutes).

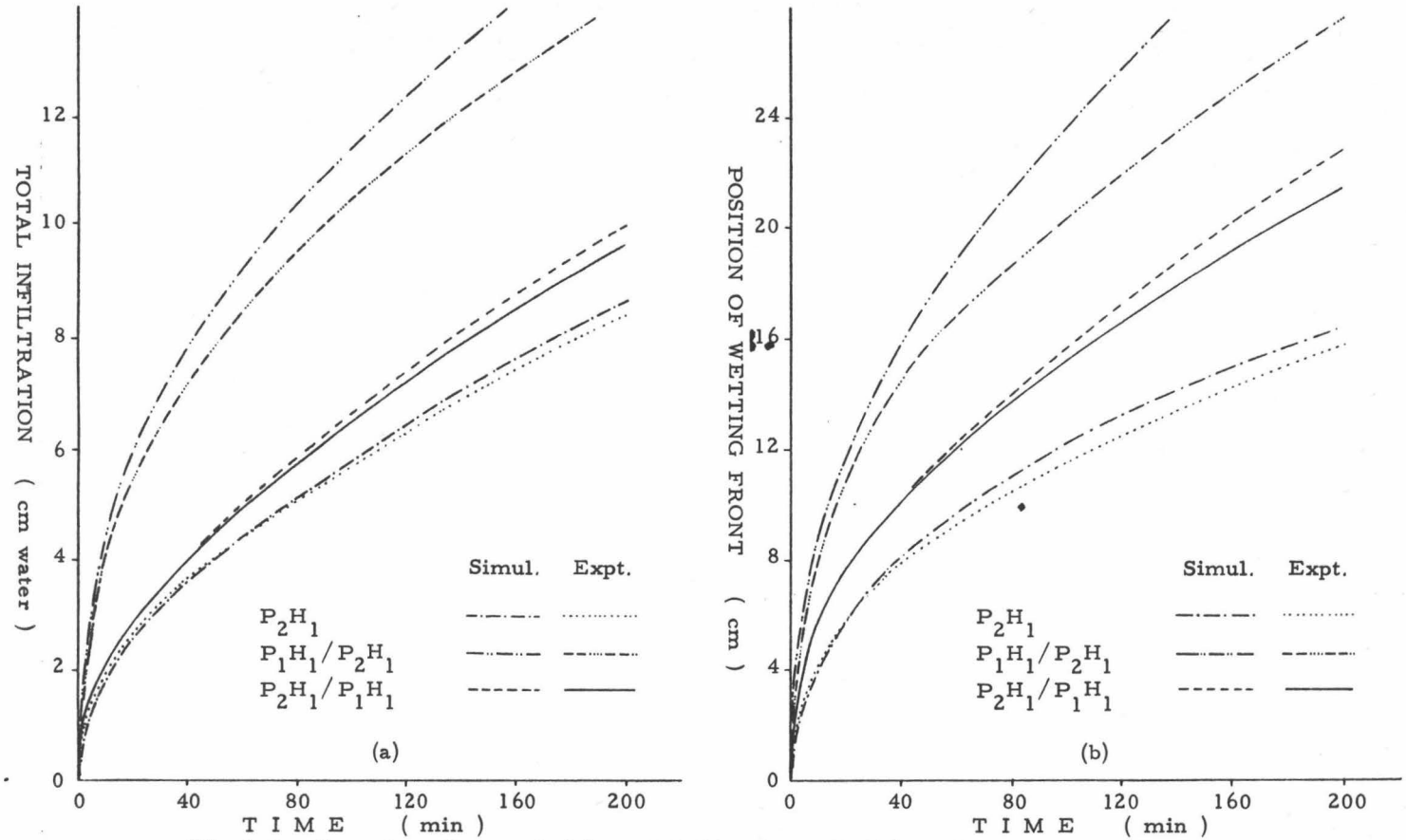


**Fig. 6.3 Time dependence of (a) total infiltration and (b) position of wetting front for vertical infiltration into air dry homogeneous and layered soils.**

and downwards into $P_1H_1$ and $P_2H_1$ respectively, as infiltration progresses (Fig. 6.1(b)). This is explained by the fact that since the lower less permeable layer can take up less water than can be potentially supplied by the upper layer, the latter soon becomes saturated. The development of positive hydrostatic pressure follows. Subsequently, the flow rate in the less permeable $P_2H_1$ layer is enhanced compared to the homogeneous $P_2H_1$ (a consequence of Darcy's Law), eventually leading to a greater uptake by the $P_2H_1$ layer underlying $P_1H_1$ than by the homogeneous $P_2H_1$ after about 160 minutes.

Another noteworthy feature of this analysis is the greater pressure head gradient in the $P_2H_1$ layer overlying the more permeable $P_1H_1$ layer soon after the water has penetrated the latter, as compared to the homogeneous $P_2H_1$. This of coarse, is due to the fact that the more permeable layer tends to transmit water downwards from the interlayer boundary much faster than can be supplied by the upper layer. As a consequence, the infiltration rate in the case of $P_2H_1$ overlying $P_1H_1$ after the water front has extended into the lower layer, is greater than that for the homogeneous $P_2H_1$ (see Fig. 6.4).

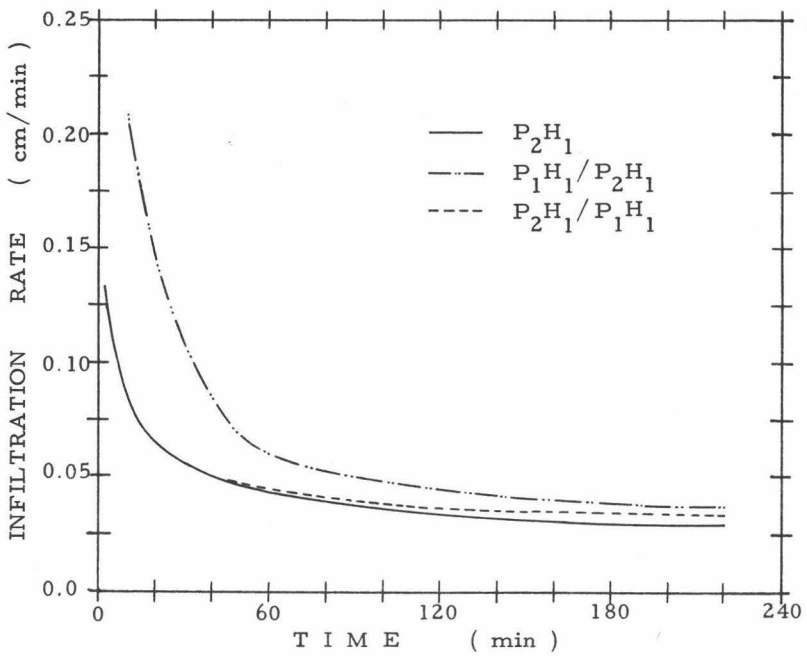


Fig. 6.4 Time dependence of infiltration rate for vertical infiltration into air dry homogeneous and layered soils.

Generally the time dependence of total infiltration and the progress of the wetting front follow the same trend as those measured, although the magnitudes involved are distinctly higher. The total infiltration from the simulation exceeds that observed by as much as 15%. Even worse are the predictions of the wetting front which are up to 35% higher than observed. These discrepancies can be ascribed to the generally poor performance of the h-based equation for very dry initial conditions demonstrated in the last chapter. It must also be noted that the differences between homogeneous $P_2H_1$ and $P_2H_1$ overlying $P_1H_1$ in terms of total infiltration, infiltration rate and progress of wetting front in these particular situations are too small to be detected by experiment because of the large error associated with the latter.

The evolution of pressure head and water content profiles appear to be in accordance with the numerical results of Hanks and Bowers (1962). However, there does seem to be a greater manifestation of the influence of the more permeable layer in the overall infiltration process compared to the results of these authors. This is likely caused by the different treatments of the interlayer boundary as discussed earlier.

The influence of the more permeable layer in the overall infiltration process is expected to be more pronounced with increasing wetness. The simulation runs are repeated, only this time, with the soil initially at field capacity. These yield similar patterns of infiltration (unpublished results). While the difference between homogeneous $P_2H_1$ and $P_2H_1$ overlying $P_1H_1$ is still small, the more permeable $P_1H_1$ overlying $P_2H_1$, however, causes a much more rapid uptake by the lower $P_2H_1$ layer than is observed with the air dry condition; the uptake by $P_2H_1$ layer underlying $P_1H_1$ exceeds that by the homogeneous $P_2H_1$ after only 100 min. infiltration.

The implication of these results to management practice is apparent. Mulching or loosening of the top soil, say up to the plough depth will contribute significantly to an increased uptake by the profile when the soil is subjected to flooded irrigation or a heavy thunderstorm that eventually causes ponding.

## 6.4 RAIN INFILTRATION INTO PROFILES OF BUNGOR SERIES

This section deals with the simulation of rain infiltration into the two disturbed profiles of the Bungor Series. Profile 1 consists of 3 horizons in the sequence 11 cm $P_1H_1$/20 cm $P_1H_2$/29 cm $P_1H_3$. Profile 2 also comprises of 3 horizons, namely, 15 cm $P_2H_1$/16 cm $P_2H_2$/29 cm $P_2H_3$.

The layering sequence corresponds to that in the field, however, the total depth is only limited to 60 cm since earlier results indicate that the wetting depth in any rainfall event is not likely to exceed this depth. Consequently, horizon 4 is not included in the analysis of either profile. Both profiles are initially at field capacity, i.e., $h(z,0) = -345$ cm. Four different rainfall intensities or events are considered. These are, (i) constant low intensity of 25 mm/hr, (ii) constant medium intensity of 50 mm/hr, (iii) constant high intensity of 75 mm/hr and (iv) variable intensity in the form of a step function:

$$q_o = \begin{cases} 25 \text{ mm/hr}, & 0 \leq t < 10 \text{ min} \\ 50 \text{ mm/hr}, & 10 \leq t < 20 \text{ min} \\ 100 \text{ mm/hr}, & 20 \leq t < 30 \text{ min} \\ 150 \text{ mm/hr}, & 30 \leq t < 40 \text{ min} \\ 100 \text{ mm/hr}, & 40 \leq t < 50 \text{ min} \\ 50 \text{ mm/hr}, & 50 \leq t < 60 \text{ min} \\ 25 \text{ mm/hr}, & 60 \leq t < 70 \text{ min} \\ 0 \text{ mm/hr}, & 70 \text{ min} \leq t \end{cases}$$

For the purpose of observing the influence of surface detention capacity all rainfall events are initially simulated with DETCAP = 0 cm. Rainfall events (iii) and (iv) are then repeated with DETCAP = 1 cm for each profile.

The resulting water content profiles during a two-hour period are shown in Fig. 6.5 and 6.6 for the two profiles, 1 and 2, respectively, while the times of the occurrence of ponding or runoff, the wetting depths at ponding and the water balance at 60 and 120 minutes are given in Table 6.1. Only the top two horizons of Profile 2 are shown in Fig. 6.6 because the third horizon is unaffected by any of the rainfall events during the 2-hour period.

The results are qualitatively predictable, but the order of the magnitudes of the effects are worth noting. No ponding or runoff occurs in Profile 1 in the case of the 25 mm/hr rain, this being smaller than the saturated conductivity of the top $P_1H_1$ horizon. Neither is there ponding during the 2-hour period for rain of 50 mm/hr which is approximately 10% higher than the saturated conductivity of $P_1H_1$. For Profile 2, with the 25 mm/hr rain, which is about twice the magnitude of the saturated conductivity of the surface $P_2H_1$ layer, ponding begins only after 72 min. These being so, it can be concluded that only rain of much greater intensity than the saturated conductivity of the surface horizon can

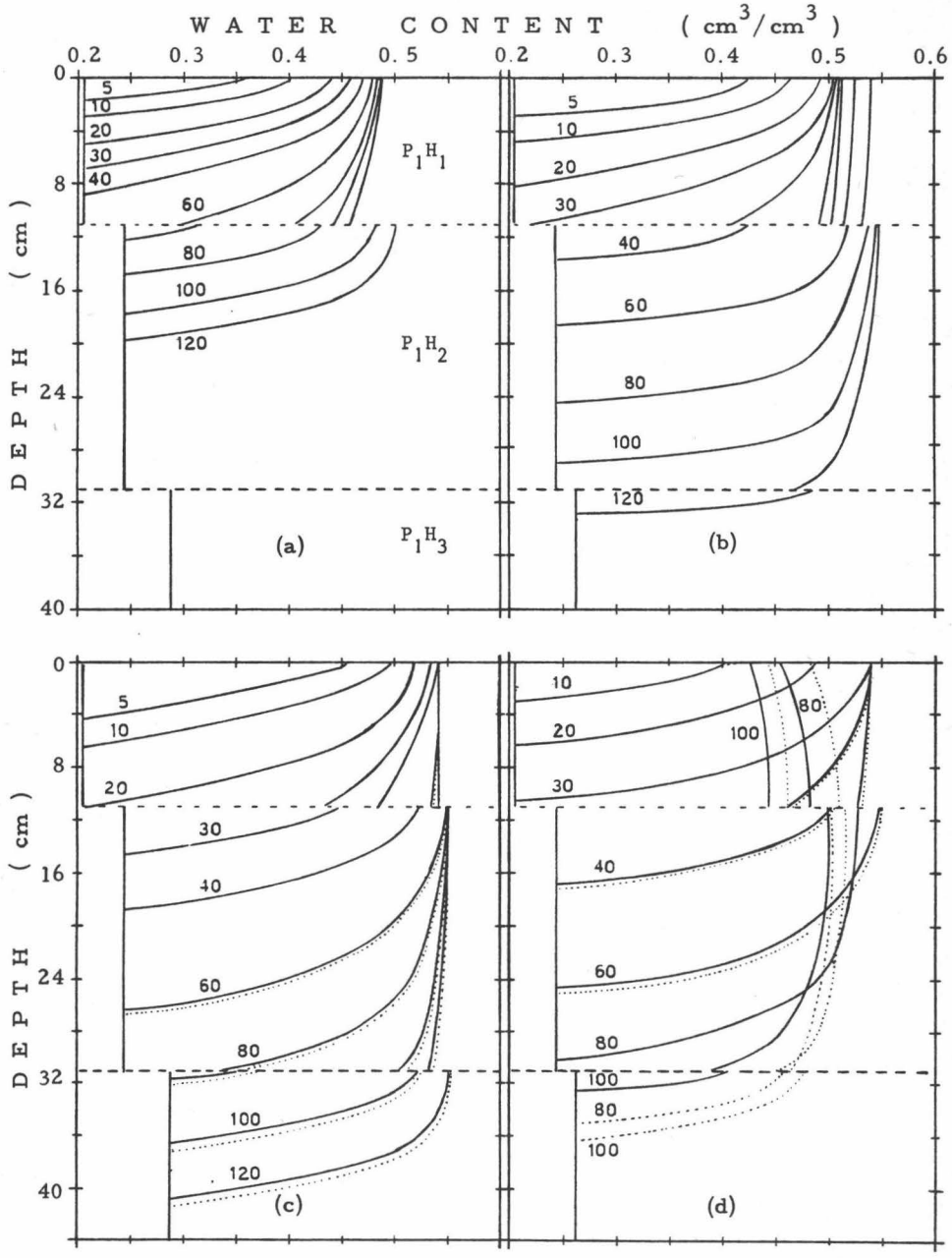


Fig. 6.5 Water content profiles during simulated rain infiltration into Profile 1 of Bungor Series for various rainfall events: (a) 25 mm/hr, (b) 50 mm/hr. (c) 75 mm/hr and (d) stepwise constant intensity. (Numbers alongside the curves indicate time in minutes. Dotted lines in (c) and (d) are water content profiles for the case of DETCAP=1 cm).

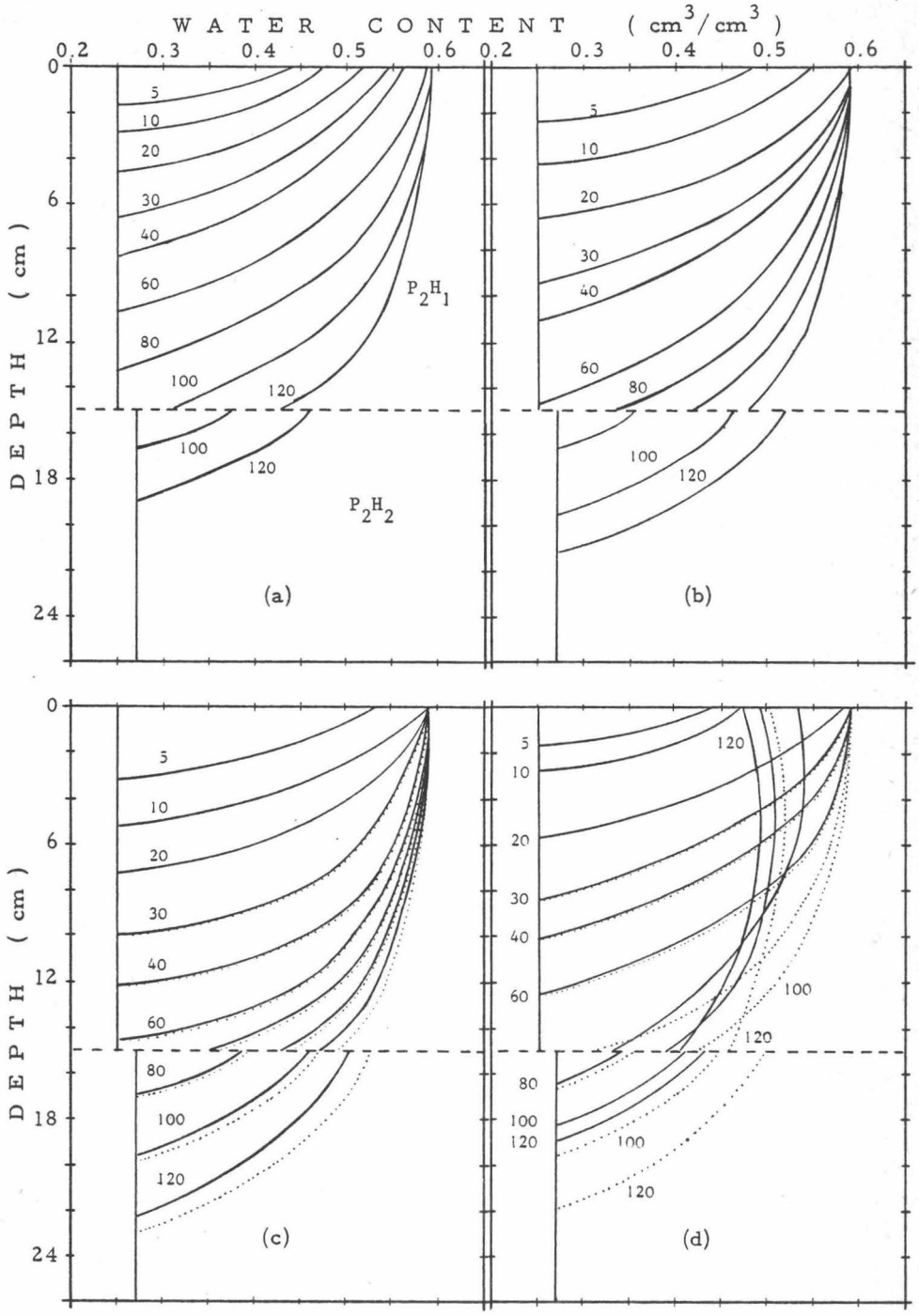


Fig. 6.6 Water content profiles during simulated rain infiltration into Profile 2 of Bungor Series for various rainfall events: (a) 25 mm/hr, (b) 50 mm/hr, (c) 75 mm/hr and (d) stepwise constant intensity. (Numbers alongside the curves indicate time in minutes. Dotted lines in (c) and (d) are water content profiles for the case of DETCAP=1 cm).

initiate ponding or runoff, assuming of coarse, that there is no deterioration of the surface properties of the soil.

Also of interest is the total water uptake and depth of wetting at incipient ponding. In general, the wetting depths are rather shallow at the time of ponding. Steady rain of intensity slightly greater than the saturated conductivity of the surface horizon is conducive to the development of deep moisture profiles and maximum water uptake before ponding. Heavy intensity rainfall results in very shallow wetting depths and low total uptake prior to ponding. For example, the 75 mm/hr rain penetrates only 4.5 cm of Profile 2 before ponding occurs. The corresponding uptake is only 1.01 cm. In contrast the 25 mm/hr rain penetrates as deep as 12.5 cm with a corresponding uptake of 2.96 cm prior to the commencement of ponding.

The efficiency of Profile 1 to Profile 2 in absorbing and conducting rain water is obvious. The total uptake and depth of wetting in the case of Profile 1 are approximately twice those of Profile 2. Less obvious is the influence of the lower horizons, or rather, the lack of it in the absorption of rain water prior to ponding. For Profile 1, the time of ponding during rainfall event (iv) is 29.8 minutes which is practically the same as the 29.6 minutes obtained with the homogeneous $P_1H_1$ (Chapter 5). Profile 2, on the other hand, experiences ponding for all rainfall events before the wetting front arrives at the next horizon. Thus, in both profiles the top horizon is too deep for any influence of an accelerated or retarded water movement in the next layer to be felt at the surface. The influence of the lower horizons would only be manifest after a prolonged period of ponding.

The presence of a surface detention capacity can delay the runoff process significantly and this will increase more than proportionately the total water uptake before runoff starts. For instance, a detention capacity of just 1 cm delays runoff by nearly 45 minutes for the case of the 75 mm/hr rain falling on Profile 1. Larger values of DETCAP would produce more dramatic effects since the detention capacity plays a dual role. First, it detains the excess water or a portion of it from being lost as runoff and, secondly, it provides an excess pressure head equal to the depth of ponded or detained water, which in turn causes a more rapid infiltrat on rate. A similar trend has been reported by Hillel, van Bavel and Talpaz (1975), in which the detention capacity was provided by a mulch of hydrophobic aggregates. This positive role of the surface detention capacity can thus be effectively used in the control of erosion.

Table 6.1. Summary of results for 4 simulated rainfall events on Profile 1 and Profile 2 of the disturbed Bungor Series.

| Rainfall Event | $T_p$ | $WD_p$ | $T_r$ | Total uptake in cm | | | Detained water cm | | Total Runoff cm | |
|---|---|---|---|---|---|---|---|---|---|---|
| | | | | $T_p$ | 60 | 120 | 60 | 120 | 60 | 120 |
| | min | cm | min | min | min | min | min | min | min | min |
| PROFILE 1 | | | | | | | | | | |
| 1. 25 mm/hr | - | - | - | - | 2.47 | 4.92 | - | - | - | - |
| 2. 50 mm/hr | - | - | - | - | 4.92 | 9.85 | - | - | - | - |
| 3. 75 mm/hr | | | | | | | | | | |
| DETCAP = 0 | 39.6 | 17.0 | 39.6 | 4.91 | 7.26 | 12.1 | - | - | 0.19 | 2.90 |
| DETCAP = 1 cm | 39.6 | 17.0 | 84.0 | 4.91 | 7.35 | 12.7 | 0.19 | 1.00 | 0.00 | 1.42 |
| 4. Variable Intensity | | | | | | | | | | |
| DETCAP = 0 | 29.8 | 10.2 | 29.8 | 2.84 | 6.82 | 7.06 | - | - | 1.39 | 1.39 |
| DETCAP = 1 cm | 29.8 | 10.2 | 42.0 | 2.84 | 6.90 | 8.17 | 0.71 | 0.00 | 0.26 | 0.26 |
| PROFILE 2 | | | | | | | | | | |
| 1. 25 mm/hr | 72.0 | 12.5 | 72.0 | 2.96 | 2.48 | 4.65 | - | - | - | 0.35 |
| 2. 50 mm/hr | 16.5 | 6.0 | 16.5 | 1.34 | 3.54 | 5.59 | - | - | - | 4.41 |
| 3. 75 mm/hr | | | | | | | | | | |
| DETCAP = 0 | 8.3 | 4.5 | 8.3 | 1.01 | 3.69 | 5.71 | - | - | 3.85 | 9.40 |
| DETCAP = 1 cm | 8.3 | 4.5 | 25.5 | 1.01 | 3.78 | 5.92 | 1.00 | 1.00 | 3.72 | 8.12 |
| 4. Variable Intensity | | | | | | | | | | |
| DETCAP = 0 | 20.4 | 6.0 | 20.4 | 1.24 | 3.34 | 3.68 | - | - | 4.63 | 4.71 |
| DETCAP = 1 cm | 20.4 | 6.0 | 31.0 | 1.24 | 3.42 | 4.79 | 1.00 | 0.00 | 3.57 | 3.65 |

$T_p$ = Time of commencement of ponding

$WD_p$ = Wetting depth at ponding

$T_r$ = Time of occurrence of runoff

Referring to Fig. 6.5(d) and 6.6(d), redistribution occurs when either rain stops (for DETCAP = 0) or when depth of ponded water is reduced to zero (for DETCAP = 1 cm). An arbitrary potential evaporation rate of 2 mm/day is assigned. The redistribution process does not take account of hysteresis and, therefore, the computed redistribution profiles are flatter and deeper than would be expected. This inadequacy though, has no direct consequence on this particular study. The examples are used mainly to illustrate the usefulness of the detention capacity in conserving water and reducing runoff.

As mentioned previously (Chapter 3) , the conductivity, diffusivity and porosity values for these disturbed profiles are generally much higher than those expected in the field. On the other hand, the rain intensities used in the simulations are fairly representative of the tropical rain in Malaysia. Therefore, it can be said that for similar soil types of heavy texture, rain penetration would be very shallow, of the order of several centimetres only, before ponding or runoff occurs. The latter comes about quite early. The amount lost as runoff during medium to high intensity rain would be generally greater than that taken up by the soil profile.

## 6.5 EFFECT OF SURFACE DEGRADATION ON INFILTRATION-RUNOFF RELATIONSHIP

The incidence of rain water on a bare soil causes large changes in the hydraulic properties of the soil surface. Structural deterioration occurs accompanied by a reduction in the surface conductivity. Although the thickness of the rain-affected layer rarely exceeds a few millimetres, Edwards and Larson (1969) and Hillel and Gardner (1969, 1970) have shown that the reduced permeability of this layer can markedly reduce infiltration.

Data on the rate of deterioration of the surface conductivity is scarce and difficult to obtain because of the multiplicity of factors involved, such as rain intensity, stability and size of aggregates and antecedent moisture condition. Edwards and Larson (1969), however, have obtained measurements of the saturated conductivity of the soil surface after different exposure times to rain of a given intensity. The change in the saturated conductivity of the affected surface appeared to follow an exponential decay. This trend of decay was later used by Farrell and Larson (1972) to provide an analytical solution of the soil water flow based on the Green and Ampt approach, for certain restricted conditions.

One of the claimed advantages of a numerical model is that it can be used to simulate situations which are too difficult to be studied experimentally or analytically. By additional assumptions on the relationship between unsaturated and saturated conductivities and the moisture characteristic of the rain-affected surface, the influence of surface degradation due to raindrop impact can be readily incorporated in the numerical model and various conditions simulated.

6.5.a Changing Hydraulic Characteristics of the Surface Layer

Results of Edwards and Larson suggest the relationship

$$\frac{K_s(t) - K_f}{K_o - K_f} = e^{-\alpha t}$$

where $K_s(t)$ is the saturated conductivity after exposure time t, $K_o$ is the saturated conductivity of the unaffected soil (i.e., at t = 0), $K_f$ is the final limiting value of the saturated conductivity and $\alpha$ is a constant. Qualitatively, one expects that for a given soil $K_f$ would decrease while $\alpha$ would increase with increasing intensity of rain, and vice versa. From the results of Edwards and Larson (1969) it would appear that the maximum degradation for a given rain intensity is reached quite early, soon after ponding or runoff has occurred. Further degradation is minimal because the thin film of water provides protection to the surface.

The second assumption pertaining to the problem is regarding the unsaturated conductivity of the affected surface layer as a function of pressure head or water content. van Keulen and van Beek (1971) assumed the surface to be saturated from the onset of rain and, hence, did not require a knowledge of the unsaturated conductivity function. For long term simulation, such an assumption should be adequate but for simulating one rainfall event a more detailed behaviour of the surface layer is necessary. In the simulations to follow, the conductivity model of Mualem (1978) will be used. This model is $K_r = S^n$, where, $K_r$ is the relative conductivity, S is the dimensionless water content and n is a constant. This model has been shown to be most adaptable with fairly constant n for different soils of a given textural class. In this study, n is assigned the value of 7.5, this being representative for the 8 soil horizons being investigated (unpublished results).

The final information required is the soil water characteristic or retentivity of the surface layer. In the present study, a simplification

is made by assuming the water retentivity to be the same as that of the unaffected soil.

6.5.b Simulation of Rain Infiltration with Soil Surface Degradation

The transient uptake of rain water by Profile 1 of the Bungor Series is simulated for different conditions of changing surface conductivity or "seal" development, an assumed seal thickness of 0.75 cm and for a rain intensity of 75 mm/hr. The soil is initially at field capacity moisture condition. Table 6.2 summarizes the simulation results for various combinations of $K_f$ and $\alpha$. The values of $\alpha$ considered represent fairly rapid seal development. For instance, with $K_f/K_o = 0.1$ and $\alpha = 0.002$ $sec^{-1}$, the saturated conductivity of the surface layer decreases to within 3% of the final limiting value, $K_f$, within 30 minutes of exposure to rain.

Table 6.2 Results of simulated rain infiltration on Profile 1 of Bungor Series with changing surface hydraulic properties.

| Simul. run | $K_f/K_o$ | $\alpha$ $sec^{-1}$ | $T_r$ min | $WD_r$ cm | Total Uptake cm | | Total Runoff cm | |
|---|---|---|---|---|---|---|---|---|
| | | | | | 40 min | 60 min | 40 min | 60 min |
| 1 | 0.5 | 0.002 | 31.7 | 10.5 | 4.41 | 6.31 | 0.50 | 1.10 |
| 2 | 0.1 | 0.002 | 15.4 | 7.8 | 4.04 | 5.62 | 0.88 | 1.79 |
| 3 | 0.02 | 0.002 | 13.4 | 6.5 | 3.12 | 3.99 | 1.80 | 3.41 |
| 4 | 0.1 | 0.001 | 24.5 | 9.2 | 4.25 | 5.75 | 0.65 | 1.66 |
| 5 | 0.1 | 0.003 | 13.8 | 6.7 | 3.93 | 5.25 | 0.99 | 2.18 |
| - | 1.0 | 0.0 | 39.6 | 17.0 | 4.90 | 7.26 | 0.00 | 0.19 |

$T_r$ - Time of occurrence of runoff;

$WD_r$ - Wetting depth at the time of occurrence of runoff;

+ The last entries with $K_f/K_o = 1.0$ and $\alpha = 0.0$ are values taken from Table 6.1 for the unaffected surface.

As expected runoff in all cases occurs sooner than if the surface were unaffected. However, the reduction is not proportional to the decrease in the saturated conductivity of the surface. This is due to the transient nature of the process as well as the steep pressure-head gradient developed in the seal, the latter being a direct consequence of the greater conductivity of the unaffected subseal layer. The flow pattern is depicted in Fig.6.7 for the case of $K_f/K_o = 0.1$ and $\alpha = 0.002$ $sec^{-1}$; here, the steepness of the pressure-head gradient in the affected surface is reflected accordingly by the steep water content gradient.

If a comparison were to be made, say, with rain infiltration into $P_2H_1$ (with protected surface), the runoff times indicated in Table 6.2 would appear reasonable. In the former, ponding or runoff occurs at 8.3 minutes, much earlier than in any of the cases simulated. Consider, for example, simulation run 3: the saturated conductivity of the developing seal at time 8.3 minutes is 0.0294 cm/min , which is greater than the value of 0.0197 cm/min for $P_2H_1$, hence, runoff would occur later.

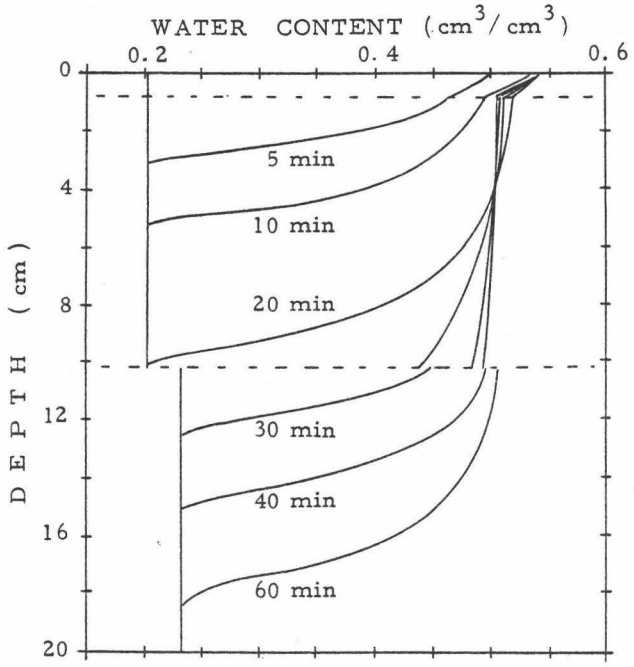


Fig. 6.7 Water content profiles in Profile 1 of Bungor Series during rain infiltration onto unprotected surface.

The reduced infiltration rates after the commencement of runoff appear to be in accordance with the measurements reported by Hillel and Gardner (1970), where, the uptake by an uncrusted soil during the first 2 hours of ponded infiltration was 7 cm while the corresponding uptake through a 1-cm crust with saturated conductivity equal to 2% of that of the uncrusted soil was 2 cm, i.e., approximately 30% of the former. In this study, a comparison between simulation run 3 and the unaffected soil (the last entries of Table 6.2) yields a similar magnitude of change: in the period between 40 minutes and 60 minutes, uptake by the unaffected soil is 2.36 cm while that through a 0.75 cm thick seal having a saturated conductivity varying from

2.8% to 2% of the saturated conductivity of the unaffected subseal layer is 0.87 cm.

The above comparison provides further evidence of the appropriateness of the assumption used herein for handling layered soils. Nevertheless, it is important to note that an inadequate representation of the rain-affected surface in the flow region would yield erroneous results. In specific terms, if the thickness were assumed to be half of the nodal distance ($\Delta z$), for instance, the consequence would be a much delayed runoff time since the constants at $\Delta z/2$, which in essence, are averages of the seal and the unaffected layer will be weighted towards the unaffected layer, thereby resulting in a greater potential infiltration rate. Such an anomaly can be avoided by letting the seal cover at least two nodes, hence the reason for assuming a thickness of 0.75 cm in the simulation runs where the distance step is set as 0.5 cm.

Returning to Fig.6.7, another important feature in addition to the steep moisture gradient at the surface, is that the subsurface soil will never attain saturation. The reason is that this layer is capable of transmitting more water than can be supplied by the seal. Thus, after the conductivity of the latter has reached its limiting value of $K_f$, the water content profile in the upper portion of the subseal layer approaches a steady state condition with unit hydraulic gradient. The pressure head and water content at the boundary will be determined by the interaction of the properties of the seal and subseal layers. Edwards and Larson (1969) have also reported similar findings.

## 6.6 CONCLUSIONS

In any simulation study, there are a great number of comparisons that can be made. Compared to the possibilities, the simulation cases presented in this chapter are meagre indeed. In deciding the kind of simulation and comparisons to be made, only those cases which are most relevant and most closely approximate the field conditions have been chosen.

The important conclusions that can be derived from this chapter are as follows:-

(i) flow in layered soils can be adequately described by using the h-based equation and assuming flow to be governed only by the hydraulic characteristics of the various layers without having to resort to flux specifications at the interlayer boundaries,

(ii) when water flows downwards from a more permeable to a less permeable layer, positive pressure heads can develop in the vicinity of the inter-layer boundary and this will lead to an accelerated movement in the less permeable layer; likewise, a more permeable layer below a less permeable one can lead to a more rapid movement of water in the latter because of the great pressure-head gradient developed at the boundary between the two layers,

(iii) only rain of intensity far exceeding the saturated conductivity of the top horizon can initiate ponding or runoff,

(iv) the wetting depths at the time of occurrence of ponding or runoff in the Bungor Series and likewise, in other soils of heavy texture, during rainfall are generally shallow, hence, the lower horizons would hardly have any influence on short term considerations of rain infiltration,

(v) the presence of surface depressions can delay runoff by a considerable period by both detaining the excess water as well as creating an excess pressure head at the surface,

(vi) by assuming certain relationships for the hydraulic properties of the surface layer it is possible to simulate the influence of surface seal development on the infiltration-runoff pattern during rain; while ponding or runoff commences at an earlier period, the overall reduction in infiltration is not as dramatic as one would expect from a mere consideration of the limiting conductivity of the seal; the greatly reduced conductivity of the seal is partially offset by the steep pressure-head gradient within it.

CHAPTER 7

# NUMERICAL SOLUTIONS FOR A TWO-DIMENSIONAL FLOW

## 7.1. INTRODUCTION

This chapter is a consequence of Chapter 5 where it was shown that the finite element approximation of the pressure-based equation, by virtue of its non-diagonal capacity matrix, yields poor mass balance in the one-dimensional flow for a significant range of moisture conditions of interest in unsaturated soils.

For two-dimensional problems, the non-diagonal capacity matrix have been found to lead to numerical and conceptual difficulties (Emery and Carson, 1971 ; Neuman, 1973). This can be remedied by defining the time derivative of the nodal pressure head as a weighted average over the entire flow region, thereby, resulting in a diagonalized capacity matrix. Such a procedure, which is more of a strategy for obtaining convergent solutions and for the maintenance of local mass balance rather than as a remedy for improving the global mass balance, when applied to the one-dimensional case (Chapter 5) was found to yield a slight improvement in the overall mass balance.

This chapter is exploratory in nature; its purpose is to examine if the anomaly for the one-dimensional problem is also manifest in the two-dimensional case. A simple two-dimensional problem is considered for the case of the predominantly horizontal infiltration into a soil slab of non-negligible thickness. Logistics leads to the consideration of the solution with the diagonalized capacity matrix first. To provide a basis of comparison, the problem is also solved by the finite difference method which has been shown to yield reliable results (Rubin, 1968).

## 7.2. TWO-DIMENSIONAL PROBLEM STATEMENT

For the predominantly horizontal infiltration into a soil slab of non-negligible height, the governing equation (Richards' equation) can be written as

$$C \frac{\partial h}{\partial t} = \frac{\partial}{\partial x} [K(h) \frac{\partial h}{\partial x}] + \frac{\partial}{\partial z} [K(h) \frac{\partial h}{\partial z} - K(h)] \qquad (7.1)$$

with initial conditions

$$h(x,z,0) = h^{o}(x,z) \qquad (7.2)$$

and boundary conditions of specified pressure heads on vertical faces AB, DC (Fig. 7.1)

$$h(0,z,t) = z - H_w \quad \text{on AB} \qquad (7.3.a)$$

$$h(L,z,t) = h_L - z \quad \text{on DC} \qquad (7.3.b)$$

and zero flux along the horizontal faces AD and BC

$$(K \frac{\partial h}{\partial z} - K)_{x,0} = 0 \quad \text{on AD} \qquad (7.3.c)$$

$$(K \frac{\partial h}{\partial z} - K)_{x,d} = 0 \quad \text{on AB} \qquad (7.3.d)$$

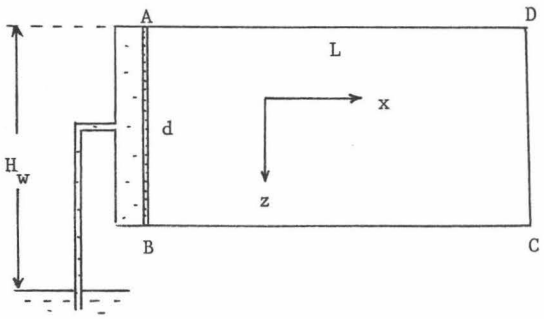


Fig. 7.1. Schematic representation of predominantly horizontal two-dimensional flow into a soil slab of non-negligible thickness, d and length, L.

## 7.3. FINITE DIFFERENCE DISCRETIZATION

### 7.3.a. The Alternating-direction Implicit (ADI) Technique

A very efficient finite difference method for the type of problem considered here is the alternating-direction implicit or "ADI" scheme of Peaceman and Rachford (1955). Let the x,z plane be divided into rectangular grid with increments $\Delta x$, $\Delta z$ such that

$$x = i\,\Delta x \qquad , i = 0,1,\ldots,N$$

and $$z = (j-1)\,\Delta z \qquad , i = 0,1,\ldots,M$$

The slab boundaries, x = 0, x = L, z = 0 and z = d correspond to i = 0, i = N-1, j = 1 and j = M-1, respectively. Thus, on all sides except along AB, the grid is extended one grid-increment beyond the slab. This is done to facilitate the handling of the derivative boundary conditions along these sides.

In brief, the ADI technique requires two advanced time levels, 2n+1 and 2n+2 levels for one complete application. In the first increment, 2n → 2n+1, the derivative of h with respect to z is expressed explicitly in terms of known values at the 2n-time level while the derivative with respect to x is expressed implicitly in terms of unknown values at the (2n+1)-time level. The resulting difference equations with unknowns $h_{i,j}^{2n+1}$, i = 1,...,N-1 are solved for each j, j = 1,...,M-1. To advance from time level 2n+1 to 2n+2, the derivative with respect to x is now expressed explicitly while that with respect to z, implicitly and the resulting equations with unknowns $h_{i,j}^{2n+2}$, j = 0,...,M are solved for each i = 1,...,N-1. Thus, in essence, the solution process consists of solving a tridiagonal system of (N-1) equations (M-1) times and (M+1) equations (N-1) times. This is significantly easier than solving (N-1)(M+1) equations twice. For linear problems stability is ascertained for all ratios of $\Delta x/(\Delta t)^2$ and $\Delta z/(\Delta t)^2$ providing $\Delta t$ is kept constant for each complete application.

### 7.3.b. Difference Equations

If the constants are evaluated at the half time step, then for advancing from 2n to 2n+1 time level, we have, for j = 1,...,M-1

$$C^{2n+\frac{1}{2}}\frac{h_{i,j}^{2n+1}-h_{i,j}^{2n}}{\Delta t^{2n}}=\frac{1}{\Delta x}\left[K_{i+\frac{1}{2}}^{2n+\frac{1}{2}}\frac{h_{i+1,j}^{2n+1}-h_{i,j}^{2n+1}}{\Delta x}-K_{i-\frac{1}{2},j}^{2n+\frac{1}{2}}\frac{h_{i,j}^{2n+1}-h_{i-1,j}^{2n+1}}{\Delta x}\right]$$

$$+\frac{1}{\Delta z}\left[K_{i,j+\frac{1}{2}}^{2n+\frac{1}{2}}\frac{h_{i,j+1}^{2n}-h_{i,j}^{2n}}{\Delta z}-K_{i,j-\frac{1}{2}}^{2n+\frac{1}{2}}\frac{h_{i,j}^{2n}-h_{i,j-1}^{2n}}{\Delta x}\right]-\frac{K_{i,j+\frac{1}{2}}^{2n+\frac{1}{2}}-K_{i,j-\frac{1}{2}}^{2n+\frac{1}{2}}}{\Delta z}$$

$$i=1,\ldots,N-1 \qquad (7.4)$$

which on simplification results in

$$a_i h_{i-1,j}^{2n+1}+b_i h_{i,j}^{2n+1}+c_i h_{i+1,j}^{2n+1}=d_i h_{i,j-1}^{2n}+e_i h_{i,j}^{2n}+f_i h_{i,j+1}^{2n}$$

$$+\frac{\Delta t}{2\Delta z}\left(K_{i,j-1}^{2n+\frac{1}{2}}-K_{i,j+1}^{2n+\frac{1}{2}}\right)\quad i=1,\ldots,N-1 \qquad (7.5)$$

where $a_i=-\frac{r_x}{2}\left(K_{i-1,j}^{2n+\frac{1}{2}}+K_{i,j}^{2n+\frac{1}{2}}\right)$

$$b_i=C_{i,j}^{2n+\frac{1}{2}}+\frac{r_x}{2}\left(K_{i-1,j}^{2n+\frac{1}{2}}+2K_{i,j}^{2n+\frac{1}{2}}+K_{i+1,j}^{2n+\frac{1}{2}}\right)$$

$$c_i=a_{i+1}$$

$$d_i=\frac{r_z}{2}\left(K_{i,j-1}^{2n+\frac{1}{2}}+K_{i,j}^{2n+\frac{1}{2}}\right)$$

$$e_i=C_{i,j}^{2n+\frac{1}{2}}-\frac{r_z}{2}\left(K_{i,j-1}^{2n+\frac{1}{2}}+2K_{i,j}^{2n+\frac{1}{2}}+K_{i,j+1}^{2n+\frac{1}{2}}\right)$$

$$f_i=d_{i+1}$$

where $r_x=\Delta t/(\Delta x)^2$ and $r_z=\Delta t/(\Delta z)^2$.

In advancing from 2n+1 to 2n+2 time level, the resulting difference equations, for i = 1,...,N-1, are

$$a_j h_{i,j-1}^{2n+2}+b_j h_{i,j}^{2n+2}+c_j h_{i,j+1}^{2n+2}=d_j h_{i-1,j}^{2n+1}+e_j h_{i,j}^{2n+1}+f_j h_{i+1,j}^{2n+1}$$

$$+\frac{\Delta t}{2\Delta z}\left(K_{i,j-1}^{2n+1\frac{1}{2}}-K_{i,j+1}^{2n+1\frac{1}{2}}\right)\quad j=1,\ldots,M-1 \qquad (7.6)$$

where $a_j = -\frac{r_z}{2}\left(K^{2n+1\frac{1}{2}}_{i,j-1} + K^{2n+1\frac{1}{2}}_{i,j}\right)$

$$b_j = C^{2n+1\frac{1}{2}}_{i,j} + \frac{r_z}{2}\left(K^{2n+1\frac{1}{2}}_{i,j-1} + 2K^{2n+1\frac{1}{2}}_{i,j} + K^{2n+1\frac{1}{2}}_{i,j+1}\right)$$

$$c_j = a_{j+1}$$

$$d_j = \frac{r_x}{2}\left(K^{2n+1\frac{1}{2}}_{i-1,j} + K^{2n+1\frac{1}{2}}_{i,j}\right)$$

$$e_j = C^{2n+1\frac{1}{2}}_{i,j} - \frac{r_x}{2}\left(K^{2n+1\frac{1}{2}}_{i-1,j} + 2K^{2n+1\frac{1}{2}}_{i,j} + K^{2n+1\frac{1}{2}}_{i+1,j}\right)$$

$$f_j = d_{j+1}$$

The conditions of zero flux at j = 1 and j = M-1 represented by

$$h^{2n+2}_{i,j+1} - h^{2n+2}_{i,j} = \Delta z \qquad , j = 0, M-1 \tag{7.7}$$

complete the system of M+1 equations in M+1 unknowns for each abscissa position, i = 1,2,...,N-1.

7.3.c. Computer Implementation

The same iterative marching procedure described in Chapter 2 is employed with an additional constraint of $\Delta t^{2n} = \Delta t^{2n+1}$ for ensuring stability. Equal spatial increments of $\Delta x = \Delta z = 2$cm are used for a slab height of 10 cm and length 14 cm. A value of $H_w = -12$ cm is used for the different runs.

## 7.4. FINITE ELEMENT DISCRETIZATION

### 7.4.a. System Equations

The finite element discretization for flow in an incompressible unsaturated and partly saturated soil was first developed by Neuman (1973). The same approach but more specific applies to the Galerkin finite element formulation of Eq. (7.1). The resulting system of ODE's is of the form

$$[D]\{h(t)\} + [A]\{\frac{dh}{dt}\} = \{Q\} - \{B\} \tag{7.8}$$

where, for triangular elements with local coordinate functions $\xi_i^e(x,z)$ (see Appendix IV) and the assumptions that K and C vary linearly according to

$$K = K_1 \xi_1^e$$

$$C = C_1 \xi_1^e$$

where 1 denotes the corners of the triangle, the elements of the coefficient matrices and of the vectors are given by

$$D_{ij} = \sum_e \int_{D^e} K_1 \xi_1^e \left( \frac{\partial \xi_i^e}{\partial x} \cdot \frac{\partial \xi_j^e}{dx} + \frac{\partial \xi_i^e}{\partial z} \cdot \frac{\partial \xi_j^e}{dz} \right) dD^e$$

$$= \sum_e \frac{1}{4\Delta} \bar{K} (b_i b_j + c_i c_j) \qquad j,i = 1,2,\ldots,N$$

$$A_{ij} = \sum_e \int_{D^e} C_1 \xi_1^e \xi_i^e \, dD^e = \sum_e \frac{\Delta}{12} (2C_i + C_p + C_q) \quad \text{if } i = j \tag{7.9}$$

$$A_{ij} = 0 \quad \text{if } i \neq j$$

$$Q_i = - \sum_e \int_{S^e} V \xi_i^e \, dS = - \sum_e [(L_s V)_i / 2]$$

$$B_i = \sum_e \int_{D^e} K_1 \xi_1^e \frac{\partial \xi_i^e}{\partial z} \, dD^e = \sum_e \frac{\bar{K}}{2} C_i$$

The subscripts i, p and q refer to the three corners of each triangle, $\Delta$ is the area of triangle e, b and c are geometric coefficients defined in Appendix IV, $\bar{K}$ is the average conductivity over a triangle, i.e., $\bar{K} = (K_i + K_p + K_q)/3$, $D^e$ and $S^e$ are the interior and surface of e, respectively and N is the total number of nodes. The summation sign applies to all elements adjacent to nodal point i. The term $(L_s V)_i$ represents the flow rate across any side $L_s$ of the triangle which includes nodal point i. Here, the flux V is assumed to be uniform on $L_s$. In the present problem $Q_i$ is zero for all nodes except on the face AB where it is unspecified. The evaluation of the above integrals has been performed with the aid of Eq.(A.IV.2) and Table IV.1. The matrix [A] is diagonal as a consequence of defining $\partial h_i/\partial t$ as a weighted average over the entire flow region.

7.4.b. Geometrical Representation of Flow Region

For the computer implementation of the problem (7.1), the soil slab is divided into quadrilateral triangles, with the horizontal and vertical sides of length 2 cm (Fig. 7.2). This results in a total of 48 nodes and 70 elements.

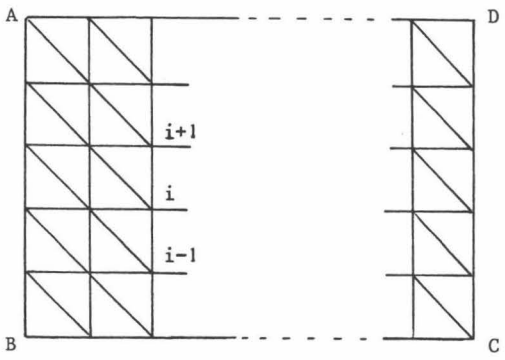


Fig. 7.2. Flow region with network of triangular elements.

7.4.c. Time Integration

The time marching procedure described in Chapter 2 applies unaltered to the system of equations (7.8) to yield the vector difference equation

$$\{[A]^{n+\frac{1}{2}} + \Delta t^n \nu\,[D]^{n+\frac{1}{2}}\}\{h\}^{n+1} = \{[A]^{n+\frac{1}{2}} - \Delta t^n(1-\nu)[D]^{n+\frac{1}{2}}\}\{h\}^n + \Delta t^n \{Q\}^{n+\frac{1}{2}} - \Delta t^n\{B\}^{n+\frac{1}{2}} \quad (7.10)$$

Equation (7.10) is no longer tridiagonal but sparse and symmetric, each equation, say the i-th, containing as many unknowns as there are elements associated with node i.

7.4.d. Boundary Conditions

For nodal points lying on AB and DC (Fig. 7.2), where values of $h_i^n$ are specified for all n, the condition is handled by a simple procedure. Suppose p is one of the nodes in question. The p-th equation in (7.10) is now replaced by a dummy expression

$$P_{pp}\, h_p^{n+1} = h_p \quad \text{(known)}$$

where $P_{pp} = 1$, and at the same time, the values of $h_p^{n+1}$ in all other remaining equations are replaced by $h_p$ and the corresponding terms trans-

ferred to the right hand side. In this way, the size of the coefficient matrix of $\{h\}^{n+1}$ remains unaltered.

For nodal points lying on AD and BC where a condition of zero flux across the faces prevails the corresponding values of $Q_i^{n+1/2}$ are set equal to zero.

## 7.5. RESULTS AND DISCUSSION

The predominantly one-dimensional horizontal infiltration into soil $P_1H_1$ is solved by the two-dimensional finite difference and finite element schemes for three initial conditions of (a) $h(x,z,0) = -345$ cm, (b) $h(x,z,0) = -1{,}000$ cm and (c) $h(x,z,0) = -15{,}000$ cm. The pressure head and water content fields after 7 minutes of infiltration for the three simulation runs are shown in Fig. 7.3. The curves are all extrapolated from outputs of nodal values at times immediately prior to and after 7 minutes.

At first glance there appears to be quite a large difference between the two solutions for initial conditions (a) and (b) because of large differences in the locations of the contour lines. However, when translated into total infiltration, the results are not that discrepant, the differences being less than 15% (Table 7.1). With initial condition (c), however, the difference is quite striking with the finite element result being less than half of the finite difference. On the basis of previous knowledge on infiltration behaviour of $P_1H_1$ (Chapters 3 and 5), the finite difference result is definitely the better in the case of initial condition (c).

Table 7.1. Total infiltration after 7 minutes for different initial conditions.

| Numerical | Total infiltration $cm^3/10\ cm^2$ | | |
|---|---|---|---|
| Method | (a)h(x,z,0)=-345cm | (b)h(x,z,0)=-1000cm | (c)h(x,z,0)=-15000cm |
| F D | 19.71 | 20.90 | 20.18 |
| F E | 22.71 | 22.80 | 9.79 |

Thus, the finite element method with a diagonalized capacity matrix, while giving a slight overprediction but still a fair comparison with the finite difference method for a wide range in the lower suctions, becomes inaccurate at high suction heads approaching wilting conditions.

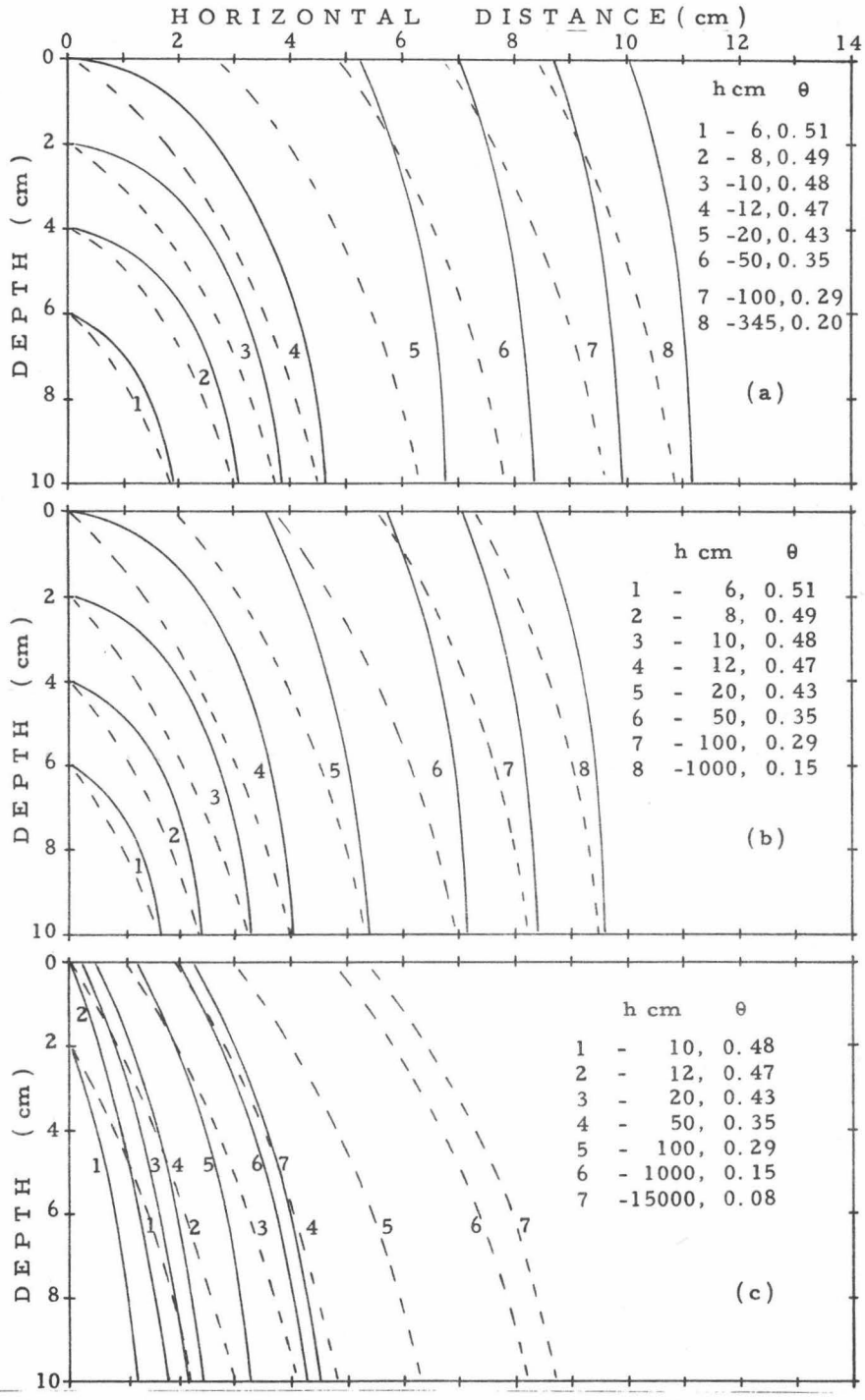


**Fig. 7. 3 Pressure head and water content fields at t=7 min during horizontal infiltration into soil slab of non-negligible height initially at (a) h(x, z, 0)=-345 cm, (b) h(x, z, 0)=-1000 cm (c) h(x, z, 0)=-15000 cm . (solid line - FE method, dashed line - FD method).**

The difference observed at the high suction also appears to be in the range that could have resulted in the 10 - 25% underprediction (in relation to the finite difference) observed in the results of Feddes et. al. (1975).

Two different strategies were then tried in an attempt at obtaining improved predictions. Firstly, it is recalled that in the one-dimensional case, diagonalizing the capacity matrix resulted in a slight increase in the total infiltration as well as an improvement in the mass balance for the initial condition of $h(z,0) = -345$ cm. A reverse process is, therefore, effected here, using a capacity matrix derived by the usual finite element technique, where for an element

$$\int_{D^e} C_1 \frac{\partial h^e}{\partial t} \xi_i^e \, dD^e = \begin{bmatrix} 6C_1+2C_2+2C_3 & 2C_1+2C_2+C_3 & 2C_1+C_2+2C_3 \\ 2C_1+2C_2+C_3 & 2C_1+6C_2+2C_3 & C_1+2C_2+2C_3 \\ 2C_1+C_2+2C_3 & C_1+2C_2+2C_3 & 2C_1+2C_2+6C_3 \end{bmatrix} \begin{Bmatrix} \frac{dh_1}{dt} \\ \frac{dh_2}{dt} \\ \frac{dh_3}{dt} \end{Bmatrix}$$

where the subscripts 1, 2 and 3 refer to the corners of the element (Note that diagonalizing by lumping all the capacity terms together results in the capacity matrix of the form in Eq. 7.9). The global relation analogous to (7.9) is obtained by summing over all elements. This strategy, however, did not yield a convergent solution for the one initial condition tried, namely, $h(x,z,0) = -345$ cm, hence confirming the claim of Neuman (1975).

It is also recalled that in the one-dimensional case, if the diagonal term were replaced by only the soil water capacity term corresponding to the given node this would result in a finite difference formulation for which mass balance is satisfied. Performing this operation on the two-dimensional case resulted in overestimation of up to 40% compared to the finite difference results in the case of the initial condition $h(x,z,0) = -15,000$ cm.

Thus, diagonalizing of the capacity matrix by taking a weighted average over the entire flow domain, in the finite element method, achieves two desirable results. These are, the attainment of convergent solutions as well as an improvement in the mass balance.

Before concluding it is worthwhile to mention other aspects of the problem solving process. In terms of input or resources necessary in effecting the two methods of solution, for deriving the required difference approximation until its successful computer implementation, the ADI finite difference technique requires negligible effort in comparison to the finite element method. Also, for this problem of simple geometry the computer time

required is very much smaller with the finite difference method. On the other hand, the handling of prescribed flux conditions by the finite difference, in this case, with the aid of imaginary nodes, is certainly less precise than in the case of the finite element method. Moreover, the essence of finite element, i.e., deriving the relationship elementwise and then assembling these together provides the flexibility of using different element sizes to suit the conditions of the problem. For example, in the case of rain infiltration on unprotected surface (Chapter 6), very small elements can be used to describe the rain-affected region while larger elements can be used for the more homogeneous subsurface soil. With finite difference, variable grid sizes is possible but entailing a lower order of accuracy.

## 7.5. CONCLUSION

Numerical results for the two-dimensional flow of water into a horizontal soil slab using the finite difference ADI technique and the Galerkin finite element method feature an inconsistency in the performance of the latter method for unsaturated flow as was inferred from the one-dimensional problems in Chapter 5. The diagonalized capacity matrix leads to a much greater pressure head range for which the results are considered acceptable. However, in view of an even wider range of pressure heads occurring in the soil, the advantage in flexibility is outweighed by the inconsistency and greater preparatory effort involved with this method. The easier and more consistent finite difference method is certainly preferred in soil water studies.

# CHAPTER 8

## SUMMARY AND GENERAL CONCLUSIONS

This study was designed with dual objectives, namely, to simulate water movement in the Bungor Series (Typic Paleudult) and to assess the relative merits of the finite difference and finite element numerical procedures employed in the solution of the unsaturated flow equation or Richards' equation. It was prompted, on the one hand, by the desire to examine the water flow behaviour in some Malaysian soils which are prone to erosion and the extent of the influence of the soil profile as a whole on the infiltration-runoff relationship during rain, and on the other, by the recent interest towards the usage of the finite element method in numerical procedures for unsaturated and saturated soil water flow. For the purpose of the study, disturbed samples from the top four horizons of two profiles of the Bungor Series were used.

The sequence of the simulation study, following the choice of the Richards' equation as the working model, is as follows :

(i) development of finite difference and finite element numerical approximations for the solution of the two variants of Richards' equation, that is, the moisture-based and the pressure-based equations.

(ii) characterization of the soil hydraulic properties required for the solution of Richards' equation ; this entails laboratory measurements of the specific water capacity for wetting, the soil water diffusivity and saturated conductivity and the structure characterization of the first two by the pattern recognition approach.

(iii) validation of the water flow model and evaluation of the numerical models.

(iv) simulation of water flow in the Bungor Series for different rainfall and surface conditions, and

(v) exploratory study on two-dimensional solutions by the finite difference and finite element methods.

The following summarizes the pertinent findings and conclusions from the study :

1. The pattern recognition approach can provide a convenient alternative for the structure characterization of poorly defined systems.

2. The Richards' model is valid for the description of water movement in the soils studied.

3. Within its range of applicability, that is, for unsaturated and homogeneous soil, the moisture-based equation is much superior to the pressure-based equation in all aspects of computation. With the moisture-based equation also, there is virtually no difference in the overall performance of the two numerical approximation methods. The finite element method gives a slightly superior mass balance but loses out in terms of computational time and effort.

4. The finite element method applied to the pressure-based equation, is reliable only for the moisture range wetter than field capacity. For drier initial conditions, the method gives very poor predictions. This stems from the non-diagonal nature of the capacity matrix derived using this method. The finite difference approximation to the h-based equation also shows rather poor accuracy for very dry initial conditions. The latter, however, can be remedied by the use of the Kirchoff integral transformation which effectively reduces the non-linearity in the conductivity-pressure head relationship thus allowing for a more efficient solution of the pressure-based equation when large pressure head gradients exist in the soil.

5. The inconsistency of the finite element method for unsaturated flow in one dimension is also evident in the two-dimensional case. However, diagonalizing the capacity matrix increases the range for which the solutions are acceptable. In view of these findings usage of the finite element method in unsaturated soil water studies appears to be very restricted, specifically, to the wetter soil conditions and because of the generally wide range of moisture condition naturally occurring in the soil, the more consistent finite difference technique would be more preferable.

6. For layered soils use of the h-based equation where the pressure head is assumed to vary continuously across the boundary and the flow rate

completely governed by the different layer properties gives useful and predictable results and, therefore, subsequently used as the basis for simulating movement in the Bungor Series.

7. With regard to the response to rain, it is gathered that rain which is capable of causing runoff within a reasonable period is one with intensity of about twice the magnitude of the saturated conductivity of the surface horizon. The extent of wetting and the total uptake before ponding or runoff occurs is small in the case of the heavy-textured soils considered. The depth of penetration is only of the order of several centimetres when runoff is initiated, so that, rarely will the hydraulic properties of the lower soil horizons affect the time of occurrence of runoff and hence the total uptake prior to ponding.

8. The two profiles of the Bungor Series exhibit significant differences in the hydraulic properties mainly due to the higher organic matter content in the upper horizons of the second profile and the generally higher clay content in it. Because of the greater permeability of Profile 1, it is generally about twice as efficient as the other profile in safely disposing away the rain water. In either case, the presence of a surface detention capacity can delay runoff for a considerable period of time and this property can be effectively used in the control of erosion.

9. The time of occurrence of ponding should be shortened by changes in the hydraulic properties of the rain-affected surface. Using some hypothetical relationships for the changing hydraulic properties, it is possible to simulate the flow pattern for unprotected soil surface. The soil beneath the rain-affected layer will not attain saturation inspite of the very small thickness of the latter. This particular simulation, while generating little information over what is already expected in practice, however, lends support to the appropriateness of the assumptions for treating layered soil.

Finally, it must be mentioned that this study is an attempt at applying some systems engineering techniques to the solution of an environmental problem of interest, hence, the problem aspect of the thesis is duly limited in its scope. In this regard too, we are encountered with a situation whereby, the tool is more refined than the object it is supposed to work on and one eventually has to reconcile the precise results of the present systems approach with the real field observations. It is the author's hope that this study is not an end in itself but only

the beginning of a series of more extensive as well as intensive studies towards generating more information about the soil environment in Malaysia.

# CHAPTER 9

# SAMENVATTING EN ALGEMENE BESLUITEN

Deze studie werd opgezet met een dubbel objektief, namelijk het simuleren van de waterbeweging in de Bungor Series (Typic Paleudult) en het bepalen van de waarde van 'de finite difference'- en de 'finite element' - numerische technieken gebruikt voor de oplossing van de onverzadigde stroomvergelijking of de Richards' vergelijking. Dit werd enerzijds ingegeven door het verlangen om het gedrag te onderzoeken van de waterbeweging in enkele Maleisische gronden die gevoelig zijn voor erosie en om de invloed van het bodemprofiel als geheel na te gaan op de infiltratie-runoff relatie gedurende de regen, en anderzijds door de recente interesse voor het gebruik van de finite element methode in numerische technieken voor onverzadigde en verzadigde grondwaterstromingen. Om dit studiedoel te bereiken werden monsters van de bovenste vier horizonten van 2 profielen van de Bungor Series gebruikt.

Het deel van de simulatiestudie volgend op de keuze van Richards' vergelijking als werkmodel, ziet eruit als volgt :

(i) ontwikkeling van de finite difference en finite element numerische benaderingen voor het oplossen van de 2 varianten van Richards vergelijking nl. deze op vocht-basis en deze op druk-basis.

(ii) karakterisatie van de hydrologische bodemkenmerken vereist voor de oplossing van Richards vergelijking. Dit brengt laboratoriummetingen met zich van de specifieke watercapaciteit in natte toestand, van de bodem water verplaatsing en van de verzadigde geleidbaarheid en de struktuurkarakterisatie van de eerste twee door middel van patroonherkenning.

(iii) nagaan van de waarde van het waterstromingsmodel en evaluatie van de numerische modellen.

(iv) simulatie van de waterbeweging in de Bungor Series voor verschillende regenval- en oppervlakvoorwaarden en

(v) verkennende studie omtrent twee-dimentionale oplossingen met behulp van de finite difference- en de finite element - methodes.

Het volgende overzicht geeft de bijzonderste bevindingen en besluiten van de studie :

1. De benadering via patroonherkenning kan een behoorlijk alternatief vormen voor de struktuur-karakterisatie van slecht gedefinieerde systemen.

2. De Richards vergelijking is geldig voor de beschrijving van waterbeweging in de bestudeerde bodems.

3. Binnen de grenzen van de toepasbaarheid, dat is voor onverzadigde en homogene gronden, is de vergelijking op vochtigheidsbasis veel beter dan de vergelijking op basis van druk en dit in alle aspecten van de berekening. Voor de vergelijking op druk-basis is er, uitgezonderd het feit dat de finite element - methode een iets hogere massa-balans geeft maar anderzijds iets meer rekentijd vraagt, virtueel geen verschil in het gebruik van de twee numerische benaderingsmethoden.

4. De finite element - methode, toegepast op de vergelijking op basis van druk, is alleen betrouwbaar voor de vochtigheidsgraad hoger dan veldcapaciteit. Voor drogere beginvoorwaarden geeft de methode zeer slechte schattingen. Dit komt door de niet-diagonale aard van de capaciteitsmatrix die afgeleid werd bij deze methode. De finite difference benadering van de vergelijking op h-basis vertoont ook eerder een lage nauwkeurigheid voor de zeer droge beginvoorwaarden. Dit laatste kan evenwel verholpen worden door het gebruik van de Kirchoff integraaltransformatie die de niet-lineariteit in de relatie geleidingsvermogen-stroomdruk effectief reduceert en aldus een meer efficiënte oplossing geeft voor de vergelijking op druk-basis wanneer grotere stroomdrukgradiënten bestaan in de bodem.

5. De inconsistentie van de finite element methode voor onverzadigde stroming in één dimensie is ook evident in het twee-dimensionale geval. Nochtans door diagonaliseren van de capaciteitsmatrix verhoogt de graad van aanvaardbaarheid van de oplossingen. Deze bevindingen indachtig schijnt het gebruik van de finite element - methode in onverzadigde grondwater-studies zeer beperkt en speciaal enkel voor natte bodems bestemd. Omwille van de algemeen brede variatie in de natuurlijke vochttoestanden van de bodem verdient de meer consistente finite difference - techniek de voorkeur.

6. Voor gelaagde gronden geeft het gebruik van de op h-gebaseerde vergelijking, waar men aanneemt dat de stroomdruk continu varieert doorheen de grensvlakken en de stroomsnelheid volledig afhangt van de verschillende laageigenschappen, goede en voorspelbare resultaten. Daarom wordt deze vergelijking gebruikt als basis voor de simulatie van de waterbeweging in de Bungor Series.

7. Met betrekking tot de respons op regen, kan men besluiten dat regen runoff kan veroorzaken binnen een redelijke periode indien de intensiteit ongeveer tweemaal deze is van de verzadigde geleidbaarheid van de bovenste horizont. De mate van natheid en de totale opname vóór de plasvorming of runoff is laag bij gronden met zware textuur. De bezakkingsdiepte is slechts van de orde van enige centimeters wanneer de runoff begint, zodat slechts zelden de hydrologische eigenschappen van de lagere horizonten de tijd waarop runoff voorkomt zullen beïnvloeden en bijgevolg ook de totale opname vóór de plasvorming.

8. De twee profielen van de Bungor Series vertonen significante verschillen in de hydraulische eigenschappen die hoofdzakelijk te wijten zijn aan het hoger gehalte organisch materiaal in de bovenste horizonten van het tweede profiel en aan zijn algemeen hoger kleigehalte. Wegens de grotere permeabiliteit is profiel 1 in het algemeen ongeveer tweemaal zo efficiënt als het andere qua veilig opbergen van het regenwater. In elk geval kan de aanwezigheid van een oppervlakkige opslagcapaciteit de runoff voor een aanzienlijke tijd uitstellen en deze eigenschap kan effektief gebruikt worden in de kontrole van de erosie.

9. De tijd, gedurende dewelke plasvorming optreedt, zou moeten ingekort worden door veranderingen in de hydrologische eigenschappen van het door de regen getroffen oppervlak. Door gebruik van enige hypothetische verbanden voor het veranderen van de hydrologische eigenschappen is het mogelijk het stromingspatroon voor niet beschermde gronden te simuleren. De bodem onder de door de regen getroffen laag zal geen verzadiging bereiken, ondanks de geringe dikte van deze laatste. Deze simulatie verleent, hoewel er algemeen weinig geweten is over wat de praktijk verwacht, toch steun aan de stellingname om gelaagde gronden te behandelen.

Uiteindelijk moet eraan herinnerd worden dat deze studie een poging is om enige systeem-ingenierurs-technieken toe te passen op een belangrik milieuprobleem, vandaar dat de omvang van de problemen in dit werk eerder beperkt is. Evenzo komen we in een situatie waar het doel

meer verfijnd is dan het onderwerp waarover gewerkt wordt en men moet eventueel de preciese resultaten van de huidige systeembenadering in verzoening brengen met de reële veldwaarnemingen. De auteur hoopt dat deze studie niet een einde betekent maar enkel een start is voor een reeks meer uitvoerige en meer intensieve studies omtrent het verzamelen van meer informatie van de bodems in Maleisië.

APPENDIX I

In the derivation of the finite element approximation to a partial differential equation, say in one dimension, the Galerkin criterion entails the evaluation of the integral in the form

$$I_{\alpha\beta} = \int_{z_1}^{z_2} \psi_1^{\alpha} \psi_2^{\beta} \, dz \qquad \text{(A.I.1)}$$

where $\alpha$ and $\beta$ are integer exponents.

Consider, for example, the evaluation of the first component in the Galerkin criterion (Eq. 2.26), i.e.

$$I = \int_{z_o}^{z_N} \psi_m \frac{\partial u^*}{\partial t} \, dz \qquad m = 0,\ldots,N$$

where $\psi_m$ has the property

$$\psi_m(z) = 1 - \frac{|z - z_m|}{\Delta z} \qquad |z - z_m| \leqslant \Delta z$$

$$\psi_m(z) = 0 \qquad |z - z_m| > \Delta z$$

Substituting for $u^*$ given by $u^* = \sum_{i=0}^{N} \psi_i u_i$ leads to

$$I = \int_{z_o}^{z_N} \psi_m \sum_{i=0}^{N} \psi_i \frac{du_i}{dt} \, . \, dz \qquad m = 0,\ldots,N$$

Expanding and making use of the properties of $\psi_m$ above, we arrive at

$$I = \int_{z_{m-1}}^{z_m} \psi_m \psi_{m-1} \, dz \, . \, \frac{du_{m-1}}{dt} + \int_{z_{m-1}}^{z_{m+1}} \psi_m \psi_m \, dz \, . \, \frac{du_m}{dt} + \int_{z_m}^{z_{m+1}} \psi_m \psi_{m+1} dz \, . \, \frac{du_{m+1}}{dt}$$

Evaluation of the above integrals (having the form of $I_{\alpha\beta}$, as in Eq. (A.I.1)) can be performed by direct means to yield for all interior nodes (i.e. $z_o$, $z_N$ excluded).

$$I = \frac{\Delta z}{6} \left[ \frac{du_{m-1}}{dt} + 4 \frac{du_m}{dt} + \frac{du_{m+1}}{dt} \right] \qquad m = 1,\ldots,N-1$$

In general, however, integration of $I_{\alpha\beta}$ is simplified with the aid of the following convenient formula

$$\int_{z_1}^{z_2} \psi_1^{\alpha} \psi_2^{\beta} \, dz = \frac{\alpha! \, \beta! (z_2 - z_1)}{(\alpha + \beta + 1)!} \qquad \text{(A.I.2)}$$

where, for instance, $\alpha!$ is the factorial of $\alpha$.

Tables of values of Eq. (A.I.2) for various integers $\alpha$ and $\beta$ can be found in a number of textbooks (as for example, Huebner, 1975). Part of the table given in the above reference is reproduced below, following the notations used in this thesis.

Table A.I.1. Integrals of basis functions (after Huebner, 1975)

$$I_{\alpha\beta} = \frac{1}{z_2 - z_1} \int_{z_1}^{z_2} \psi_1^{\alpha} \psi_2^{\beta} \, dz = \frac{A}{B}$$

| $\alpha + \beta$ | $\alpha$ | $\beta$ | A | B |
|---|---|---|---|---|
| 0 | 0 | 0 | 1 | 1 |
| 1 | 1 | 0 | 1 | 2 |
| 2 | 2 | 0 | 2 | 6 |
| 2 | 1 | 1 | 1 | 6 |
| 3 | 3 | 0 | 3 | 12 |
| 3 | 2 | 1 | 1 | 12 |

Thus for $\alpha = 1$, $\beta = 1$ and $z_2 - z_1 = \Delta z$, we have

$$I_{11} = \frac{1}{6}$$

and $$\int_{z_1}^{z_2} \psi_1 \, \psi_2 \, dz = \frac{\Delta z}{6}$$

APPENDIX II

The system of equation generated from the time integration of the finite difference or finite element approximation is of the form

$$[T]\{u\} = \{R\}$$

where

$$[T] = \begin{bmatrix} b_1 & c_1 & 0 & \cdots & 0 \\ a_2 & b_2 & c_2 & \ddots & \vdots \\ 0 & \ddots & \ddots & \ddots & 0 \\ \vdots & \ddots & \ddots & \ddots & c_{n-1} \\ 0 & \cdots & 0 & a_n & b_n \end{bmatrix}$$

$$\{u\} = [u_1 \quad u_2 \quad \cdots\cdots \quad u_n]^T$$

and

$$\{R\} = [R_1 \quad R_2 \quad \cdots\cdots \quad R_n]^T$$

To solve for $\{u\}$, the tridiagonal matrix $[T]$ is factorized into an $[L]$ and $[U]$ matrix

$$[T] = [L][U] = \begin{bmatrix} \alpha_1 & 0 & \cdots & 0 \\ a_2 & \alpha_2 & \ddots & \vdots \\ 0 & \ddots & \ddots & 0 \\ 0 & \cdots & a_n & \alpha_n \end{bmatrix} \begin{bmatrix} 1 & \beta_1 & 0 & \cdots & 0 \\ 0 & 1 & \beta_2 & \ddots & \vdots \\ \vdots & \ddots & \ddots & \ddots & 0 \\ \vdots & \ddots & \ddots & \ddots & \beta_{n-1} \\ 0 & \cdots & \cdots & 0 & 1 \end{bmatrix}$$

where $\alpha_1 = b_1$

$$\beta_i = \frac{c_i}{\alpha_i} \qquad i = 1,2,\ldots, n-1$$

$$\alpha_i = b_i - a_i b_{i-1} \qquad i = 2,3, \ldots, n$$

For the above computation to be valid $\alpha_i \neq 0$ for all i.

The solution is now accomplished by letting $\{v\} = [U]\{u\}$. Then, $[L]\{v\} = \{R\}$ which can be solved for $\{v\}$ by forward substitution

$$v_1 = R_1/\alpha_1$$

$$v_i = (R_i - a_i v_{i-1})/\alpha_i \qquad i = 2,3,\ldots, n$$

Finally, $[U]\{u\} = \{v\}$ is solved by backward substitution

$$u_n = v_n$$

$$u_i = v_i - \beta_i u_{i+1} \qquad i = n-1,\ n-2,\ \ldots,\ 1$$

One should be cautious in using this algorithm since the latter may converge to a wrong solution which may look reasonable to the casual observer. In order to obtain a correct solution, the following conditions are sufficient (although not necessary)

(i) $|b_1| > |c_1| > 0$

(ii) $|b_i| \geq |a_i| + |c_i|$ , $a_i c_i \neq 0$, $i = 2,3,\ldots,\ n-1$

(iii) $|b_n| > |a_n| > 0$

If the elements of $[T]$ satisfy these conditions, $[T]$ is said to be diagonally dominant. This is true in cases considered herein. An example when conditions (i) and (ii) are not necessary is when $[T]$ is symmetric and positive definite.

The algorithm above is attributed to Thomas (1949) and has been shown to be extremely stable with respect to round-off errors (Douglas, 1959).

APPENDIX III

Classification and description of the two profiles of the Bungor Series

PROFILE 1

Soil Name : Colluvium from Bungor Series

Classification : (a) Taxonomy : Clayey over clayey-skeletal kaolinitic isohyperthermic Typic Paleudult

(b) FAO : Dystric Nitosol

Authors of Description : S. Paramananthan, Luc Maene, Mokhtaruddin and Shamsuddin

Location : Universiti Pertanian Malaysia Campus, Pasture Field No. 10

Elevation : 30 m (100 ft)

Landforms : Lower midslope of moderately dissected undulating hills

Slopes : 6°

Climate : Moisture Regime : Udic

Temperature Regime : Isohyperthermic

Parent Material : Sandstones/shales

Drainage : Moderately well drained

Moisture Condition of the soil : Moist

Water-table 1.3 m

The soil consists of colluvial material overlying the weathered shales and sandstone. The colluvium is believed to be derived from Bungor Series and also laterites from the surrounding areas.

Profile Description

| | | |
|---|---|---|
| Ap | 0-12 cm | Brown (10YR 5/3) fine sandy loam ; strong medium and fine subangular blocky ; slightly friable ; no clay-skins ; common pores ; few charcoal fragments ; few channels ; abundant fine roots ; rather sharp boundary. |
| $B_1$ | 12-30 cm | Yellow (10YR 7/6) fine sandy clay loam ; moderate medium and coarse subangular blocky ; friable to firm ; patchy clayskins on ped faces and occasional organic stains on ped faces ; few pores ; few charcoal fragments ; occasional channel ; many fine roots ; diffuse boundary. |
| $B_{2t}$ | 30-86 cm | Very pale brown (10YR 7/4) clay ; weak medium and coarse subangular blocky ; friable ; discontinuous to continuous clayskins on ped faces ; few pores ; occasional pieces of vein quartz ; occasional termite chamber (2 cm) few fine roots ; rather sharp boundary. |

| | | |
|---|---|---|
| $IIC_1$ | 86-140 cm | Pale yellow (2.5Y 7/4) with few (5%) medium distinct dusky red (10R 3/4) mottles ; gravelly clay ; weak medium and coarse angular blocky ; friable to slightly sticky ; patchy clayskins on ped faces ; gravels consist mainly of petroplinthite concretions ; very few fine roots ; diffuse boundary. |
| $IIC_2$ | 140-190 cm | Light gray (10YR 7/1) with few (10%) medium distinct red (10R 4/6) mottles ; clay ; massive ; sticky ; a band of vein quartz cuts across the profile. |

PROFILE 2

Soil Name : Bungor Series (lateritic phase)

Classification : (a) Taxonomy : Clayey over clayey-skeletal, kaolinitic isohyperthermic Typic Paleudult

(b) FAO : Dystric Nitosol

Authors of Description : S. Paramananthan, Luc Maene, Mokhtaruddin and Shamsuddin

Location : Universiti Pertanian Malaysia Campus, Pasture Field No. 10

Elevation : 30 m (100 ft)

Landform : Crest of hill in undulating terrain

Slope : 3°

Climate : Moisture Regime : Udic

Temperature Regime : Isohyperthermic

Parent Material : Sandstones/shales

Drainage : Moderately well drained

Moisture Condition of the soil : Moist

Water-table 1.3 m

The soil consists of colluvial material overlying the weathered shales/sandstone. The colluvium is believed to be derived from the surrounding Bungor/Serdang Series while the laterite from the Malacca or Prang Series.

Profile Description

| | | |
|---|---|---|
| Ap | 0-15 cm | Brown (10YR 4/3) sandy loam; medium to coarse strong subangular blocky ; firm, no clayskins ; few pores ; few charcoal fragments ; many medium and fine roots ; sharp boundary. |

| | | |
|---|---|---|
| $B_1$ | 15-31 cm | Yellowish brown (10YR 5/8) fine sandy clay ; strong coarse subangular blocky ; firm ; patchy clayskins ; some organic coatings on ped faces and along old root channels ; common pores ; few channels ; many fine and a few coarse roots, diffuse boundary. |
| $B_{2t}$ | 31-50/62cm | Brownish yellow (10YR 6/6) clay ; weak medium and fine subangular blocky ; friable ; thin discontinuous clay-skins ; occasional organic stains ; few pores ; few channels ; occasional charcoal fragments ; few fine roots ; sharp wavy boundary. |
| $IIB_{31cn}$ | 50/62-120cm | Reddish yellow (7.5YR 6/8) gravelly clay ; weak medium subangular blocky friable ; discontinuous clayskins on ped faces ; gravels consist mainly of subrounded ironstone concretions ; few fine roots ; few pores ; diffuse boundary. |
| $IIB_{32cn}$ | 120-144cm | Yellow (2.5Y 7/6) gravelly clay ; weak coarse angular blocky ; friable ; patchy clayskins on ped faces ; gravels consist of ironstone and vein quartz fragments; sharp boundary. |
| IIIC | 144cm+ | Pale yellow (2.5Y 7/4) with few (10%) medium distinct dusky red (10R 3/6) mottles ; clay ; massive ; friable; patchy coatings ; occasional channel, red mottles are sandier and tend to form soft concretions. |

APPENDIX IV : LOCAL COORDINATE FUNCTIONS IN TWO DIMENSIONS

It is desired to choose local coordinates $\xi_1^e$, $\xi_2^e$ and $\xi_3^e$ to describe the location of a point $P(x_p, z_p)$ within an element or on its boundary (Fig.IV.1).

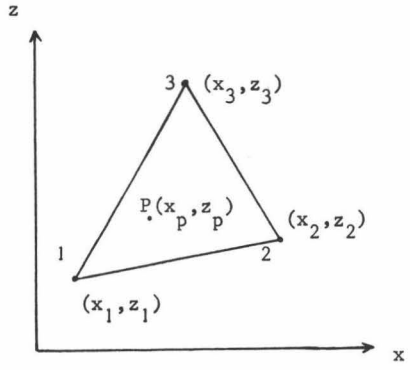


Fig. IV.1. Three-node triangle element with global coordinates $(x_p,z_p)$ defining some point within the element.

The original cartesian coordinates (x,y) is linearly related to the natural or local coordinates by the following equations (Huebner, 1975)

$$x = \xi_1^e x_1 + \xi_2^e x_2 + \xi_3^e x_3$$

$$z = \xi_1^e z_1 + \xi_2^e z_2 + \xi_3^e z_3$$

Furthermore $\xi_1^e + \xi_2^e + \xi_3^e = 1$.

Inversion of the above equation gives the local coordinates in terms of the cartesian coordinates. Thus

$$\xi_1^e(x,z) = \frac{1}{2\Delta}(a_1 + b_1 x + c_1 z)$$

$$\xi_2^e(x,z) = \frac{1}{2\Delta}(a_2 + b_2 x + c_2 z) \qquad \text{(A.IV.1)}$$

$$\xi_3^e(x,z) = \frac{1}{2\Delta}(a_3 + b_3 x + c_3 z)$$

where $2\Delta = \begin{vmatrix} 1 & x_1 & z_1 \\ 1 & x_2 & z_2 \\ 1 & x_3 & z_3 \end{vmatrix}$ = 2 x area of triangle 1-2-3

and $a_1 = x_2 z_3 - x_3 z_2$ , $b_1 = z_2 - z_3$ , $c_1 = x_3 - x_2$.

The other coefficients are obtained by cyclically permuting the subscripts. In addition, Eq. (A.IV.1) gives

$$\frac{\partial \xi_i^e}{\partial x} = \frac{b_i}{2\Delta} \quad ; \quad \frac{\partial \xi_i^e}{\partial z} = \frac{c_i}{2\Delta} \quad , \; i = 1,2,3 \tag{A.IV.2}$$

For integrating area coordinates over the area of a triangular element we allude to the following convenient formula :

$$\int_{D^e} (\xi_1^e)^{\alpha} \, (\xi_2^e)^{\beta} \, (\xi_3^e)^{\gamma} \, dD^e = \frac{\alpha!\, \beta!\, \gamma!}{(\alpha + \beta + \gamma + 2)!} \, 2\Delta$$

Table IV.1, which is reproduced, in part, from Huebner (1975), gives the values of the above equation for various integers $\alpha$, $\beta$ and $\gamma$.

Table IV.1. Integrals of area coordinates

$$I = \frac{1}{\Delta} \int_{D^e} (\xi_1^e)^{\alpha} \, (\xi_2^e)^{\beta} \, (\xi_3^e)^{\gamma} \, dD^e = \frac{A}{B}$$

| $\alpha+\beta+\gamma$ | $\alpha$ | $\beta$ | $\gamma$ | A | B |
|---|---|---|---|---|---|
| 0 | 0 | 0 | 0 | 1 | 1 |
| 1 | 1 | 0 | 0 | 1 | 3 |
| 2 | 2 | 0 | 0 | 2 | 12 |
| 2 | 1 | 1 | 0 | 1 | 12 |
| 3 | 3 | 0 | 0 | 6 | 60 |
| 3 | 2 | 1 | 0 | 2 | 60 |
| 3 | 1 | 1 | 1 | 1 | 60 |

APPENDIX V

Results of regression analyses on horizontal infiltration data

| Soil Horizon | Replicate | $x = t^{1/2} + a_\lambda$ ($\lambda$ = penetrability) | $Q = St^{1/2} + a_S$ (S = sorptivity) |
|---|---|---|---|
| P | 1 | $2.041t^{1/2} + 0.398$ | $0.982t^{1/2} + 0.200$ |
| $P_1H_1$ | 2 | $2.087t^{1/2} + 0.463$ | $1.018t^{1/2} + 0.132$ |
| | 3 | $2.153t^{1/2} + 0.356$ | $1.059t^{1/2} + 0.177$ |
| | 1 | $1.935t^{1/2} + 0.265$ | $0.971t^{1/2} + 0.051$ |
| $P_1H_2$ | 2 | $2.005t^{1/2} + 0.035$ | $1.050t^{1/2} - 0.153$ |
| | 3 | $1.960t^{1/2} + 0.294$ | $0.977t^{1/2} - 0.085$ |
| | 1 | $1.670t^{1/2} + 0.210$ | $0.866t^{1/2} - 0.090$ |
| $P_1H_3$ | 2 | $1.807t^{1/2} + 0.279$ | $0.934t^{1/2} - 0.158$ |
| | 3 | $1.823t^{1/2} + 0.231$ | $0.935t^{1/2} - 0.087$ |
| | 1 | $1.606t^{1/2} + 0.337$ | $0.851t^{1/2} + 0.004$ |
| $P_1H_4$ | 2 | $1.682t^{1/2} + 0.240$ | $0.834t^{1/2} - 0.025$ |
| | 3 | $1.741t^{1/2} + 0.391$ | $0.902t^{1/2} - 0.150$ |
| | 1 | $1.039t^{1/2} + 0.937$ | $0.566t^{1/2} - 0.038$ |
| $P_2H_1$ | 2 | $0.990t^{1/2} + 0.964$ | $0.482t^{1/2} + 0.122$ |
| | 3 | $1.089t^{1/2} + 0.807$ | $0.532t^{1/2} - 0.139$ |
| | 1 | $1.196t^{1/2} + 0.705$ | $0.599t^{1/2} - 0.008$ |
| $P_2H_2$ | 2 | $1.131t^{1/2} + 0.950$ | $0.623t^{1/2} + 0.027$ |
| | 3 | $1.162t^{1/2} + 0.807$ | $0.619t^{1/2} + 0.090$ |
| | 1 | $1.380t^{1/2} + 0.427$ | $0.751t^{1/2} - 0.015$ |
| $P_2H_3$ | 2 | $1.241t^{1/2} + 0.580$ | $0.657t^{1/2} - 0.173$ |
| | 3 | $1.336t^{1/2} + 0.501$ | $0.701t^{1/2} - 0.100$ |
| | 1 | $1.459t^{1/2} + 0.132$ | $0.780t^{1/2} - 0.040$ |
| $P_2H_4$ | 2 | $1.419t^{1/2} + 0.101$ | $0.750t^{1/2} - 0.031$ |
| | 3 | $1.453t^{1/2} + 0.112$ | $0.705t^{1/2} + 0.039$ |

x = distance of wetting front from water source;

Q = total infiltration.

APPENDIX VI

1. Statistical analyses on penetrability

(a) Profile 1

Analysis of variance:

| Source of variance | Degrees of freedom | Sum of squares | Mean of squares | F - value |
|---|---|---|---|---|
| Horizons | 3 | 0.322084 | 0.107361 | 26.75** |
| Error | 8 | 0.032085 | 0.004013 | |
| Total | 11 | 0.354169 | | |

LSD (least significant difference) at 5% level = 0.119 $cm/min^{1/2}$

Duncan's New Multiple Range Test:

| Horizon | $P_1H_1$ | $P_1H_2$ | $P_1H_3$ | $P_1H_4$ |
|---|---|---|---|---|
| Mean penetrability ($cm/min^{1/2}$) | 2.094 | 1.967 | 1.767 | 1.676 |

(b) Profile 2

Analysis of variance:

| Source of variance | Degrees of freedom | Sum of squares | Mean of squares | F - value |
|---|---|---|---|---|
| Horizons | 3 | 0.281733 | 0.093911 | 41.65** |
| Error | 8 | 0.018039 | 0.002255 | |
| Total | 11 | 0.299772 | | |

LSD at 5% level = 0.089 $cm/min^{1/2}$

Duncan's New Multiple Range Test:

| Horizon | $P_2H_4$ | $P_2H_3$ | $P_2H_2$ | $P_2H_1$ |
|---|---|---|---|---|
| Mean penetrability ($cm/min^{1/2}$) | 1.444 | 1.319 | 1.163 | 1.039 |

2. Statistical analyses on sorptivity

(a) Profile 1

Analysis of variance:

| Source of variance | Degrees of freedom | Sum of squares | Mean of squares | F - value |
|---|---|---|---|---|
| Horizons | 3 | 0.051368 | 0.017123 | 11.55** |
| Error | 8 | 0.011887 | 0.001483 | |
| Total | 11 | 0.063255 | | |

LSD at 5% level = 0.073 cm/min$^{1/2}$

Duncan's New Multiple Range Test:

| Horizon | $P_1H_1$ | $P_1H_2$ | $P_1H_3$ | $P_1H_4$ |
|---|---|---|---|---|
| Mean sorptivity (cm/min$^{1/2}$) | 1.020 | 1.006 | 0.912 | 0.862 |

(b) Profile 2

Analysis of variance:

| Source of variance | Degrees of freedom | Sum of squares | Mean of squares | F - value |
|---|---|---|---|---|
| Horizons | 3 | 0.085086 | 0.028362 | 20.27** |
| Error | 8 | 0.011196 | 0.001399 | |
| Total | 11 | 0.096282 | | |

LSD at 5% level = 0.070 cm/min$^{1/2}$

Duncan's New Multiple Range Test:

| Horizon | $P_2H_4$ | $P_2H_3$ | $P_2H_2$ | $P_2H_1$ |
|---|---|---|---|---|
| Mean sorptivity (cm/min$^{1/2}$) | 0.745 | 0.703 | 0.614 | 0.527 |

** significant at 1% level

———— not significant at 5% level

-------- not significant at 1% level

# BIBLIOGRAPHY

AHUJA, L.R. and D. SWARTZENDRUBER (1972). An improved form of soil-water diffusivity function. Soil Sci. Soc. Amer. Proc., 36, 9-14.

AYLOR, D.E. and Y. PARLANGE (1973). Vertical infiltration into a layered soil. Soil Sci. Soc. Amer. Proc., 37, 673-676.

BAKER, D.N., J.R. LAMBERT, C.J. PHAENE and J.M. McKINION (1976). GOSSYN - A simulation of cotton crop dynamics. Proc. of Sem. on the Application of Computers to the Management of Large Scale Agr./Indust. Complexes, Sci. Res. Inst. Planning, Latvian, Gosplan, Regia, Russia.

BAVER, L.D., W.H. GARDNER and W.R. GARDNER (1972). Soil Physics, 4th ed. Wiley, New York.

BRAESTER, C. (1973). Moisture variation at the soil surface and the advance of the wetting front during infiltration at constant flux Water Resour. Res., 9, 687-694.

BROOKS, R.H. and A.T. COREY (1964). Hydraulic Properties of porous media. Hydrol. Pap. 3, Colo. State Univ. Fort Collins.

BRUCE, R. and A. KLUTE (1956). The measurement of soil moisture diffusivity. Soil Sci. Soc. Amer. Proc., 20, 458-462.

BRUCE, R. and A. WHISLER (1973). Infiltration of water into layered field soils. In "Physical aspects of soil, water and salts in ecosystems", Ed., Hadas, A., D. Swartzendruber, P. Rijtema, M. Fuchs and B. Yaron. Springer-Verlag, Heidelberg, New York, 77-79.

CHILDS, E.C. (1969). The physical basis of soil water phenomena. John Wiley & Sons, London, New York.

CHILDS, E.C. and N. COLLIS-GEORGE (1950). The permeability of porous materials. Proc. Roy. Soc., 201A, 392-405.

CHILDS, E.C. and A. POULOVASSILIS (1960). An oscillating permeameter. Soil Sci., 90, 326-328.

COLMAN, E.S. and G.B. BODMAN (1944). Moisture and energy conditions during downward entry of water into moist and layered soils. Soil Sci. Soc. Amer. Proc., 9, 3-11.

CUSHMAN, J. and D. KIRKHAM (1978). A two-dimensional linearized view of one-dimensional unsaturated-saturated flow. Water Resour. Res., 14, 319-323.

D'HOLLANDER, E. (1976). Two-dimensional water flow simulation of an evaporating soil. Med. Fac. Landbouww. Rijksuniv. Gent, 41, 351-359.

D'HOLLANDER, E. and I. IMPENS (1975). Hybrid simulation of a dynamic model for water movement in a soil-plant-atmospheric continuum. In "Modeling and simulation of water resources systems", Ed., Vansteenkiste, G.C. North-Holland Publ., pp. 349-360.

DOUGLAS, J.J. (1959). Round-off errors in the numerical solution of the heat equation. J. Assoc. Computing Mach., 6, 48-58.

EAGLEMAN, J.R. and V.C. JAMISON (1962). Soil layering and compaction effects on unsaturated water movement. Soil Sci. Soc. Amer. Proc., 26, 519-522.

EDWARDS, W.R. and W.E. LARSON (1969). Infiltration of water into soils as influenced by surface seal development. Trans. ASAE, 12, 463-465, 470.

EMERY, A.F. and W.W. CARSON (1971). An evaluation of the finite element method in the computation of temperature. Jour. Heat Transfer, Trans. ASME, 93, 136-145.

FANG, C.S. and S.N. WANG (1972). Groundwater flow in a sandy tidal beach 2. Two-dimensional finite element analysis. Water Resour. Res., 8, 121-128.

FARRELL, D.A. and W.E. LARSON (1972). Dynamics of the soil-water system during a rainstorm. Soil Sci., 113, 88-95.

FEDDES, R.A., E. BRESLER and S.P. NEUMAN (1974). Field test of a modified model for water uptake by root systems. Water Resour. Res., 10, 1199-1206.

FEDDES, R.A., S.P. NEUMAN and E. BRESLER (1975). Finite element analysis of two-dimensional flow in soils considering water uptake by roots. II. Field applications. Soil Sci. Soc. Amer. Proc., 39, 231-237.

FORSYTHE, G.E. and W.R. WASOW (1960). Finite-difference methods for partial differential equations. New York, John Wiley and Sons.

FREEZE, R.A. (1969). The mechanism of natural ground-water recharge and discharge, 1. One-dimensional, vertical, unsteady, unsaturated flow above a recharging or discharging ground-water flow system. Water Resour. Res., 5, 153-171.

GARDNER, W.R. and M.S. MAYHUGH (1958). Solution and tests of the diffusion equation for the movement of water in soil. Soil Sci. Soc. Amer. Proc., 22, 197-201.

GARDNER, W.R. and F.J. MIKLICH (1962). Unsaturated conductivity and diffusivity measurements by constant flux method. Soil Sci., 93, 271-274.

GORDON, G. (1969). System simulation. Prentice Hall, New Jersey.

GREEN, W.H. and G.A. AMPT (1911). Studies in soil physics: I. The flow of air and water through soils. J. Agr. Sci., 4, 1-24.

GREEN, R.E., R.J. HANKS and W.E. LARSON (1964). Estimates of field infiltration by numerical solution of the moisture flow equation. Soil Sci. Soc. Amer. Proc., 28, 15-19.

GUYMON, G.L., V.H. SCOTT and L.R. HERMANN (1970). A finite element solution of one-dimensional diffusion-convection equation. Water Resour. Res., 6, 204-210.

HANKS, R.J. and S.A. BOWERS (1962). Numerical solution of the moisture flow equation for infiltration into layered soils. Soil Sci. Soc. Amer. Proc., 26, 530-534.

HANKS, R.J. and S.A. BOWERS (1963). Influence of variations of the diffusivity water content relation on infiltration. Soil Sci. Soc. Amer. Proc., 27, 263-265.

HAVERKAMP, R., M. VAUCLIN, J. TOUMA, P.J. WIERENGA and G. VACHAUD (1977). A comparison of numerical simulation models for one-dimensional infiltration. Soil Sci. Soc. Amer. Proc., 41, 285-294.

HERUDJITO, D. (1977). Contribution to the study of vertical water movement in a natural and conditioned silty loam soil. Doctorate Thesis, State Univ. Ghent.

HILLEL, D., C.H.M. VAN BAVEL and W. TALPAZ (1975). Dynamic simulation of storage in fallow soil as affected by mulch of hydrophobic aggregates. Soil Sci. Soc. Amer. Proc., 39, 826-833.

HILLEL, D. and W.R. GARDNER (1969). Steady infiltration into crust-topped profiles. Soil Sci., 108, 137-142.

HILLEL, D. and W.R. GARDNER (1970). Transient infiltration into crust-topped profiles. Soil Sci., 109, 69-76.

HUDSON, N. (1971). Soil conservation. Batsford Ltd., London.

HUEBNER, K.H. (1975). The finite element methods for engineers. John Wiley & Sons, New York.

ISAACSON, E. and H. KELLER (1966). Analysis of numerical methods. John Wiley & Sons, New York.

ISERMANN, R. (1975). Modeling and identification of dynamic process - an extract. In "Modeling and simulation of water resources systems", Ed.,Vansteenkiste, G.C. North-Holland Publ., pp. 7-33.

IVE, J.R., C.W. ROSE, B.H. WALL and B.W.R. TORSSELL (1976). Estimation and simulation of sheet run-off. Aust. J. Soil Res., 14, 129-138.

JACKSON, R.D. (1963). Porosity and soil-water diffusivity relations. Soil Sci. Soc. Amer. Proc., 27, 123-126.

KANAL, L. (1974). Patterns in pattern recognition 1968-1974. IEEE Trans. on information theory, November, IT 20.

KARPLUS, W.J. (1972). System identification and simulation, a pattern recognition approach. Proc. Fall Joint Compt. Conf., 385-392.

KLUTE, A. (1952). A numerical method for solving the flow equation for water in unsaturated materials. Soil Sci., 73, 105-116.

KLUTE, A. (1972). The measurement of the hydraulic conductivity and diffusivity of unsaturated soils. Soil Sci., 113, 264-276.

KLUTE, A., F.D. WHISLER and E.J. SCOTT (1965). Numerical solution of the nonlinear diffusion equation for water flow in a horizontal soil column of finite length. Soil Sci. Soc. Amer. Proc., 29, 353-358.

KUNZ, K.S. (1957). Numerical Analysis. McGraw Hill, New York.

LAMBERT, J.R., D.N. BAKER and C.J. PHENE (1976). Dynamics of processes in the soil under growing row crops : RHIZOS. Proc. of Sem. on Application of Computers to the Management of Large Scale Agr. & Indust. Complexes : Sci. Res. Institute of Planning, Latvian, Gosplan, Regia, Russia.

MAENE, L.J., L.K. HUAN, G.G. MAESSCHALCK and M. MOKHTARUDDIN (1977). Soil physics project: Annual report of Belgian technical cooperation programme, Universiti Pertanian Malaysia.

MILLER, D.E. and W.H. GARDNER (1962). Water infiltration into stratified soil. Soil Sci. Soc. Amer. Proc., 26, 115-119.

MUALEM, Y. (1978). Hydraulic conductivity of unsaturated porous media: Generalized macroscopic approach. Water Resour. Res., 14, 324-334.

NEUMAN, S.P. (1973). Saturated-unsaturated seepage by finite elements. Jour. Hydraulic Div., ASCE, 99, 2233-2250.

NEUMAN, S.P., R.A. FEDDES and E. BRESLER (1975). Finite element analysis of two-dimensional flow in soils considering water uptake by roots.

Soil Sci. Soc. Amer. Proc., 39, 224-230.

NEUMAN S.P. and T.N. NARASIMHAN (1977). Mixed explicit-implicit iterative finite element scheme for diffusion-type problems: I. Theory. Int. J. num. Meth. Engng , 11, 309-323.

NIELSEN, D.R., J.W. BIGGAR and J.M. DAVIDSON (1962). Experimental consideration of diffusion analysis in unsaturated flow problems. Soil Sci. Soc. Amer. Proc., 26, 107-111.

NIELSEN, D.R., J.M. DAVIDSON, J.W. BIGGAR and R.J. MILLER (1964). Water movement through Panoche clay loam soil. Hilgardia, 35, 491-506.

NILSSON, N.J. (1965). Learning machines - Foundations of trainable pattern-classifying systems. McGraw Hill, New York.

NIMAH, M.N. and R.J. HANKS (1973). Model for estimating soil water, plant and atmospheric interrelations. I. Description and Sensitivity. Soil Sci. Soc. Amer. Proc., 37, 522-527.

O'BRIEN, F.E.M. (1948). The control of humidity by saturated salt solutions. J. Sci. Instr., 25, 73-76.

PARLANGE, Y. (1971). Theory of water movement in soils. 2. One-dimensional infiltration. Soil Sci., 111, 170-174.

PARLANGE, Y. (1972). One-dimensional infiltration with constant flux at the surface. Soil Sci., 114, 1-4.

PARLANGE, Y. (1977). A note on the use of infiltration equations. Soil Sci. Soc. Amer. J., 41, 654-655.

PEACEMAN, D.W. and H.H. RACHFORD (1955). The numerical solution of parabolic and elliptic differential equations. J. Soc. Industr. Appl. Math., 3, 28-41.

PHILIP, J.R. (1957). The theory of infiltration: 1. The infiltration equation and its solution. Soil Sci., 83, 345-357.

PHILIP, J.R. (1957a). The theory of infiltration : 4. Sorptivity and algebraic infiltration equations. Soil Sci., 84, 257-264.

PHILIP, J.R. (1957b). The theory of infiltration : 6. Effect of water depth over soil. Soil Sci., 85, 278-286.

PHILIP, J.R. (1972). Future problems of soil research. Soil Sci., 113, 294-300.

PINDER, G.F. and E.D. FRIND (1972). Application of Galerkin's procedure to aquifer analysis. Water Resour. Res., 8, 108-120.

RAATS, P.A.C. and W.R. GARDNER (1974). Movement of water in the unsaturated zone near a water table. In "Drainage for Agriculture", Ed., van Schilfgaarde, J. Agronomy 17, 311-405, Amer. Soc. Agron. Madison, Wis.

RAATS, P.A.C. (1973). Unstable wetting fronts in uniform and non-uniform soils. Soil Sci. Soc. Amer. Proc., 37, 681-685.

RAMSER, C.E. (1927). Run-off from small agricultural areas. J. Agr. Res., 34, 797-823.

REICHARDT, K., D.R. NIELSEN and J.W. BIGGAR (1972). Horizontal infiltration into layered soils. Soil Sci. Soc. Amer. Proc., 36, 858-863.

REMSON, I., G.M. HORNBERGER and F.J. MOLZ (1971). Numerical methods in subsurface hydrology. Wiley-Interscience, New York.

REMSON, I., M. RESNICOFF and B.B. SCOTT (1967). Numerical studies of drainage of unsaturated soils. Trans. ASCE, 10, 388-390.

RICHARDS, L.A. (1931). The conduction of liquids through porous medium. Physics, 1, 318-313.

RICHARDSON, L.F. (1910). The approximate arithmetical solution by finite differences of physical problems involving differential equations with an application to the stresses in masonry dam. Phil. Trans. Royal Soc. A210, 307-357.

RICHTMEYER, R.D. and K.W. MORTON (1967). Difference methods for initial-value problems. Interscience, New York.

ROGERS, J.S. and A. KLUTE (1971). The hydraulic conductivity water content relationship during non-steady flow through a sand column. Soil Sci. Soc. Amer. Proc., 35, 695-700.

RUBIN, J. (1968). Theoretical analysis of two-dimensional transient flow of water in unsaturated and partly saturated soils. Soil Sci. Soc. Amer. Proc., 32, 607-615.

RUBIN,J. and R. STEINHARDT (1963). Soil water relations during rain infiltration: I. Theory. Soil Sci. Soc. Amer. Proc., 27, 246-251.

RUBIN, J. and R. STEINHARDT (1964). Soil water relations during rain infiltration: III. Water uptake at incipient ponding. Soil Sci. Soc. Amer. Proc., 28, 614-619.

SARIDIS, G.N. and R.F. HOFSTADTER (1974). A pattern recognition approach to the classification of non-linear systems. IEEE Trans. on Systems, Man and Cybernatics, SMC-4, 362-370.

SCHWAB, G.O., R.K. FREVERT, T.W. EDMINSTER and K.K. BARNES (1966). Soil and water conservation engineering , 2nd ed. Wiley, New York.

SIMUNDICH, T.M. (1975). System characterization: a pattern recognition approach. Ph.D. Thesis, UCLA, School of Engineering and Applied Sciences, Los Angeles.

SMITH, I.M., R.V. FARRADAY and B.A. O'CONNOR (1973). Rayleigh-Ritz and Galerkin finite element for diffusion-convection problem. Water Resour. Res. 9, 593-606.

STAPLE, W.J. (1966). Infiltration and redistribution of water in vertical columns of a loam soil. Soil Sci. Soc. Amer. Proc., 30, 553-558.

STROOSNIJDER, L., H. VAN KEULEN and G. VACHAUD (1972). Water movement in layered soils - 2. Experimental confirmation of a simulation model. Neth. J. agric. Sci., 20, 67-72.

SWARTZENDRUBER, D. (1969). The flow of water in unsaturated soils. In "Flow through porous media", Ed., De Wiest, R.J.M. Academic Press, New York.

SWARTZENDRUBER, D. and D. HILLEL (1973). The physics of infiltration. In "Physical aspects of soil, water and salts in ecosystems", Ed., Hadas, A., D. Swartzendruber, P. Rijtema, M. Fuchs and B. Yaron. Springer Verlag, Heidelberg, New York, 3-15.

THOMAS, L.H. (1949). Elliptic problems in linear difference equations over a network. Report of Watson Science Computing Laboratory - New York, Columbia University.

VACHAUD, G. (1967). Determination of hydraulic conductivity of unsaturated soils from analysis of transient flow data. Water Resour. Res., 3, 697-705.

VACHAUD, G. and J.L. THONY (1971). Hysteresis during infiltration and redistribution in a soil column at different initial water contents. Water Resour. Res., 7, 111-126.

VAN KEULEN, H. and C.H.M. VAN BEEK (1971). Water movement in layered soils - A simulation model. Neth. J. agric. Sci., 19, 138-153.

VANSTEENKISTE, G.C. (1972). Hybrid simulation of distributed parameter systems. Med. Fac. Landbouww. Rijksuniv. Gent, 37, 974-981.

VANSTEENKISTE, G.C. (1975). Modeling and simulation in environmental systems. Proc. Internl. Symp. & Course, Simulation 75, Zürich, 608-613.

VANSTEENKISTE, G.C., J. BENS and J. SPRIET (1978). Design of a linear classifier using simulation techniques. Proc. United Kingdom Simulation Conf., May (in press).

VANSTEENKISTE, G.C., J. BENS and J. SPRIET (1978a). Structure characterization for system modeling in uncertain environments. Proc. Symp. on System Simulation Methodology, Rehovot, Israel, Aug. 1978.

VERMA, R.D. and W. BRUTSAERT (1970). Unconfined aquifer seepage by capillary flow theory. J. Hydraul. Div. Amer. Soc. Civil Eng. 96 (HY 6) , 1330-1344.

VERPLANCKE, H. (1973). Studie van de wetmatigheid van de infiltratie en de diffusiviteit van water in natuurlijke en gekonditioneerde leemgronden. Ph.D. Thesis, State Univ. Ghent.

VICHNEVETSKY, R. (1975). Introduction to finite element methods for initial value problems, Rutgers.

WANG, F.W. and V. LAKSHMINARAYANA (1968). Mathematical simulation of water movement through unsaturated nonhomogeneous soils. Soil Sci. Soc. Amer. Proc., 32, 329-334.

WATSON, K.K. (1966). An instantaneous profile method for determining the hydraulic conductivity of unsaturated porous materials. Water Resour. Res., 2, 709-715.

WATSON, K.K. and A.A. CURTIS (1975). Numerical analysis of vertical water movement in a bounded profile. Aust. J. Soil Res., 13, 1-11.

WHISLER, F.D. and A. KLUTE (1965). The numerical analysis of infiltration considering hysteresis into a vertical soil column at equilibrium under gravity. Soil Sci. Soc. Amer. Proc., 29, 489-494.

WHISLER, F.D. and A. KLUTE (1967). Rainfall infiltration into a vertical soil column. Trans. of the ASAE, 10, 391-395.

WHISLER, F.D., A. KLUTE and D.B. PETERS (1968). Soil water diffusivity from horizontal infiltration. Soil Sci. Soc. Amer. Proc., 32, 6-11.

YOUNG, T.Y. and T.W. CALVERT (1974). Classification, estimation and pattern recognition. American Elsevier, New York.

YOUNGS, E.G. (1964). An infiltration method of measuring the hydraulic conductivity of unsaturated porous materials. Soil Sci., 97, 307-311.

ZARADNY, H. (1978). Boundary conditions in modeling water flow in unsaturated soils. Soil Sci., 125, 75-82.

ZIENKIEWICZ, O.C. (1971). The finite element method in engineering science. Mc Graw Hill, London.